

**Development of an Experimental Setup for Testing Scaled  
Versions of AASHTO Type IV Girders under Dynamic Impact  
Loadings**

**by**

**Luis Alberto Orozco, B.S.C.E.**

**Departmental Report**

Presented to the Faculty of the Graduate School of  
The University of Texas at Austin  
in Partial Fulfillment  
of the Requirements  
for the Degree of

**Master of Science in Engineering**

**The University of Texas at Austin**

**August 2006**

Copyright

by

Luis Alberto Orozco

2006

**Development of an Experimental Setup for Testing Scaled  
Versions of AASHTO Type IV Girders under Dynamic Impact  
Loadings**

**APPROVED BY  
SUPERVISING COMMITTEE:**

---

**Eric B. Williamson**

---

**Oguzhan Bayrak**

## **Dedication**

To my parents Felipe de Jesus Orozco (†) and Miriam Lorena Villaseñor, and to my brothers Luis Felipe and Alejandro Orozco for their encouragement and advice throughout my life.

## **Acknowledgments**

I would like to express my sincerest thanks and appreciation to Prof. Eric B. Williamson and Prof. Oguzhan Bayrak for all their help and guidance; it was a privilege learning from them.

I am grateful to all faculty members for always being available to answer my questions and for all the much needed advice they gave me. Prof. Joseph A. Yura motivated me during my first semester when I needed it the most and taught me that grades are not everything when pursuing an M.S. degree. Prof. John E. Breen was always interested in my progress and gave me a helping hand with a warm smile.

I would also like to thank the laboratory and administrative staff at Ferguson Laboratory. Mike Bell did all the welding of the buttresses; Dennis Phillip and Blake Stasney were always available to patiently answer my questions and give me invaluable advice throughout the duration of my project. An important part of my education received from The University of Texas at Austin came from them.

I would like to thank all my friends whose labor and humor was invaluable to me. In particular, Laura K. Wendling whom not only read this report and gave me her suggestions to improve the clarity of this text, but also gave me her friendship during one of the most difficult periods of my life.

Finally, I would like to thank my family to whom I will be indebted the rest of my life since they sacrificed so much without ever asking anything in return. They are the ones who made this dream come true. Thank you for believing in me.

August 8, 2006

## Table of Contents

<b>CHAPTER 1 – Introduction and Objectives .....</b>	<b>1</b>
1.1 Introduction .....	1
1.2 Objectives of this Project .....	1
1.3 Scope of this Project.....	2
<b>CHAPTER 2 – Background .....</b>	<b>3</b>
2.1 Background .....	3
2.2 Motivation for Research.....	5
<b>CHAPTER 3 – Design of Beam Specimens.....</b>	<b>12</b>
3.1 Introduction .....	12
3.2 Design Objectives .....	12
3.3 Dimensions of Specimens .....	13
3.4 Longitudinal Reinforcement of Specimens.....	15
3.5 Transverse Reinforcement of Specimens .....	19
3.6 Material Properties .....	22
3.6.1 Reinforcing Bars .....	22
3.6.2 Prestressing Strand.....	24
3.6.3 Concrete .....	25
3.7 Beam Capacities .....	26
3.8 Laminated Lumber Beam.....	27
<b>CHAPTER 4 – Test Setup .....</b>	<b>29</b>
4.1 Introduction .....	29
4.2 Impact Test Pendulum.....	30

4.3	Buttresses .....	33
4.3.1	Design and Construction .....	33
4.3.2	Modifications to Buttresses .....	38
4.4	Instrumentations of Specimen .....	41
4.4.1	External .....	41
4.4.2	Internal .....	44
 <b>CHAPTER 5 – Test Results.....</b>		<b>45</b>
5.1	Introduction .....	45
5.2	Test 1 – Reinforced Concrete Beam .....	45
5.3	Test 2 – Reinforced Concrete Beam with FRP at the Ends .....	50
5.4	Test 3 – Laminated Lumber Beam .....	56
5.4.1	Laminated Lumber Beam – 6-in drop height .....	57
5.4.2	Laminated Lumber Beam – 6-in drop height .....	61
5.4.3	Laminated Lumber Beam – 12-in drop height .....	63
5.4.4	Laminated Lumber Beam – 18-in drop height .....	67
 <b>CHAPTER 6 – Conclusion and Recommendations .....</b>		<b>73</b>
6.1	Summary .....	73
6.2	Conclusions .....	74
6.3	Recommendations for Future Research .....	74
 <b>APPENDIX A – Calculations for specimens.....</b>		<b>76</b>
A.1	Stress Calculations Using Allowable Stress Design .....	76
A.2	Flexural Design of Test Specimens .....	79
A.2.1	Prestressed Concrete Specimens .....	79
A.2.2	Reinforced Concrete Specimens .....	80

A.3 Shear Design of Test Specimens .....	82
A.3.1 Prestressed Concrete Specimens .....	82
A.3.2 Reinforced Concrete Specimens .....	89
<b>APPENDIX B – Drawings .....</b>	<b>92</b>
<b>APPENDIX C – Pictures .....</b>	<b>96</b>
<b>REFERENCES .....</b>	<b>112</b>
<b>VITA.....</b>	<b>113</b>



## List of Tables

Table 3-1: Comparison between an AASHTO Type IV Beam and proposed specimen.....	15
Table 3.1: Stresses in concrete at $50d_b$ and midspan for Type IV girder and proposed prestressed specimen at release .....	18
Table 3.3: Total bottom steel and predicted static capacity for a point load at midspan for the two types of specimens.....	19
Table 3.4: Average yield stresses of rebars.....	23
Table 3.5: Average compression strength for concrete.....	26

## List of Figures

Figure 2-1: Confederation Bridge during summer and winter (Sea Ice Studies, 2005).....	3
Figure 2-2: Weight dropping impact apparatus (Jones, 2000) .....	4
Figure 2-3: Impact test setup (Jones, 2000) .....	5
Figure 2-4: Oversize load truck accident (source is unknown).....	6
Figure 2-5: Collision of an oversize load truck with a prestressed girder bridge in Madrid, Spain (elmundo.es, 2005) .....	7
Figure 2-6: Damage to a prestressed girder bridge caused by a truck in Iowa on 2005 (source is unknown). .....	8
Figure 2-7: Damage to a prestressed girder bridge caused by a truck near Monterrey, Mexico on 2005 (courtesy of Gutierrez Ingenieros). .....	9
Figure 2-8: Roadside bomb near a bridge in Iraq (BBC News, 2005).....	10
Figure 3-1: (a) Type IV beam, (b) 1:5 scaled Type IV beam. (c) 6.5in x 11.5in specimen (units in in.) .....	14
Figure 3-2: Section profile (a) at ends (b) at midspan.....	16
Figure 3-3: Location of longitudinal reinforcement for (a) prestressed beam (b) reinforced beam.....	19
Figure 3-4: Cross section of (a) prestressed beam (b) reinforced beam.....	20
Figure 3-5: End cross section of (a) prestressed beam (b) reinforced beam... ..	21
Figure 3-6: Stirrup spacing for (a) prestressed beam (b) reinforced beam... ..	21
Figure 3-7: Stress vs. Strain curve for 6 mm and #3 rebar.....	22
Figure 3-8: (a) Tested rebars. (b) Tension test of a #3 rebar.....	24
Figure 3-9: Low relax. ½-in seven wire strand with wedges. ....	24
Figure 3-10: Load vs. Strain curve for low relax. ½-in seven wire strand (Tuchscherer, 2006).. ..	25
Figure 3-11: Moment-curvature diagram for prestressed beams .....	26
Figure 3-12: Cross section of laminated lumber beam .....	28
Figure 4-1: (a) Typical prestressed bridge. (b) Ideal test setup.....	29
Figure 4-2: Main components of the impact test pendulum.....	31
Figure 4-3: Test setup for barrier test using impact test pendulum (Mitchell, 2005).....	32

Figure 4-4: Plan view of the laboratory's tie-down floor (pendulum area only) ..	33
Figure 4-5: Reactions produced on A-frame due to 80-kip load.....	35
Figure 4-6: Reactions produced on nose of support due to the specimen's self-weight and a 40-kip rebound load.. ..	36
Figure 4-7: Final drawing for A-frames and nose (for more details refer to Appendix B).. ..	36
Figure 4-8: Welding of (a) A-frame, (b) nose of A-frame. ....	37
Figure 4-9: Plan view of test setup.....	38
Figure 4-10: Test setup for first specimen. ....	38
Figure 4-11: Concentration of stresses due to conditions of supports.. ..	39
Figure 4-12: (a) 1-in spacers between nose and A-frame (b) ½-in plates between rods and beam (plan view)... ..	39
Figure 4-13: Modifications to the supports after the first test.....	40
Figure 4-14: Modifications to the supports after the second test. ....	41
Figure 4-15: Location of LVDTs and string pots for the first two tests.....	42
Figure 4-16: Load cell on: (a) west support (b) east support (c) front of pendulum.....	43
Figure 4-17: Location of LVDTs, string pots and load cells for the third tests.. ..	43
Figure 4-18: Strain gauges on reinforcing steel and prestressing strand.....	44
Figure 5-1: Neoprene pad bonded to beam; straps are only used while epoxy set .....	46
Figure 5-2: Support displacement obtained from the first test performed.. ..	47
Figure 5-3: Video frames recorded from the overhead traveling crane.. ..	48
Figure 5-4: Local damage to east end of the beam. ....	49
Figure 5-5: (a) Bottom layer of FRP cross section view. (b) Bottom layer of FRP longitudinal view. (c) Top layer of FRP longitudinal view.. ..	50
Figure 5-6: Placing of FRP fibers on reinforced concrete beam.....	51
Figure 5-7: Midspan deflection registered by string potentiometers. ....	52
Figure 5-8: Frames from video recorded from the overhead traveling crane. ....	53
Figure 5-9: Unfiltered acceleration profile.....	54
Figure 5-10: Filtered acceleration profile.....	55
Figure 5-11: Load profile obtained from load cells (LC) at supports and front of pendulum mass.....	57
Figure 5-12: Load profile obtained from load cell (LC) in front of pendulum and from acceleration profile (6-in drop height).....	59
Figure 5-13: Midspan deflection measured using string potentiometers (SP). ....	60
Figure 5-14: Midspan deflection during impact measured using string potentiometers (SP).. ..	60

Figure 5-15: Load comparison between first two tests. ....	61
Figure 5-16: Force profile for first two tests obtained from acceleration data.. ...	62
Figure 5-17: Frames from video recorded during impact (6-in drop height).....	63
Figure 5-18: Load comparison between test 2 (6-in drop height) and test 3 (12-in drop height).. .....	64
Figure 5-19: Force profile for test 2 (6-in drop height) and test 3 (12-in drop height).....	65
Figure 5-20: Midspan displacement for test 2 (6-in drop height) and test 3 (12-in drop height).. .....	66
Figure 5-21: Frames from video recorded during impact (12-in drop height).....	66
Figure 5-22: Load comparison between test 3 (12-in drop height) and test 4 (18-in drop height).. .....	67
Figure 5-23: Force profile for test 2 (6-in drop height), test 3 (12-in drop height) and test 4 (18-in drop height).. .....	68
Figure 5-24: Pictures of laminated lumber beam after final test.....	69
Figure 5-25: Midspan displacement for test 2 (6-in drop height), test 3 (12-in drop height) and test 4 (18-in drop height).....	70
Figure 5-26: Load profile obtained from load cell (LC) in front of pendulum and from acceleration profile (12-in drop height).....	71
Figure 5-27: Load profile obtained from load cell (LC) in front of pendulum and from acceleration profile (18-in drop height).....	72

# **CHAPTER 1**

## **Introduction**

### **1.1 INTRODUCTION**

The construction of a bridge not only involves great sums of money but also a great amount of time. The whole process may take several months and often years. In most cases, the general public is affected by the construction of bridges due to traffic disruptions, noise, dirt and many others factors caused by construction sites. Due to these reasons and because bridges are extremely important for transportation purposes, current specifications consider a design life of 75 years for bridges. In the design, many types of loads are considered, including accidental loadings. However, until recently, consideration to intentional blast loading was not considered. In recent years, terrorist attacks that targeted transportation facilities forced the engineering community to start researching the potential effects of blast loads on bridges in order to develop guidelines for design.

The purpose of this project is to develop scaled versions of AAASHTO Type IV girders that can be constructed and tested safely at Ferguson Laboratory. In order to test the specimens, a test setup has to be designed and built.

### **1.2 OBJECTIVES OF THIS REPORT**

The objective of this report is to document research performed by the author under the supervision and direction of faculty members for the project titled “Blast-Resistant Highway Bridges: Design and Detailing Guidelines”. The research performed for this project includes the following:

- designing and constructing small scale specimens that represent an AASHTO Type IV girder;
- designing and constructing of the two buttresses employed as beam supports as part of the test setup;
- testing of the test setup and different types of instrumentation using concrete and lumber specimens; and
- comparing data obtained from accelerometers and load cells in order to obtain the force applied to the specimen.

A further objective of the author is that this report serves as a useful reference for future researchers involved in the use of the impact test pendulum, the buttresses, and some of the instrumentation presented in this report.

### **1.3 SCOPE OF THIS PROJECT**

This report includes the development of test specimens representative of an AASHTO Type IV girder and an appropriate test setup for this type of members. Chapter 2 includes a brief background review of dynamic tests performed on prestressed beams. Chapter 3 describes the design procedure and construction of the test specimens employed for this project. The development of the test setup, including the instrumentation used, is addressed in Chapter 4. Chapter 5 contains data obtained from three tests performed as well as the interpretation of these data. Finally, Chapter 6 includes conclusions and recommendations for future research based on the information included in this report.

## CHAPTER 2

### Background

#### 2.1 BACKGROUND

Research related to the structural response of bridges to dynamic loadings is not new. Most of the research conducted to date has focused on loading caused by natural forces like wind, earthquake, and ice (Figure 2-1) or by accidental impact like the ones caused by vessels against bridges or debris flowing through waterways (Figure 2-1). However, most of the research does not involve bridges being loaded from the bottom, opposite to the direction of gravity; and limited research has been performed on bridges subjected to accidental or intentional explosions. Loading any type of bridge in a way that it is not intended can potentially lead to catastrophic results, and prestressed concrete girder bridges are no exception. For such systems, prestressing strands are located to resist gravity loads, and such girders have low resistance to upward acting loads.



*Fig. 2-1: Confederation Bridge during summer and winter (Sea Ice Studies, 2005).*

Recent research related to dynamic loading of prestressed beams has been performed by the Department of Civil Engineering of the National Defense

Academy of Japan (Jones, 2000). The objective of the research was to determine the structural response of prestressed beams under high speed impact loading induced by a weight dropping machine (Figure 2-2). First, a high speed loading analysis was performed to find the expected limit drop height. Then, the impact test was performed using the test setup presented in Figure 2-3, and finally, an impact failure analysis was carried out to simulate the results obtained from the dynamic test. From this research, it was concluded that the limit drop height could be predicted prior to the test and that the impact failure analysis was able to represent the failure behavior of the beams tested. However, this investigation did not focus on loading the beams in the direction opposite to gravity, which would be a more critical condition.

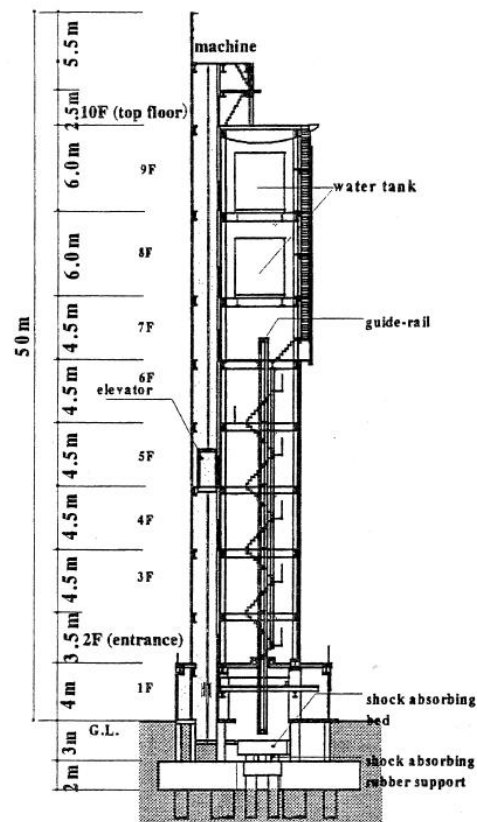


**Fig. 2-2: Weight dropping impact apparatus (Jones, 2000).**



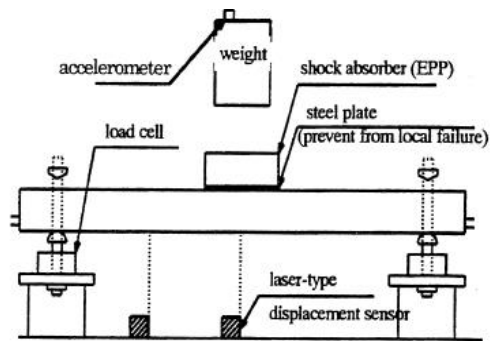


*Fig. 2-3: Impact test setup (Jones, 2000).*

Recently, Washington State Department of Transportation (WSDOT) realized that little research had been conducted on blast effects on bridges. It was also estimated that the damage expected from a blast on top of a prestressed girder bridge would cause damage to the deck and possibly one or two girders located near the blast. However, if the blast was to occur under the prestressed bridge, the damage could be extensive. In order to address this concern, the Transportation Center at Washington State University initiated the research project “Prestressed Girder Blast Test” (WSU, 2005). The objective of the project is to test and analyze the vulnerability of prestressed girder bridges under blast loading with different types of orientation. To analyze the vulnerability of the girders, WSDOT Bridge Division will conduct two full-scale prestressed girder bridge blast experiments. The two bridges will be composed of four girders, but different types of girder lengths will be used: 75 ft for the first one and for the other 150 ft. The project is expected to conclude in December 2007.

## **2.2 MOTIVATION FOR RESEARCH**

There are several types of events that can cause loading on a bridge from the bottom, but the ones that the project will focus on are those produced by accidental or intentional explosive loadings and impact loadings produced by

oversize load trucks. Figure 2-4 show an accident involving construction equipment and a bridge. It is important to point out that this bridge is not a prestressed girder bridge. Hence, the redundancy in the bridge prevented it from collapsing. However, with such extensive damage, a prestressed girder bridge may not have performed so well.



***Fig. 2-4: Oversize load truck accident (source is unknown).***

Figures 2-5 and 2-6 show damage caused to prestressed girder bridges by trucks carrying oversize loads. The first figure shows a bridge over an important highway in Madrid, Spain that was impacted by an oversize truck at a high speed. The external prestressed beam lost all of its strands due to the impact, and the

beam had to be replaced. Figure 2-6 shows a prestressed girder bridge in Iowa in which a truck carrying a large steel cylinder impacted the girders at a speed of about 70 mph. For this case, the external girder that was impacted first did not suffer extensive damage. However, in the zone of impact, the last two prestressed beams are essentially gone. The bridge did not collapse because of the redundancy provided by the slab and guardrail.



***Fig. 2-5: Collision of an oversize load truck with a prestressed girder bridge in Madrid, Spain (elmundo.es, 2005).***



***Fig. 2-6: Damage to a prestressed girder bridge caused by a truck in Iowa on 2005 (source is unknown).***

Figure 2-7 shows a prestressed girder bridge in Monterrey, Mexico composed of post-tensioned girders. In a situation similar to the one presented in the previous figure, a truck carrying an oversize steel cylinder slammed into the bridge. In this case, the external beam was seriously damaged, and the strand profile was exposed. The whole span was displaced horizontally by more than an inch after the impact. It can also be seen that steel cylinder produced an upward load to the post-tensioned beams causing tension cracks at the top of the section. This upward force was strong enough to lift the beam, and, as can be seen from the picture, the neoprene pad is no longer in contact with the abutment.



***Fig. 2-7: Damage to a prestressed girder bridge caused by a truck near Monterrey, Mexico on 2005 (courtesy of Gutierrez Ingenieros).***

The loadings produced by explosives occur rarely, but, due to recent events involving terrorists targeting transportation facilities, a new area of research evolved (Figure 2-8). The need for investigation in this area is constantly growing. In July, 2002, the National Strategy for Homeland Security was formed to try to secure the U.S. from terrorist attacks. The main purpose of homeland security is not only to prevent terrorist attacks but also to reduce vulnerability to them. States were asked to identify 15 to 20 of its most vulnerable facilities and then develop mitigation procedures for each one of them. Several bridges were included in the lists of several states (WSU, 2005). There are many different ways to mitigate the vulnerability of bridges, and one of them is by creating design guidelines that address the problem.



*Fig. 2-8: Roadside bomb near a bridge in Iraq (BBC News, 2005).*

In order to formulate guidelines for the design of bridges resistant to impact and explosive loadings, test data are needed. However, doing research in this area involves applying large loads rapidly, which makes the process complicated and expensive. In addition, these types of loadings can be extremely dangerous. For this reason, a great deal of the research that goes into this

investigation addresses designing and fabricating test specimens and a test setup that will allow for testing to be performed in a safe and relatively inexpensive manner.

## **CHAPTER 3**

### **Design of Beam Specimens**

#### **3.1 INTRODUCTION**

The design of five beams that were constructed by the author is described in this chapter. Two of the specimens consist of prestressed concrete beams, two of plain reinforced concrete, and one of 2-in×12-in pine boards. The first type of specimen is representative of a prestressed AASHTO Type IV girder for a 24-ft roadway. These sections are typically used in the construction of bridges with spans between 70 and 100 ft. The information about the girder was obtained from TxDOT Bridge Division plans. The steel reinforcement of Type IV beams can vary greatly depending on the beam length; therefore, a specific application must be selected when designing the specimens. This decision was mainly influenced by the capacity of the existing impact test pendulum designed by Geoffrey T. Mitchell (Mitchell, 2005), space limitations where the specimen will be tested, and construction feasibility. The design for the second type of specimen, the reinforced concrete beams, was based on the prestressed beams. For the laminated lumber beam, no specific design requirements were specified, but the dimensions of it were similar to the other specimens. These last two types of specimens were mainly used to verify that all the instrumentation was working properly and to obtain information on ways to improve the measurements.

#### **3.2 DESIGN OBJECTIVES**

As mentioned before, an AASHTO Type IV girder is commonly used on prestressed bridges. However, due to its large dimensions and capacities, constructing and testing a full-size Type IV girder would also require the



construction of a large test setup and a way to apply large dynamic loads. Such an experiment set up would end up being very expensive and require a lot of space. Consequently it was decided that this option could not be easily pursued. Therefore, a model to represent a Type IV had to be designed. The model should be a scaled version of the actual Type IV girder in both dimensions and amount of steel used. The following sections describe the procedure used to obtain the final specimen, which represent an AASHTO Type IV girder.

### **3.3 DIMENSIONS OF CONCRETE SPECIMENS**

To maintain the same scale for the cross section and for the length of the beam, the specimen was selected to represent an 80-ft long girder. Anything longer would require a small scale for use with the existing impact test pendulum, and, as a result, the cross section would end up being very small and difficult to construct. Anything shorter would be only representative of a span close to the ends of a bridge. Several scales were tried, and the one that most satisfied all requirements was a 1:5 scale, resulting in a specimen 16-ft long. However, an additional 4 inches on each end was included to ensure enough bearing area. This length was adequate for the space currently available in the test pendulum area, and it also allowed two beams to be cast at the same time in the existing prestressing bed.

The shape of the cross section had to be modified from the typical I-section to a rectangular section due to the complication of constructing the formwork and rebar cage for a small I-section. In addition, the rectangular cross section was made bigger in order to be able to use #3 rebar for the stirrups and still meet the cover requirements from ACI-318-05. Figure 3-1 shows the dimensions of the cross section of an AASHTO Type IV beam, a 1:5 scaled

model, and the proposed specimen. Table 3-1 shows a comparison between selected properties of an AASHTO Type IV beam and the proposed specimen, including the distance to the top outer fiber ( $Y_t$ ) and to the bottom outer fiber ( $Y_b$ ). The area of the Type IV section is approximately ten times bigger than that of the specimen due to the modifications done for construction purposes. This will roughly double the shear capacity of a Type IV girder for 1:5 scale. However, this will not affect the results, because the specimen is expected to fail in flexure.

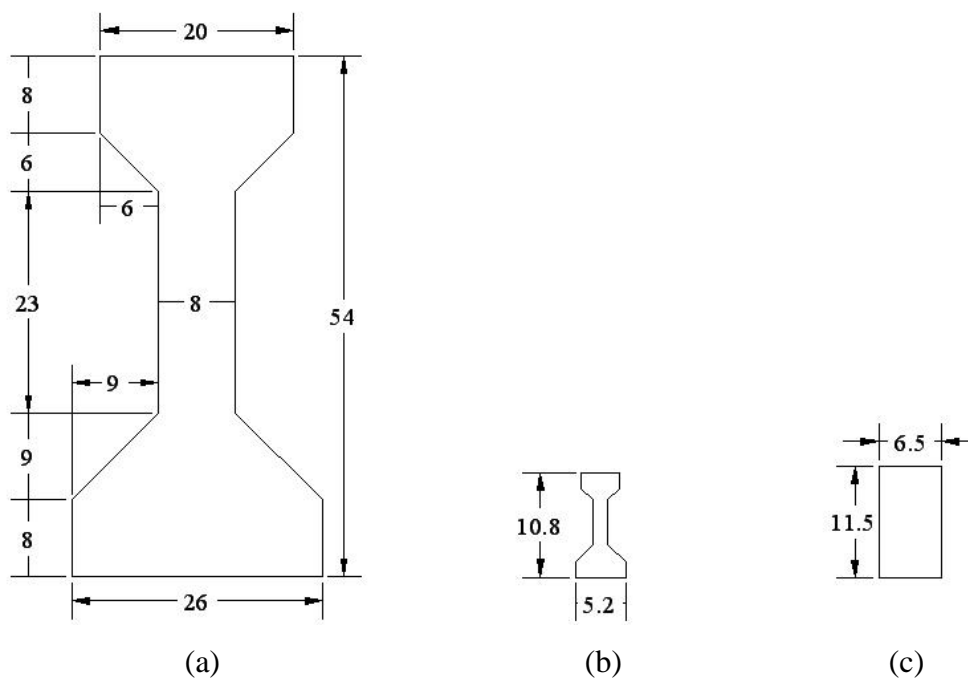


**Fig. 3-1: (a) Type IV beam, (b) 1:5 scaled Type IV beam. (c) 6.5in x 11.5in specimen (units in in.).**

**Table 3-1: Comparison between an AASHTO Type IV Beam and proposed specimen.**

<b>Beam</b>	<b>Length (ft)</b>	<b>Area (in<sup>2</sup>)</b>	<b>Width (in)</b>	<b>Depth (in)</b>	<b>Y<sub>t</sub> (in)</b>	<b>Y<sub>b</sub> (in)</b>	<b>Y<sub>b</sub>/Depth</b>
<b>AASHTO Type IV</b>	80	788.4	26	54	29.25	24.75	0.46
<b>6.5in x 11.5in</b>	16.67	74.75	6.5	11.5	5.75	5.75	0.5
<b>Ratio</b>	4.8	10.5	4	4.7	5.1	4.3	0.9

In order to be able to use the same test setup for all tests, the dimensions for the reinforced beams had to be the same as for the prestressed beams. Additionally, having all specimens be of the same size would give the opportunity to compare all tests performed and would also allow the use of the same formwork, saving valuable time and materials.

### **3.4 LONGITUDINAL REINFORCEMENT OF SPECIMENS**

The amount and location of the longitudinal reinforcement of an 80-ft AASHTO Type IV girder varies along its length. It has a total of twenty ½-in 270-ksi low relaxation strands, of which four are depressed at midspan. In addition, the section has more reinforcing bars at the ends than at midspan. Due to these differences, two sections were considered for the design and are shown in Figure 3-2.

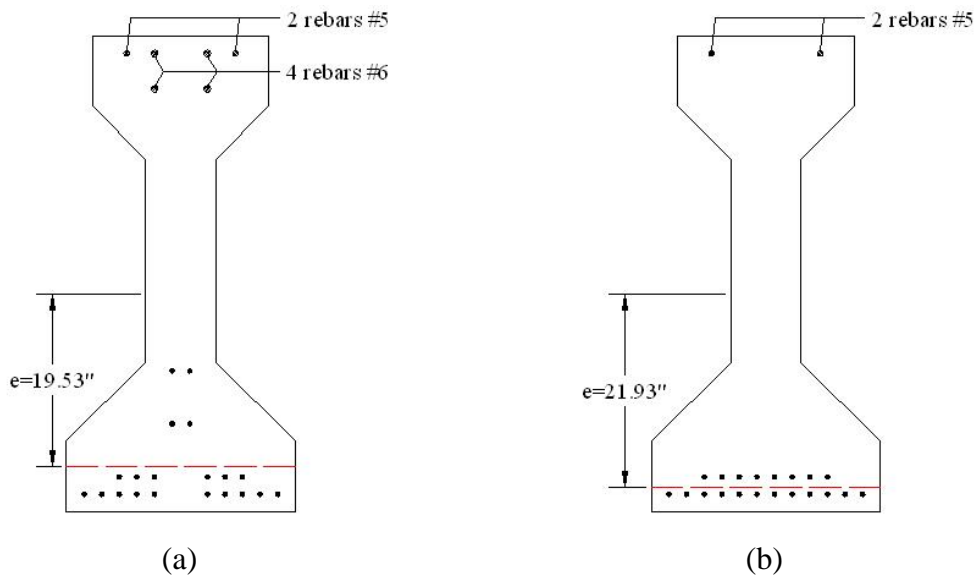


**Fig. 3-2: Section profile (a) at ends (b) at midspan.**

The amount of strands and reinforcing bars for the proposed specimen was obtained by maintaining approximately the same ratios between the area of concrete ( $A_c$ ) to area of prestressing steel ( $A_p$ ) and area of concrete to area of reinforcing bars ( $A_s$ ) of the Type IV girder. These requirements resulted in two ½-in strands, which, due to the small dimensions of the section, had to have the same eccentricity along the whole length of the beam. For the reinforcing bars, two areas of steel were obtained, 0.225-in<sup>2</sup> for the ends and 0.058-in<sup>2</sup> for midspan. However, as it will be described in the next chapter, the load will be applied to the specimen at midspan. Therefore it was decided that it was of more relevance to the project to focus on the area of steel in this region and not at the ends. For construction purposes and in order to have a symmetric rebar cage, two deformed rebars had to be used, and the smallest available were 6 mm (0.024 in) in diameter. Although the total area of steel exceeds the one at midspan for the

desired ratio, it was decided that this small difference would not have a significant effect on the results.

After obtaining the amount of steel for the specimen, the location of the strands was calculated. This was done by adjusting the eccentricity ( $e$ ) so that the stresses at the critical points do not exceed the stresses allowed by ACI-318-05 and also so they resemble those of an AASHTO Type IV girder. Originally, the two required strands were placed on the bottom corners of the stirrups, resulting in an eccentricity of 4 in. Placing the strands there, however, would have caused the failure of the beam at release due to the excessive tension stress at the top fiber. The most feasible solution to this problem would have been to place an extra strand close to the centroid of the cross section. By doing so, the eccentricity could be reduced to 2.75 in and the stresses could be within those required by the code. However, the prestressing bed at Ferguson Laboratory is intended for beams with one layer of strands, which left this option as one that could not be easily pursued. Consequently, the only way to build the prestressed beams was by locating the layer of strands approximately 1.5-in above the corner of the stirrups.

Appendix A shows the procedure used to calculate the stresses produced by the prestressing force using Allowable Stress Design. Table 3-2 shows the resulting stresses for the specimen and AASHTO IV girder at a distance of 50 times the diameter of the strand ( $50d_b$ ) from the ends and at midspan. These locations are the two critical points where stresses should be checked on a prestressed beam.

***Table 3-2: Stresses in concrete at 50d<sub>b</sub> and midspan for Type IV girder and proposed prestressed specimen at release.***

	<b>Stresses at 50d<sub>b</sub></b>		<b>Stresses at midspan</b>	
	<b>80 ft AASHTO Type IV</b>	<b>6.5in x 11.5in specimen</b>	<b>80 ft AASHTO Type IV</b>	<b>6.5in x 11.5in specimen</b>
<b>Bottom fiber</b>	-1.716 ksi	-1.892 ksi	-1.174 ksi	-1.765 ksi
<b>Top fiber</b>	0.441 ksi	0.257 ksi	-0.200 ksi	0.129 ksi

As mentioned before, the reinforcement for the prestressed beams was obtained by scaling down an actual Type IV beam. With this information, the capacity of the beam under a point load at midspan was calculated (see Appendix A). After obtaining this information, the reinforced concrete beams were designed to resist a similar point load at midspan if loaded in the direction of gravity. However, the required steel for the bottom layer was significant compared to the cross section and could not be placed in a way to meet ACI-318-05 spacing requirements. Therefore, the amount of steel used was the maximum that could be placed in one layer and still meet the standards. This resulted in three #5 grade 60 rebars with a clear spacing of 1.125 in for the bottom layer. Regarding the top layer of longitudinal reinforcement, it would have been desirable to use the same 6-mm rebar that was used for the prestressed beams. However, due to availability issues, two #3 grade 60 rebars were used. Figure 3-3 shows the cross section of the two types of specimens with the longitudinal reinforcing steel. A comparison of the amount of steel and static capacity for a point load at midspan for the two types of specimens is presented in Table 3-3.

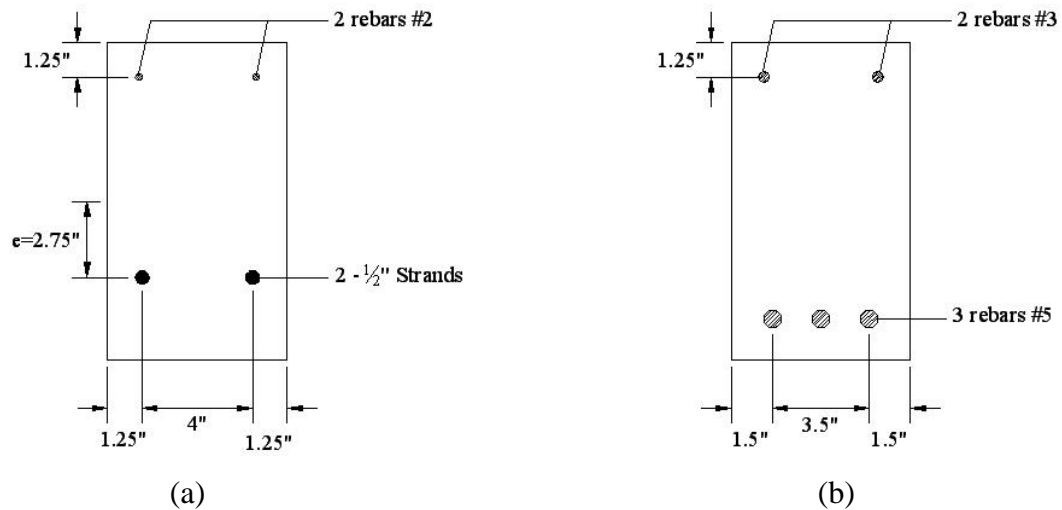


**Fig. 3-3: Location of longitudinal reinforcement for (a) prestressed beam (b) reinforced beam.**

**Table 3-3: Total bottom steel and predicted static capacity for a point load at midspan for the two types of specimens.**

Type of Specimen	Type of steel	Total area of steel	Static capacity for point load at midspan
<b>Prestressed Concrete Beam</b>	1/2-in 270-ksi low relax. strand	0.306 in <sup>2</sup>	12.5 kips
<b>Reinforced Concrete Beam</b>	#5 grade 60 rebars	0.93 in <sup>2</sup>	9.6 kips

### 3.5 TRANSVERSE REINFORCEMENT OF SPECIMENS

After having defined the amount and location of the longitudinal steel for each type of beam, the transverse reinforcement or stirrups required were calculated. It is important to point out that for the prestressed beams the design

was not based on an AASHTO Type IV girder but rather on providing sufficient reinforcement so that the specimen would fail in flexure under gravity loads. The same applies to the reinforced beams. For both types of beams, #3 grade 60 stirrups were used, but the spacing was different for each type of beam. Figure 3-4 shows the final cross section of the two types of specimens

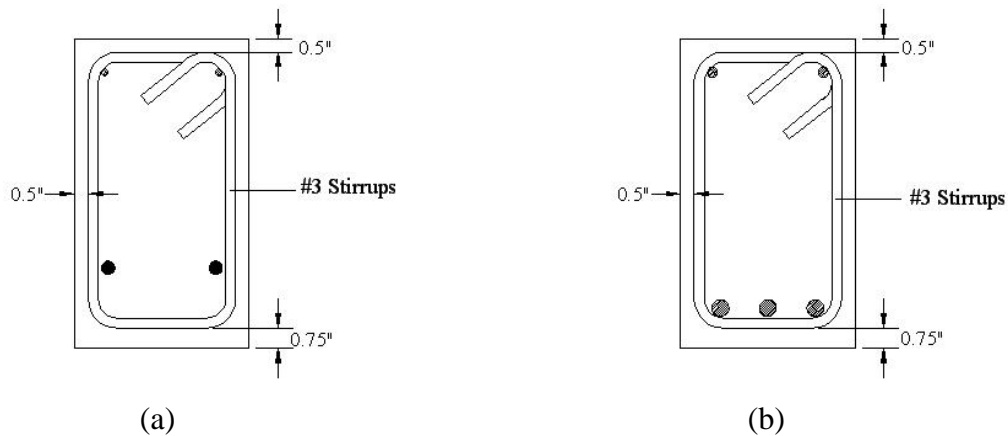


**Fig. 3-4: Cross section of (a) prestressed beam (b) reinforced beam.**

In addition to the transverse reinforcement, the ends of the prestressed beams included extra reinforcement known as bursting steel. The purpose of this steel is to prevent local failure at the ends when releasing the strands. In the case of the reinforced beams, this steel is not required. However, as will be explained in Chapter 5, results from the first test suggested that steel should also be added to the ends of the other reinforced beam. This additional steel was added in order to prevent local failures at the ends due to the support conditions of the test setup. For this reinforcement, #3 rebars were employed. Figure 3-5 shows the beam end cross sections, and Figure 3-6 shows the stirrup spacing used for each type of specimen.



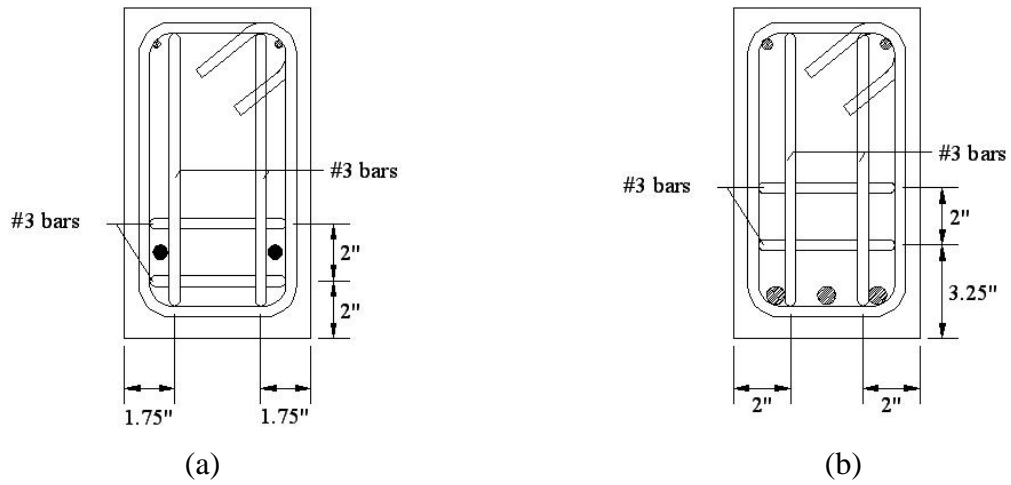


**Fig. 3-5: End cross section of (a) prestressed beam (b) reinforced beam.**

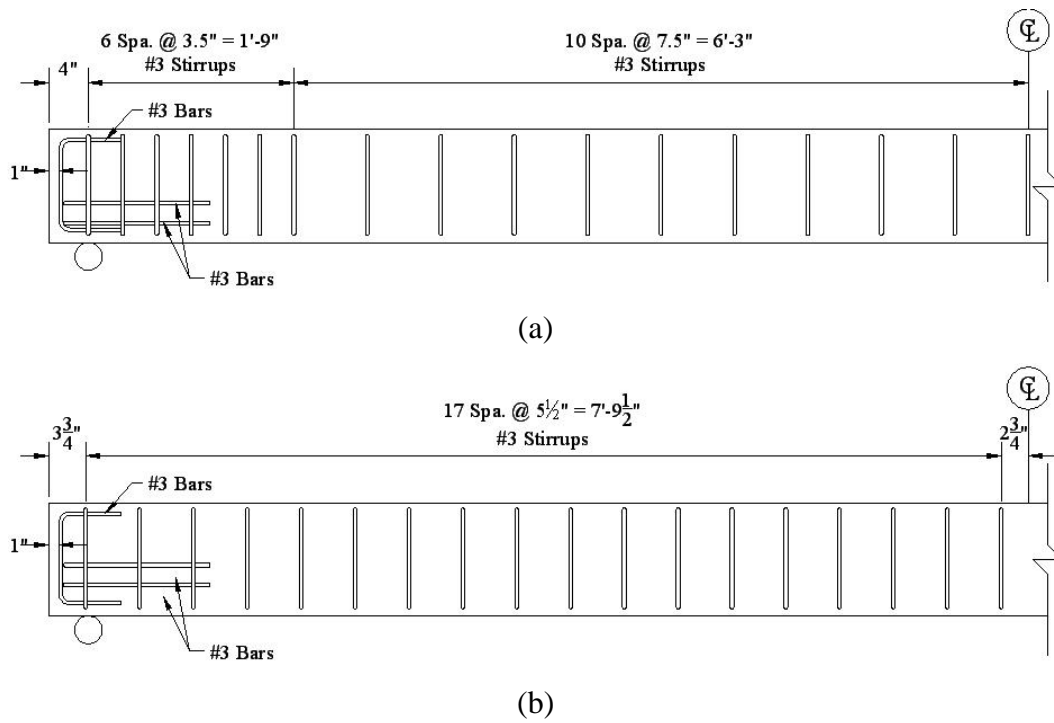


**Fig. 3-6: Stirrup spacing for (a) prestressed beam (b) reinforced beam.**

### 3.6 MATERIAL PROPERTIES

#### 3.6.1 Reinforcing bars

The longitudinal reinforcing bars used for the top layer of the prestressed specimens are a non-standard size and are not easily found commercially. Ferguson Laboratory has two stacks of this rebar, which were manufactured in two different countries, Mexico and Sweden. Both bars are deformed 6-mm rebar, which makes it difficult to distinguish between them upon visual inspection. However, they have different yield stresses ( $f_y$ ) according to the manufacturers; the rebar from Mexico yields at 90 ksi while the one from Sweden yields at 65 ksi. Because it was difficult to distinguish one from the other, tension tests were performed in accordance with ASTM A615/A in order to obtain the actual yield stress. Tests were also performed for the rebar used as shear reinforcement for both types of specimens to verify that it actually was grade 60. Figure 3-7 shows a typical stress-strain relationship for the two types of non-commercial rebar as well as for the #3 rebar used as stirrups.

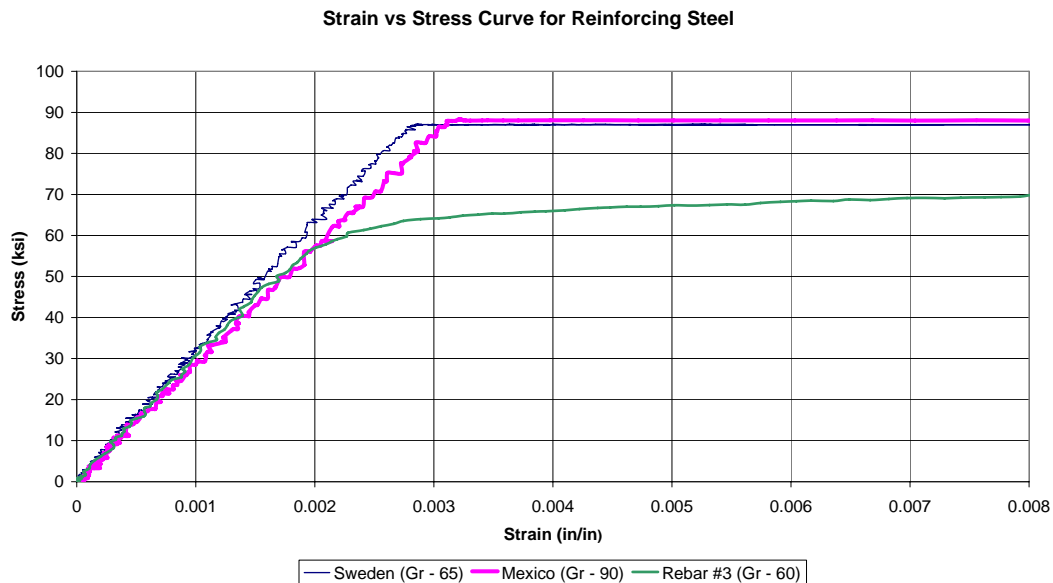


**Fig. 3-7: Stress vs. Strain curve for 6 mm and #3 rebar.**

After performing at least three tests with each type of rebar and having obtained the stress-strain relationship for each of them, the results indicated that the yield stress for all bars occurs above 60 ksi. To obtain this value, a provision in ACI-318-05 was used that states that the yield strength for bars exceeding 60 ksi can be taken as the stress corresponding to a strain of 0.0035. However, for design calculations, this value shall not exceed 80 ksi. Table 3-4 shows the average yield stress and the stress used for design calculations.

**Table 3-4: Average yield stresses of rebars.**

<b>Rebar Type</b>	<b>Area (in<sup>2</sup>)</b>	<b>Average <math>f_y</math> (ksi)</b>	<b><math>f_y</math> for design calculations (ksi)</b>
Sweden	0.044	83.87	80
Mexico	0.044	87.85	80
#3	0.11	62.97	60
#5	0.31	NA	60

Once the yield values for each rebar were available, the decision to use the 6-mm rebar from Sweden for reinforcement in the prestressed specimens was made. For the longitudinal reinforcement of the reinforced beams, #5 grade 60 rebar were used, but no tests were performed to determine the material properties of these bars. Figure 3-8 shows two pictures: one of the two different types of 6-mm rebar as well as the #3 and #5 rebars used, and the other of a tension test of a #3 rebar.



**Fig. 3-8: (a) Tested rebar. (b) Tension test of a #3 rebar.**

### **3.6.2 Prestressing strand**

The strand used for the prestressed specimens was Low Relaxation ½-in seven wire strand with an ultimate stress ( $f_{pu}$ ) of 270 ksi and an area of 0.153 in<sup>2</sup>. A picture of the strand and wedges used is presented in Figure 3-9. This strand was already available at Ferguson Laboratory, and the properties of it were obtained from tension tests performed by Robin Tuchscherer (Tuchscherer, 2006). Figure 3-10 shows a typical load-strain relationship for the strand used for the prestressed specimens.



**Fig. 3-9: Low relax. ½-in seven wire strand with wedges.**

Load vs Strain for Spool #2 (1/2-in Strand)

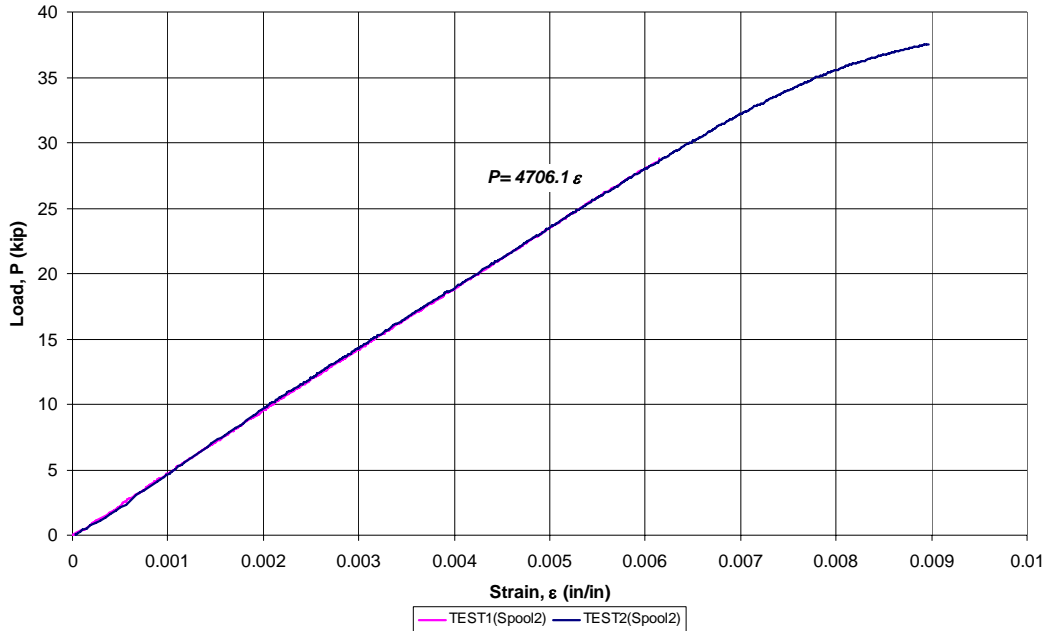


*Fig. 3-10: Load vs. Strain curve for low relax. 1/2-in seven wire strand (Tuchscherer, 2006).*

### 3.6.3 Concrete

The concrete employed for the prestressed specimens was different than that used for the reinforced concrete ones. This difference was due to the fact that the volume of concrete needed for each specimen was relatively small, only 0.32 yd<sup>3</sup>. Therefore, it was easier and more economical to coordinate the pour with another project that required a larger volume of concrete.

For the prestressed specimens, the concrete used had Type III cement, which is typically used to obtain high strengths in a short period of time. For the reinforced specimens, regular cement was used, and the aggregate size used for all

specimens was  $\frac{3}{4}$  in. Table 3-5 shows the average 28-day compressive strength ( $f'_c$ ) for each of the specimens built.

**Table 3-5: Average compression strength for concrete.**

Type of Beam	Average $f'_c$ (ksi)
Prestressed Specimens	12.41
Reinforced Concrete 1	6.90
Reinforced Concrete 2	5.20

### 3.7 BEAM CAPACITIES

Once the beam dimensions and material properties are established, the capacities of the beams can be calculated. To compute the response of the prestressed beams, a moment-curvature diagram (Figure 3-11) was constructed using a software package called RESPONSE (Felber, 1990).

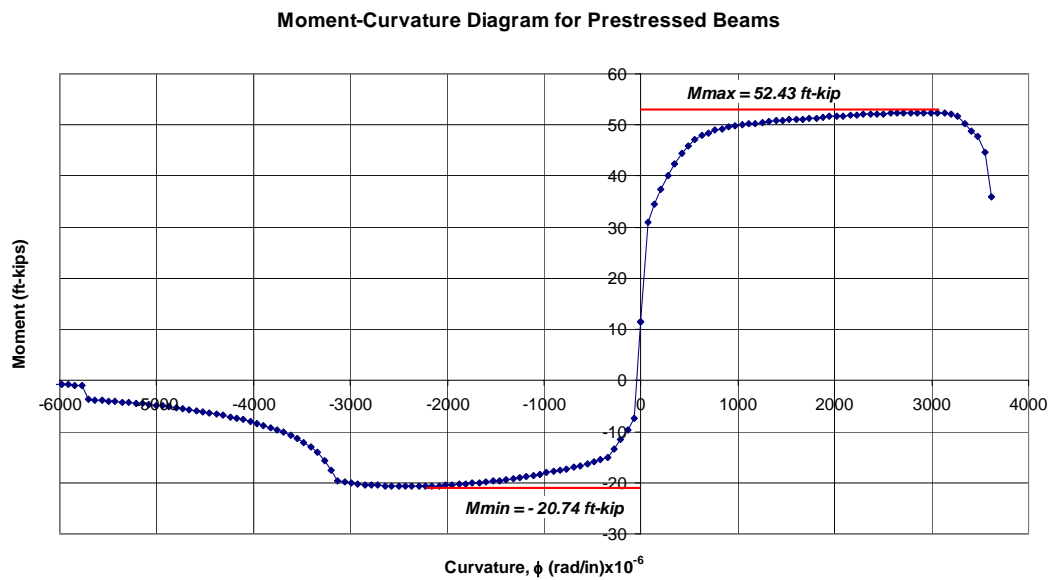


**Fig. 3-11: Moment-curvature diagram for prestressed beams.**

As mentioned before, the longitudinal steel for the reinforced concrete beams was initially calculated based on the moment capacity of the prestressed beams. The area of steel required for a moment of 52.4 ft-kip is of 1.27-in<sup>2</sup>, but this amount of steel could not be placed in one layer due to clear spacing requirements by ACI-318-05. For this reason, it was decided to use three #5 rebars, which results in an area of steel of 0.93 in<sup>2</sup> and a moment capacity of 40.9 ft-kip. All calculations regarding the concrete beams are presented in Appendix A.

### **3.8 LAMINATED LUMBER BEAM**

The idea of fabricating a laminated lumber beam was raised after performing the first two tests and realizing the need for a different type of instrumentation. This instrumentation needed to be verified before performing an actual test with a concrete beam. A simple, cost-effective way to investigate the performance of the instrumentation was by running a test on a beam with similar dimensions as the concrete ones. This beam was constructed using 2-in×12-in pine boards and ¾-in plywood. The boards are actually 1.5-in×11.25-in, and, in order to have a depth of 6 in, three boards were used with a layer of plywood added between them. The boards and plywood were attached together using a thin layer of carpenter's glue and 3-in nails. The length of this beam was 18 ft. Figure 3-12 shows the cross section of the laminated lumber beam.

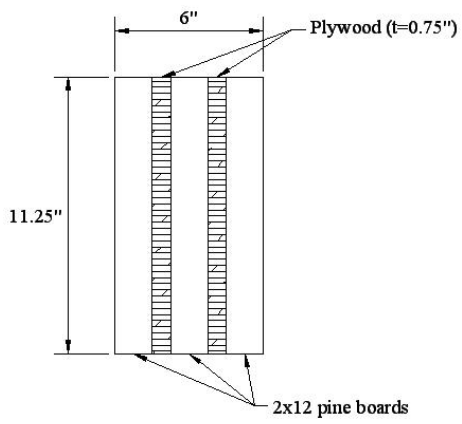


***Fig. 3-12: Cross section of laminated lumber beam.***



## CHAPTER 4

### Test Setup

#### 4.1 INTRODUCTION

This chapter addresses all issues related to the test setup, starting from the main components involved and moving on to the development of the final setup and instrumentation used. The main objective of the test setup is to reproduce the conditions of a prestressed beam in a bridge when subjected to loading from the bottom. Generally, bridges are not designed for this type of loading, but interest in loading a bridge from the bottom has increased in recent years, not only to resist accidental impact loading but also to resist a possible explosion in case the bridge is targeted by terrorists. Therefore, the test setup had to be able to hold a beam from the ends without producing moment restraint, because most prestressed girders used in bridges are simply supported. The setup also had to allow a dynamic load to be applied to the bottom of the beam.

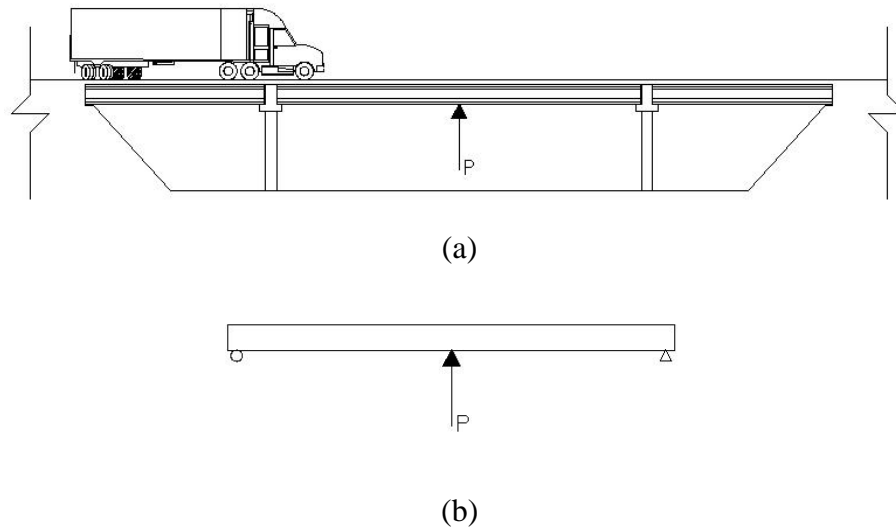


**Fig. 4-1: (a) Typical prestressed bridge. (b) Ideal test setup.**

It is relevant to mention that getting to the final test setup was an evolutionary process. With each test performed, there were modifications to the setup based on the behavior of the specimen and the results obtained from the instrumentation. The principal components used for the tests are the impact test pendulum and the A-frames or buttresses that act as supports at the ends of the beam.

#### **4.2 IMPACT TEST PENDULUM**

In this section, a description of the impact test pendulum is presented because it is one of the main components of the test setup. However, the author of this report did not participate in the design or construction of this piece of equipment. The pendulum was designed by Geoffrey T. Mitchell (Mitchell, 2005), and details not presented here can be found in his thesis. The impact test pendulum consists of an 855-kg mass made up of steel plates suspended by four steel cables from a 22-ft tall steel frame. The pendulum mass can be lifted up to a 16-ft drop height using a winch. A sketch of the pendulum's main components is shown in Figure 4-2.

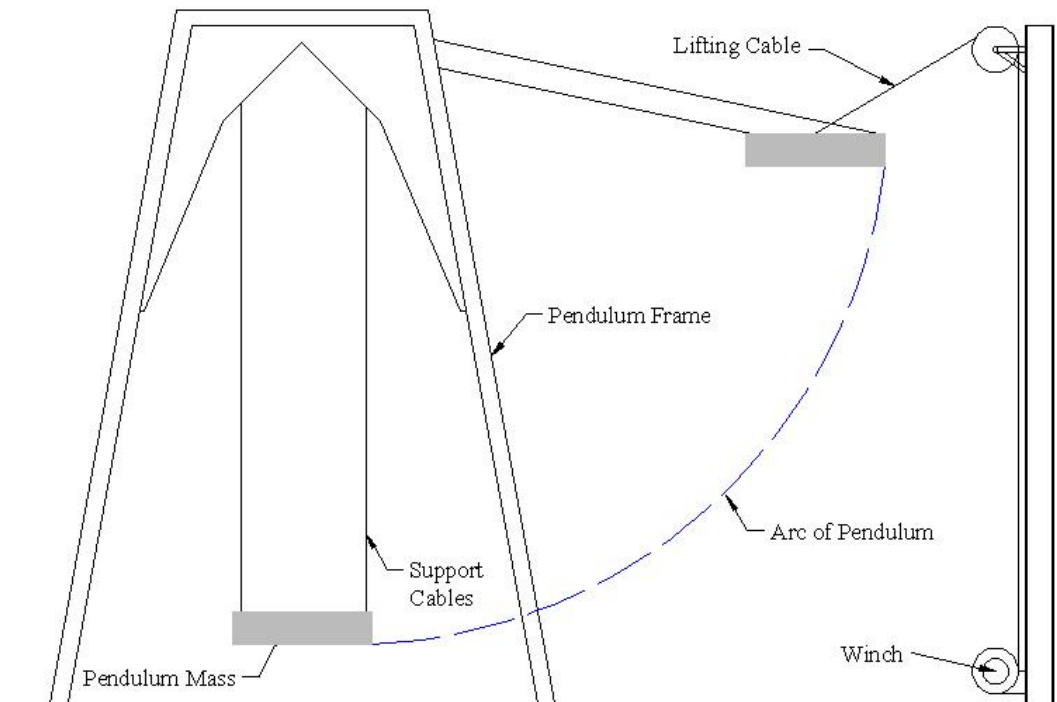


***Fig. 4-2: Main components of the impact test pendulum.***

The impact test pendulum was originally designed to simulate a vehicular impact on a bridge barrier. Figure 4-3 was obtained from Mitchell's (Mitchell, 2005) thesis, and it shows a rendering of a barrier test using the pendulum. Nevertheless, with some minor adjustments, the pendulum can be used to test other structures like the beams involved in this project.

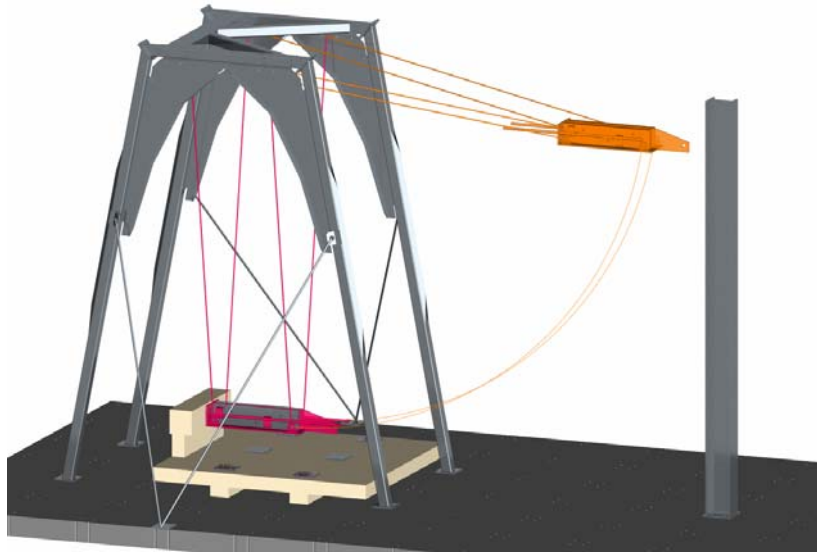


***Fig. 4-3: Test setup for barrier test using impact test pendulum (Mitchell, 2005).***

For the purposes of the current study, the impact test pendulum required only a minor modification, which was the addition of a load cell in front of the mass to record the impact force. However, the load cell was only added after two tests were performed and the need for an accurate way to obtain the impact load was identified. The reasons for this need will be discussed in a subsequent section. There were also some other additions done to the surrounding area of the pendulum. For the barrier tests, a slab was anchored to the laboratory's structural tie-down floor, and a barrier was installed on top of this slab. But for testing beams, a frame was needed to serve as a support to hold the beams at a specific height and to allow the beams to span 16-ft. The support also needed to be anchored to the tie-down floor with 1-in diameter threaded rods. Hence, the design was largely based on the clusters of bolts available in the pendulum area (Figure 4-4).

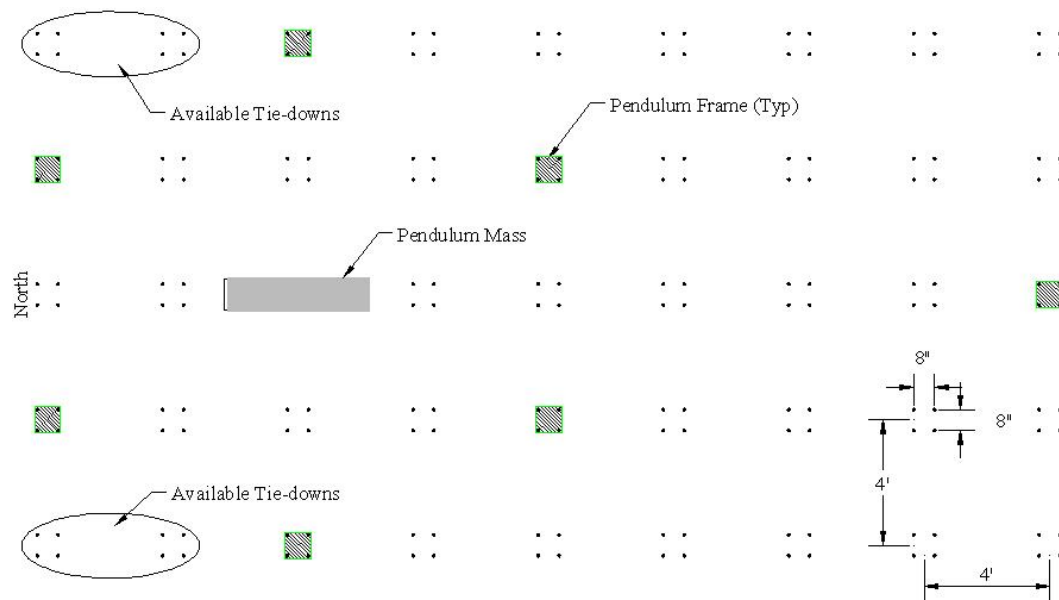


**Fig. 4-4: Plan view of the laboratory's tie-down floor (pendulum area only).**

## 4.3 BUTTRESSES

### 4.3.1 Design and construction

Once the available clusters of bolts were identified, the design for the buttresses could be started. During the initial stages of the buttress design, the dimensions and capacities of the specimens were already known, but the load that was going to be induced by the pendulum was still unknown. Computation of the impact load depends upon several factors including the stiffness of the supports, the energy absorbed at impact, and the time of contact between the pendulum mass and the beam. Thus, a convenient means of determining the impact force and its variation with time is through experimentation. Because of the initial uncertainties associated with the load imparted to the test beam by the pendulum, the A-frames had to be designed as conservatively as possible. While doing the pre-design, it was decided that before purchasing any material to build the A-

frames, special consideration had to be given to the scrap material from previous projects available at Ferguson Structural Laboratory. Therefore, a survey of the scrap yard was performed, and some W-shapes, angles, and plates were selected based on their dimensions and conditions.

As mentioned previously, the design process for the A-frames was iterative, and several models were developed, compared, and abandoned. The comparison was mainly based on constructability, capacity to resist load, and the frame's ability to distribute forces to the tie-down floor. By this point, it is already known that the maximum static capacity of the beam, if loaded in the direction of the gravity, is of 12.5 kips. However, the loading will be done in the opposite direction for this project, which means that the load is smaller than this value (5.2 kips in the case of the prestressed beam). This load, however, could not be used to design the buttresses because other types of beams with different capacities might be tested in the future using the same setup. It was also known from tests performed by Mitchell (Mitchell, 2005) that the maximum acceleration registered when testing concrete barriers was approximately 25-g ( $805 \text{ ft/sec}^2$ ). If multiplied by the mass of the pendulum ( $58.4 \text{ lbs-sec}^2/\text{ft}$ ), a force of 47 kips is obtained. This force could not be used either because, when testing barriers, a crushable package that absorbed some energy was used. So an 80-kip force was selected because it was thought to be conservative when compared to the capacity of the beam and to the forces produced by the pendulum on previous tests. If the designed model was not able to resist an 80 kip force, it was discarded. In order to compare the distribution of forces, the same 80 kip load was applied to all models at the location where the beam was going to make contact with the buttress, and then the buttress reactions were calculated. Figure 4-5 shows the reactions produced by the applied load on the selected model.

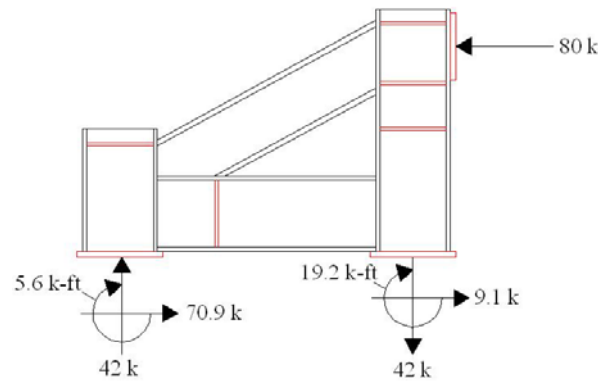


**Fig. 4-5: Reactions produced on A-frame due to 80-kip load.**

The front part of the support, which will be referred to as the nose, will hold the beam at a specific height and also prevent it from bouncing out of position after the initial impact. The dimensions of this part of the support played a big role in the design. This section could not be too long because it would hit the cables that hold down the pendulum frame, but it could not be too small because it would not be strong enough. Most of the design was based on geometry and the sections available at the scrap yard, and then it was checked by applying half of the load for which the A-frame was designed for acting as a rebound force. A 0.65 kip load was also applied to the design to account for half of the weight of the specimen. Figure 4-6 shows the reactions produced by these forces on the selected model. These same reactions were then applied with opposite magnitude to the buttress to verify the performance, which demonstrated the ability of the selected buttress to carry the maximum anticipated loads.

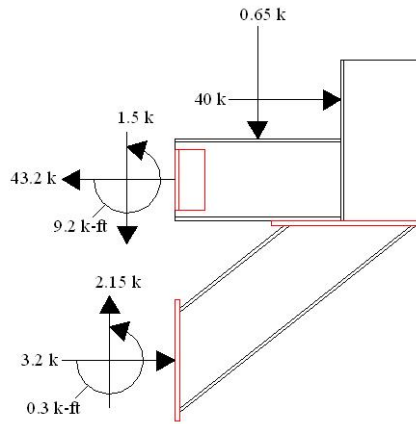


**Fig. 4-6: Reactions produced on nose of support due to the specimen's self-weight and a 40-kip rebound load.**

After obtaining the reactions and checking that the bolts to be used would not fail, 1/2-in stiffeners were added to those areas that might buckle due to the impact force. Figure 4-7 shows the final drawing for the A-frame and nose selected. More detailed information on the buttress design can be found in Appendix B. Once the design was put together, the fabrication process could begin (Figure 4-8).

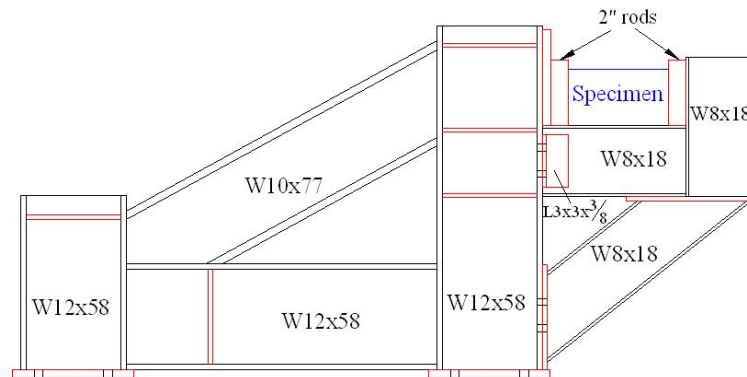


**Fig. 4-7: Final drawing for A-frames and nose (for more details refer to Appendix B).**





(a)



(b)

***Fig. 4-8: Welding of (a) A-frame, (b) nose of A-frame.***

Finally, with the two supports welded together and painted, the test setup could be assembled in the pendulum area. Each buttress was anchored to the tie-down floor using eight 1-in threaded rods (ASTM A320/A193) with a tensile stress capacity of 105 ksi. Figures 4-9 and 4-10 show a plan drawing and a picture, respectively, of the test setup configuration with a reinforced concrete beam in place.

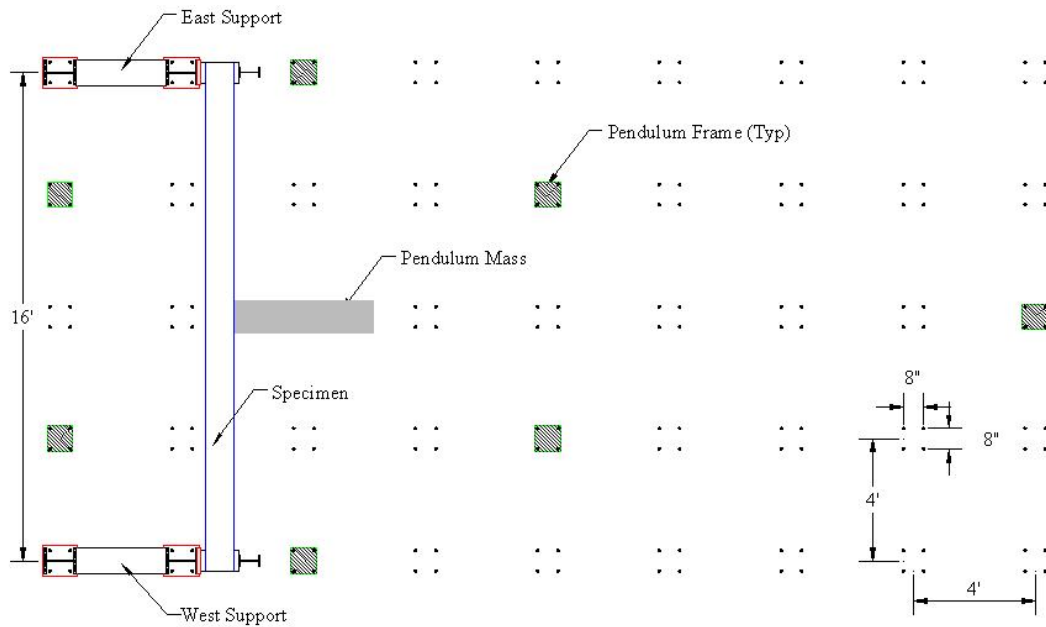


**Fig. 4-9: Plan view of test setup.**



**Fig. 4-10: Test setup for first specimen.**

#### **4.3.1 Modifications to Buttresses**

The first modification occurred before testing the first specimen. As shown previously, the nose of the A-frames has rods that hold the beam in place.

The distance between these rods was fixed to 11.5 in, which is the depth of the specimens to be tested. However, after setting the beam in place, it was clear that there was going to be localized crushing of the concrete during an impact test due to the concentration of forces in one small location (Figure 4-11). Therefore, it was decided to insert several ½-in steel plates between the rod and the beam to increase the bearing area. In order to make this adjustment, the nose had to be separated 1 in from the A-frame. To accomplish this, some spacers were fabricated out of 1-in thick steel plates and were placed between the nose and the A-frame (Figure 4-12).

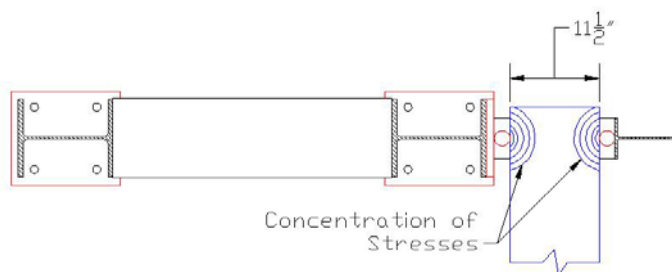


**Fig. 4-11: Concentration of stresses due to conditions of supports (plan view).**

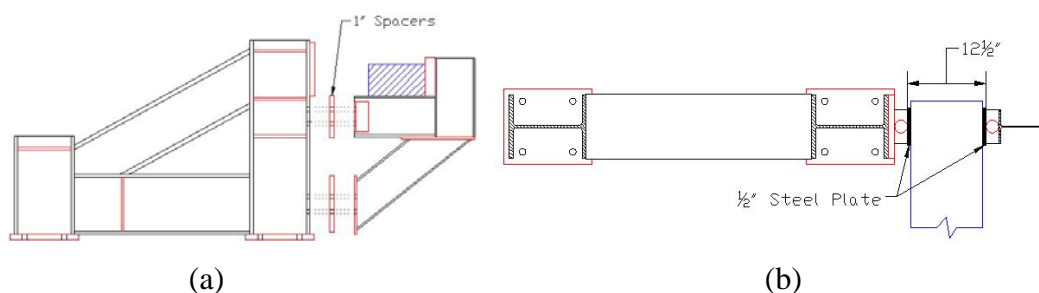


**Fig. 4-12: (a) 1-in spacers between nose and A-frame (b) ½-in plates between rods and beam (plan view).**

After performing the first test, the results indicated that the nose of the support was not acting entirely as a simple support, but it also induced some

moment restraint to the specimen. This restraint occurred because the rotation of the specimen was very large, and the space in between the rods was 12.5 in, which is exactly the depth of the beam plus the two ½-in plates. Thus, when the beam deformed there was not adequate space to allow the beam to rotate without the nose providing some restraint. The moment restriction not only caused some minor damage to the nose of the supports, but there were also some effects on the specimen that will be discussed in the next chapter. The first measure taken to correct the support conditions was to remove one of the rods in order to have a gap of 2.5 in between the specimen and the front of the nose. At first, it was thought that leaving this gap would allow the specimen to bounce or vibrate after the initial impact, but after witnessing the first test, this possibility was ruled out. The second measure taken was to strengthen the support by adding stiffeners to the angles used to bolt the nose to the rest of the A-frame. Figure 4-13 shows the modifications done to the support after the first test.

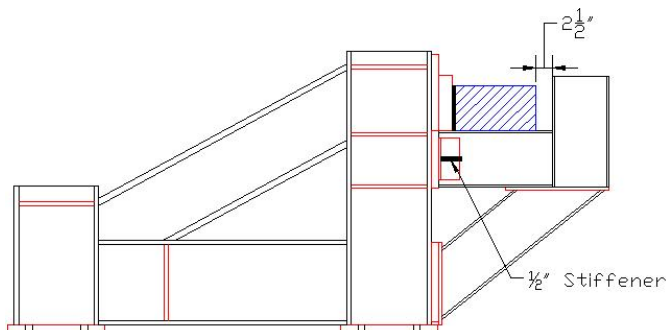


**Fig. 4-13: Modifications to the supports after the first test.**

Once the modifications were implemented, a second specimen was tested. Results from this test showed that no damage occurred to either the supports or the specimen ends. However, the supports still required some modifications in order to be able to add load cells to each of them. The first modification for adding a load cell consisted of removing the remaining rod and adding a ½-in

steel plate with tapped holes to the front part of the A-frame so the load cell could be bolted securely to the support. The second modification consisted of increasing the space where the beam is situated to be able to add a 100-kip load cell and still maintain the required gap to allow for free rotation of the specimen. In order to make this change, part of the front of the nose had to be removed (using a torch). The third measure was to add a stopper to prevent the beam from striking the load cell after the initial impact. This modification was done by welding a 1-in thick steel plate to the front part of the A-frame. The length of this plate was calculated based on allowing the beam to rotate  $12.8^\circ$  which is equivalent to a midspan deflection of 21.5-in. This rotation was the result of using the smallest possible stopper, which was 4 in in length. Anything smaller than 4 in would not protect the load cell, and anything bigger would limit the maximum allowable rotation.

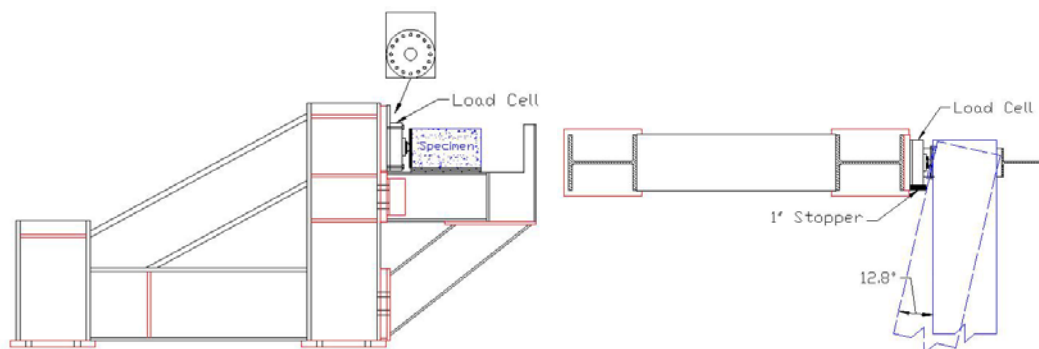


**Fig. 4-14: Modifications to the supports after the second test.**

## 4.4 INSTRUMENTATION OF SPECIMEN

### 4.4.1 External

The external instrumentation includes all measuring devices that are outside the beam. There were four different types of external instruments used to obtain data from the tests performed: linear variable differential transducers

(LVDTs), string potentiometers, accelerometers, and load cells. Similar to the rest of the test setup, selection of the instrumentation was an iterative process, and there were some changes in the instrumentation used over the course of the project in order to enhance the quality of the data collected.

The same instrumentation was used for the first two tests: two LVDTs located behind the supports to measure any possible movement of the buttresses, two LVDTs at the quarter points of the beam, two string potentiometers at midspan to measure deflections, and two accelerometers attached to the pendulum mass, one with a capacity of 100 g and the other with a capacity of 250 g. Figure 4-15 shows a drawing of the test setup with the location of the instrumentation used for the first two tests.

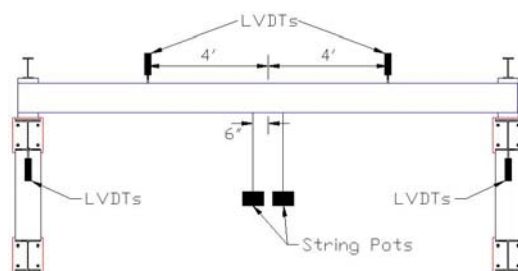


**Fig. 4-15: Location of LVDTs and string pots for the first two tests.**

After the first two tests were performed, it was decided to make some modifications to the instrumentation used. Changes were necessary because, after interpreting the data, it was seen that two of the LVDTs were not registering any useful data. Also, there were some doubts about the accelerometers working properly. These two issues will be discussed in more detail in the following chapter.

As a result, the LVDTs located at the quarter points of the beam were eliminated, and load cells were added to the test setup. Originally, only two load cells, each with a capacity of 100-kips, were going to be used, one at each

support. Later, it was decided to add a 200-kip load cell in front of the mass of the pendulum. Figure 4-16 shows the three load cells employed in the test setup.

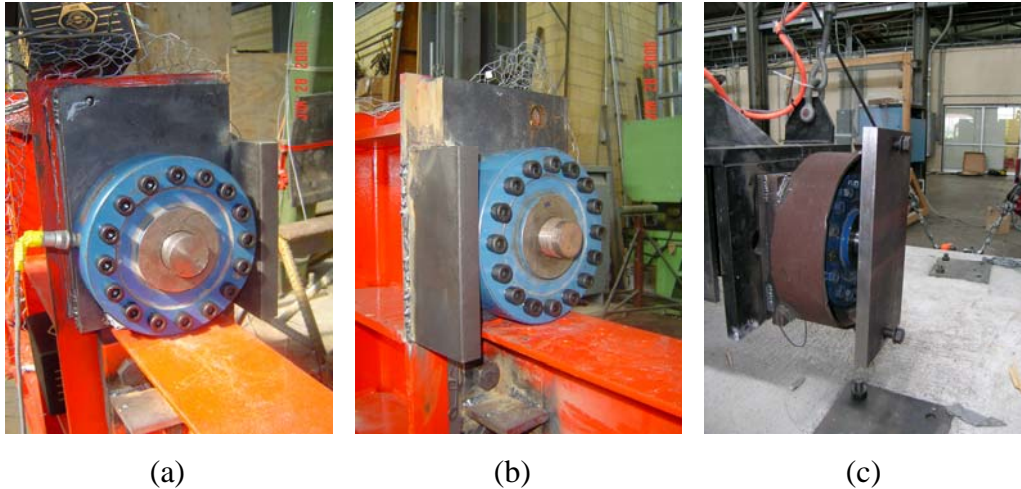


**Fig. 4-16: Load cell on: (a) west support (b) east support (c) front of pendulum.**

After having installed all the instrumentation, a test was performed with the laminated wood beam to evaluate the behavior of the load cells under impact loading. Figure 4-17 shows the location of the instrumentation used for this final test. In this case, the performance of the instrumentation worked in a satisfactory way, but as it will be explained in more detail in the following chapter, this beam was not loaded with the same magnitude as the concrete ones.

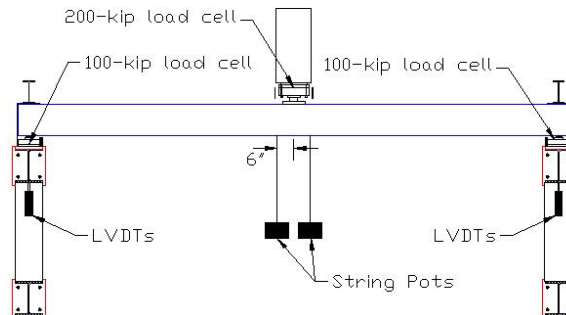


**Fig. 4-17: Location of LVDTs, string pots and load cells for the third tests.**

#### ***4.4.2 Internal***

The instrumentation inside the beam will be referred to as internal instrumentation. For the case of the reinforced concrete beams, there was no internal instrumentation used because the purpose of these beams was to make sure that the supports, impact pendulum, and external instrumentation behaved as expected. Conversely, 36 strain gauges were installed within each prestressed concrete beam. These strain gauges were placed on the strands, longitudinal rebar, and stirrups at different locations along the length of the beam. Figure 4-18 shows a section of the beam that has strain gauges on all types of reinforcement. The exact location of each can be found on a drawing presented in appendix B.



***Fig. 4-18: Strain gauges on reinforcing steel and prestressing strand.***



## **CHAPTER 5**

### **Test Results**

#### **5.1 INTRODUCTION**

The results obtained from each test performed are addressed in this chapter, and the behavior of some of the equipment used is also presented. In total, three tests were performed; for the first two tests, reinforced concrete beams were tested to failure by raising the pendulum mass to a specific drop height. For the third test, a laminated lumber beam was used to perform a series of tests using different drop heights until failure of the specimen occurred.

#### **5.2 TEST 1 – REINFORCED CONCRETE BEAM**

The first specimen tested was a reinforced concrete beam. The main purpose of this test was to verify that all the instrumentation worked properly and that the supports behaved in an adequate manner. Because this was the first test of its kind with the impact test pendulum, there was some concern about damaging the pendulum mass due to a direct impact with the beam. As a result, a 2-in neoprene pad was bonded to the beam using a high-strength epoxy (Figure 5.1). This problem did not exist when using the pendulum to test concrete barriers because a crush package that absorbed some of the energy before the impact was welded to the pendulum mass. The drop height used for testing the reinforced concrete beam was 15 ft with respect to the ground; this height is equivalent to 12 ft with respect to the pendulum mass.



*Fig. 5-1: Neoprene pad bonded to beam; straps are only used while epoxy sets.*

After performing the test, there were many significant observations. The neoprene pad served its purpose, and the pendulum mass suffered no damage. In addition, the neoprene pad fell after the initial impact without any damage and could be easily reused. An important limitation of this test was that there was not much information obtained regarding the instrumentation used because the data acquisition system was set to a sampling rate of 500 cycles per second (Hz), instead of 5000 Hz, which is the rate typically used when testing with the pendulum. Using a high sampling rate ensures that there will be enough data points collected during the short duration of the impact of the pendulum, which only lasts approximately 0.05 seconds. Even with the small amount of data obtained from the LVDTs at the supports, it was clear that the support displacement (Figure 5-2) was insignificant compared to the amount of displacement occurring at midspan. It is difficult to know the exact displacement that occurred at midspan because the pendulum not only failed the beam, but it also pushed it until it fell from the supports. However, by inspecting the video recorded from the overhead traveling crane, it is possible to make a rough

estimate of the magnitude. Figure 5-3 shows four frames obtained from the video of the test. The large black and white rectangles each measure 4 in, and the small ones measure 2 in. Based on this scale, it can be determined that the midspan deflection was larger than 28 in.

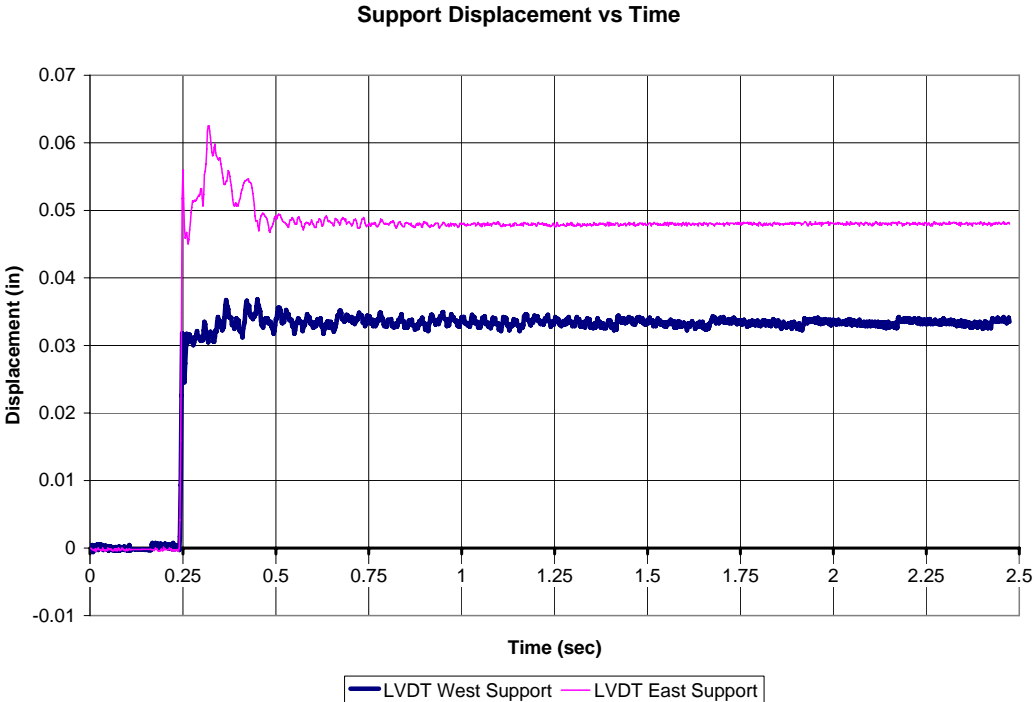


*Fig. 5-2: Support displacement obtained from the first test performed.*

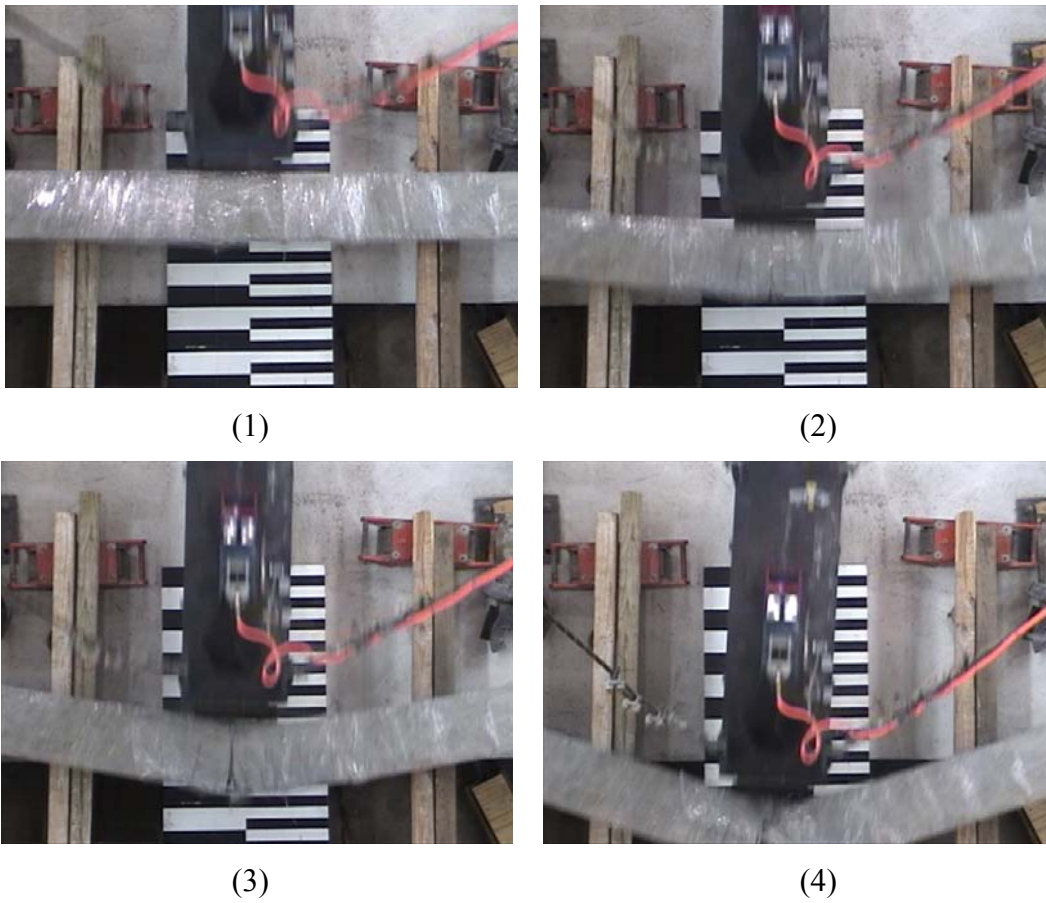


***Fig. 5-3: Video frames recorded from the overhead traveling crane.***

Although the A-frame supports performed well, the nose of the supports restricted rotation at the ends of the beam, and some minor damage occurred to the nose of the east support. As mentioned in the previous chapter, this problem was corrected by removing a roller, but the specimen also suffered a local failure at one of the ends (Figure 5-4), which required another modification.

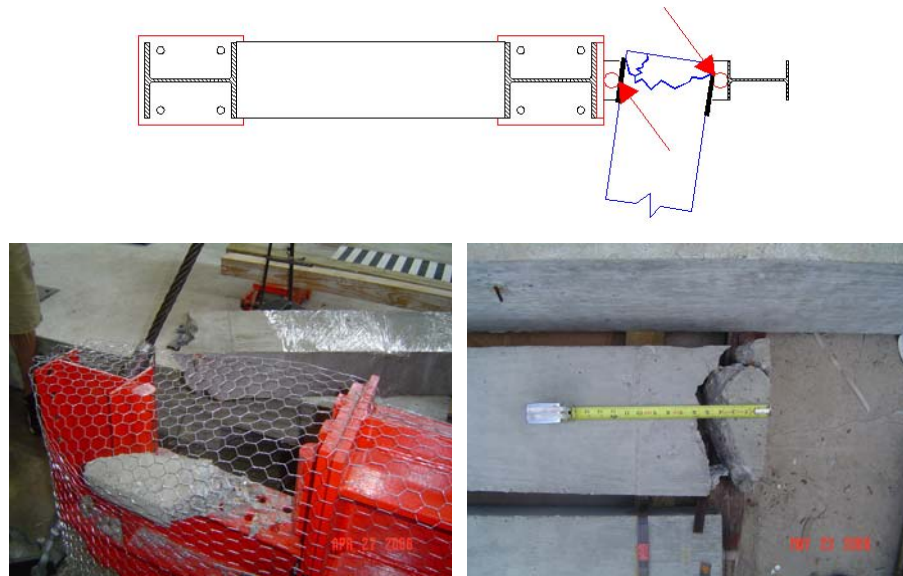


***Fig. 5-4: Local damage to east end of the beam.***

To prevent local failure at the ends, additional steel was included in the second reinforced concrete specimen as mentioned previously in Chapter 3. Because it was unknown if the additional steel was going to be sufficient to prevent failure at the ends, it was decided to add external reinforcement. Several options were considered, but most of them involved the purchase of material and adequate construction time. One of the options included the use of Fiber Reinforced Polymer (FRP), which is an expensive material. However, Ferguson Laboratory had adequate supplies in stock that were available for use. In addition, FRP can be easily installed in a short period of time. Therefore, it was decided to use this material on the next specimen to evaluate its behavior. As can be seen from Figure 5-5, two layers of FRP were used; the bottom layer wrapped the beam 10 inches in the longitudinal direction, and the top layer wrapped the beam 10 inches in the transverse direction.

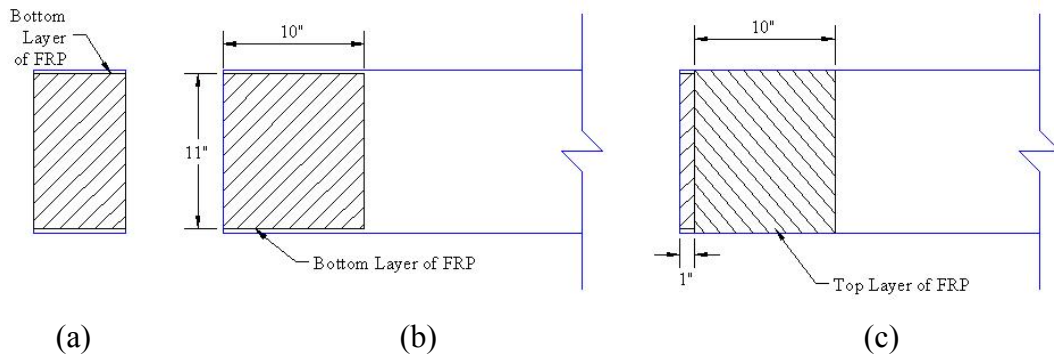


**Fig. 5-5: (a) Bottom layer of FRP cross section view. (b) Bottom layer of FRP longitudinal view. (c) Top layer of FRP longitudinal view.**

### **5.3 TEST 2 – REINFORCED CONCRETE BEAM WITH FRP AT ENDS**

The second specimen tested was also a reinforced concrete beam. This specimen was reinforced at the ends with FRP as shown in Figure 5-6. The purpose of this test was to verify that the modifications to the supports eliminated the moment restraint observed during the first test, that the FRP installed would prevent local failure at the ends, and that the instrumentation used worked properly since on the first test this could not be verified due to the small sampling rate used. The drop height used for this test was also 15 ft with respect to the ground.



***Fig. 5-6: Placing of FRP fibers on reinforced concrete beam.***

The modifications to the support and the FRP added at the beam ends eliminated the problems encountered on the first test regarding the ends. Therefore, it was decided to install FRP on the two prestressed beams, which were previously fabricated but not yet tested.

On this occasion, enough data points were obtained from the data acquisition system, and most instruments provided some useful information. The LVDTs located on the supports indicated that there were insignificant support displacements. Therefore, the displacement registered on the previous test can be interpreted as the settling of the supports after which there will be no additional considerable movement. The string potentiometers located at midspan registered the data used to obtain the chart presented in Figure 5-7. The difference in the initial condition is due to the fact that the string potentiometer on the west side has a 15-in run and was initially extended about 11.5 in while the one on the east has a maximum capacity of 10 in and was extended approximately 9.75 in. After the impact, the string potentiometer cables reeled back all the way to zero

displacement. However, the accuracy of the midspan displacement information was unknown because it could be possible that the beam moved faster than the spring in the string potentiometer rewinding the cable. It would have been ideal to compare this measured displacement with the one from the quarter points, but for unknown reasons, the LVDTs at these locations did not register any data.

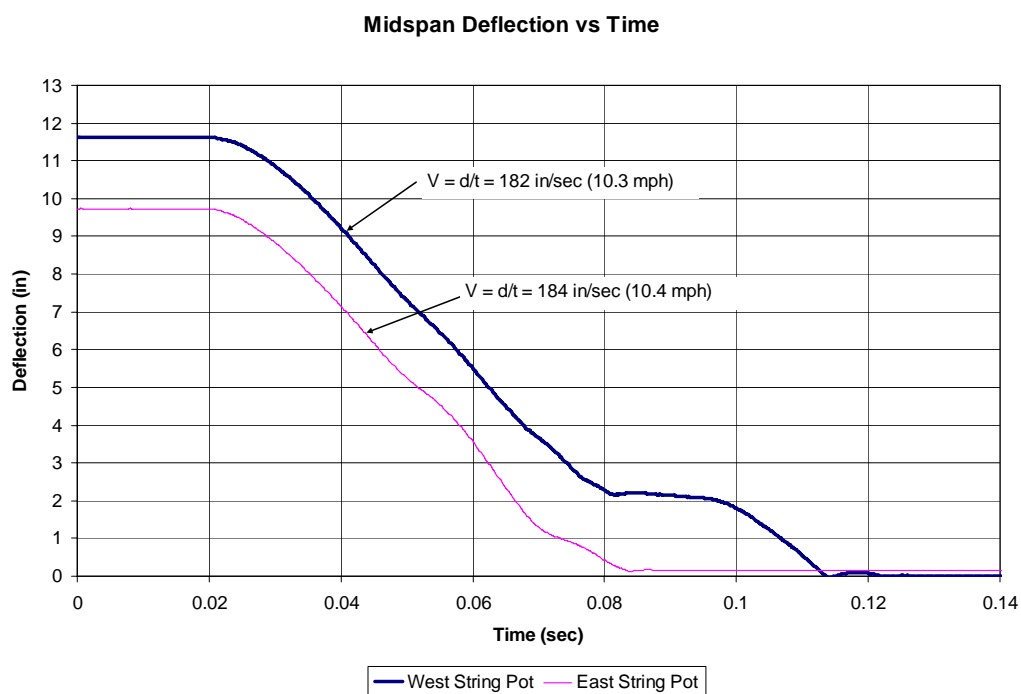
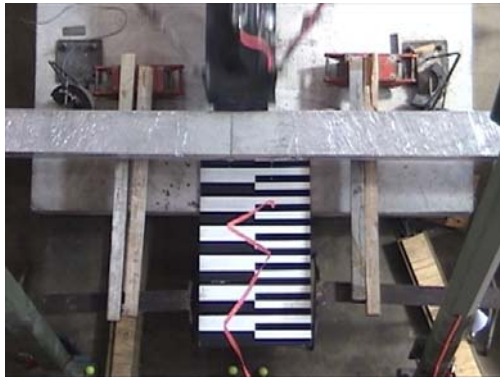


***Fig. 5-7: Midspan deflection registered by string potentiometers.***

Once again, it was concluded that the exact midspan displacement could not be determined with the instrumentation used. It can only be concluded that it is known to be several feet in magnitude. Figure 5-8 shows six frames obtained from a recorded video from the overhead traveling crane during the impact.





(1)



(2)



(3)



(4)



(5)



(6)

***Fig. 5-8: Frames from video recorded from the overhead traveling crane.***

The two accelerometers located behind the pendulum mass provided useful data. The raw data is presented in the chart shown in Figure 5-9. The figure shows that accelerometer B, with a maximum capacity of 100 g, is saturating or exceeding its capacity, and accelerometer A, with a 250 g capacity, performs much better. However, because the pendulum mass is constructed from steel plates, it vibrates after the initial impact, and the accelerometers record this vibration, which is sometimes referred to as “ringing”. To eliminate most of this ringing, a low-pass filter designed by Geoffrey T. Mitchell (Mitchell, 2005) was used to filter the data obtained from the second test. Figure 5-10 shows a filtered acceleration profile using only the data of accelerometer A because the data obtained from accelerometer B was inaccurate.

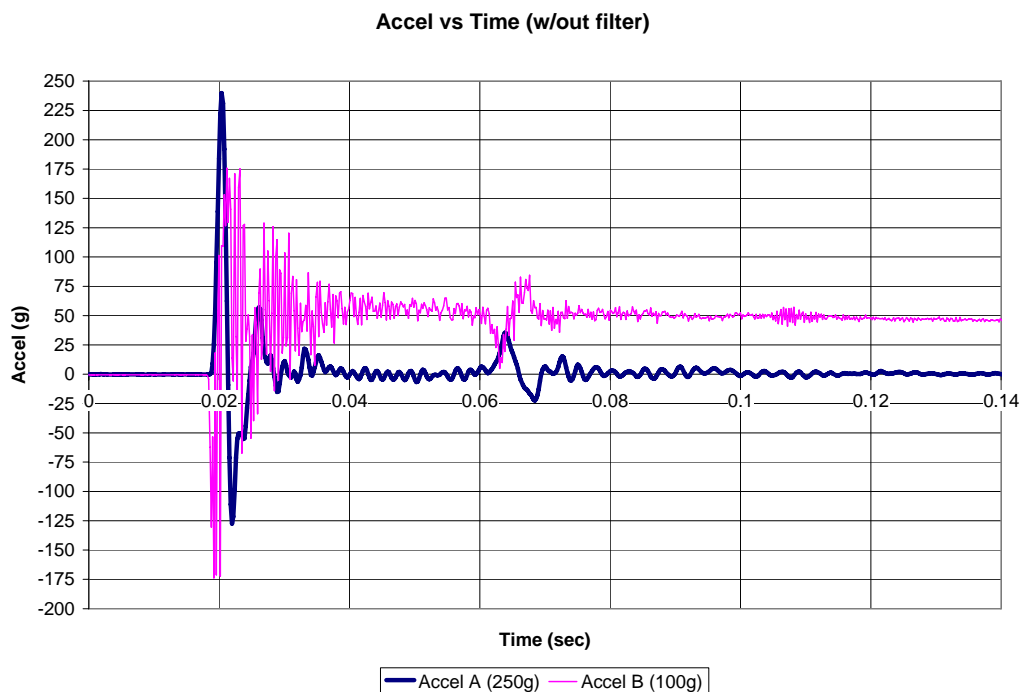


***Fig. 5-9: Unfiltered acceleration profile.***

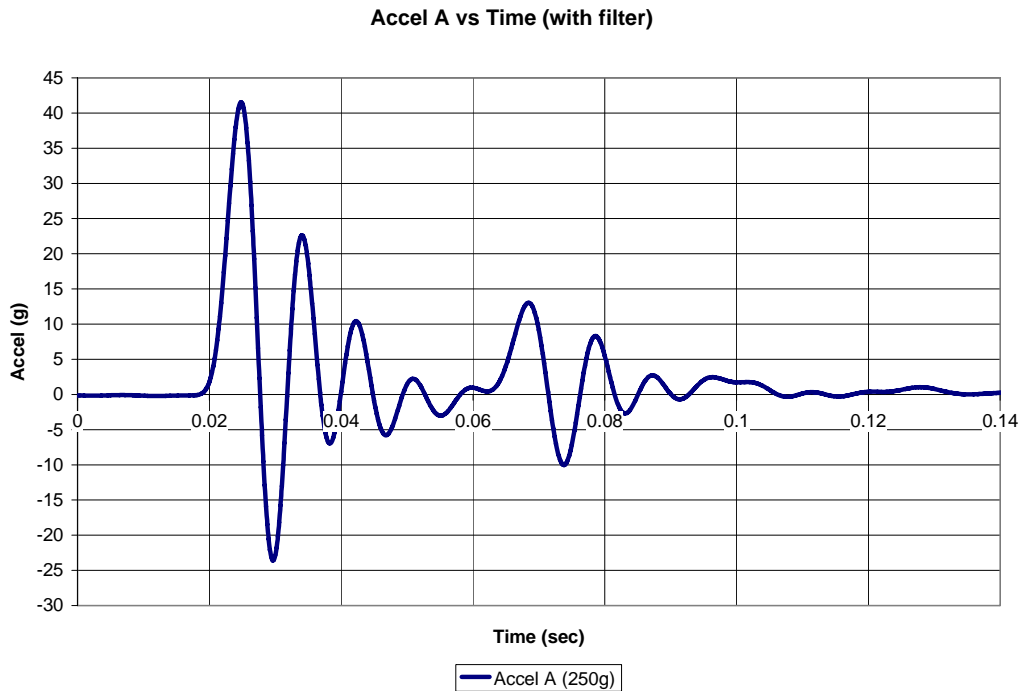


***Fig. 5-10: Filtered acceleration profile.***

The main purpose for registering the acceleration of the pendulum was to be able to obtain a force from the acceleration profile. This approach had not been used previously when analyzing the data from the accelerometer for the barrier tests. The acceleration data obtained for the barrier project was used to validate the impact test pendulum by comparing acceleration histories from the pendulum and actual crash tests (Mitchell, 2005). To obtain the force, the curve shown in Figure 5-10 is converted to units of acceleration by multiplying each value by the acceleration of gravity ( $32.2 \text{ ft/sec}^2$ ), and the new curve is then multiplied by the mass of the pendulum ( $58.5 \text{ lbs-sec}^2/\text{ft}$ ). The resulting curve gives force versus time. If the area under the curve of the force versus time graph is calculated, the impulse is obtained. If the impulse is then divided by the duration of the impact ( $\Delta t$ ), a force in pounds can be calculated. However, it was realized that the

duration of the impact could not be determined by simply analyzing the acceleration profile.

Although most of the information obtained from the instrumentation was useful, there were doubts regarding the accuracy of the data obtained from the string potentiometers. Also, the time of contact between the pendulum mass and the specimen was still unknown, and the load could not be easily determined from the acceleration data. To solve the displacement issues, it was decided that a high-speed camera should be used. The camera employed for the first two tests can record approximately 30 frames per second (fps), and a typical high-speed camera can easily record 1,000 fps. By recording this many fps, super slow-motion playback can be achieved, which would allow the measuring of displacements to be obtained visually. However, the use of a high-speed camera implied a high cost and could not be obtained for this project in the time frame available. To obtain the load, it was decided to employ load cells, one at each support and one in front of the pendulum. It is important to point out that adding a load cell to the front of pendulum increased the weight of the pendulum by 165 pounds.

#### **5.4 TEST 3 – LAMINATED LUMBER BEAM**

The purpose of the third test was to evaluate the behavior of the load cells installed in front of the pendulum mass and at the supports. In order to carry out this evaluation, a laminated lumber beam was employed, and the pendulum mass was lifted to different drop heights. In total, four tests were performed — two with a 6-in drop height, one with a 12-in drop height, and one with a 18-in drop height. At the 18-in drop height, the laminated lumber beam partially failed.

### 5.4.1 Laminated lumber beam – 6-in drop height

For the first test performed with the laminated lumber beam, a 6-in drop height with respect to the pendulum mass was used. The load profile registered from the load cells is shown in Figure 5-11. In this chart, the loads from the two load cells at each support are added together and compared with data obtained from the load cell in front of the pendulum mass. The maximum load registered for the sum of the reactions was 17.03 kips, and the maximum load obtained from the load cell located in front of the pendulum was 17 kips. These loads, however, were out of phase by 0.0052 seconds with respect to each other. This might be a small fraction of time, but at a sampling rate of 5000 Hz, 26 channels can be read in 0.0052 secs.

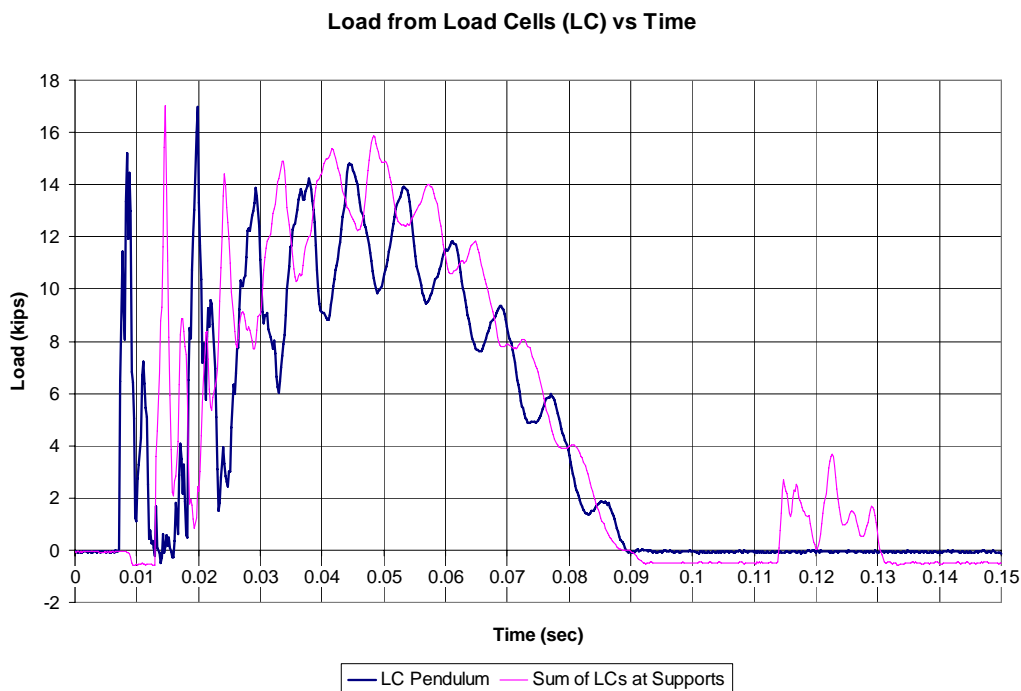


**Fig. 5-11: Load profile obtained from load cells (LC) at supports and front of pendulum mass.**

The acceleration obtained from the 250-g accelerometer was filtered and then multiplied by the new mass of the pendulum ( $63.6 \text{ lbs-sec}^2/\text{ft}$ ) to obtain a force profile. Figure 5-12 shows a comparison between the force obtained from the acceleration profile and the one obtained from the load cell in front of the pendulum. It can be seen that a similar behavior is obtained from the load cells and the accelerometer, but the magnitudes differ along the entire duration of the impact, especially at the beginning. An explanation for the differences in magnitudes could be that the load cell had a steel plate in front of the load button for protection purposes. The plate impacted the load button with the initial impact, and this impact would cause an increase in the load registered by the load cell relative to the case in which the load were applied slowly without impact. However, since the mass of the plate ( $1.23 \text{ lbs-sec}^2/\text{ft}$ ) is a small percentage of the total mass of the pendulum, the increment in load that it may cause would be insignificant compared to the total load. A more reasonable explanation would be that the filter used for the acceleration data removed information corresponding to the impact and not only to the “ringing”. The filter works by eliminating high frequencies and allowing low frequencies to pass. Therefore, it is possible that the initial impact caused high frequencies similar to the ones produced by the “ringing” of the pendulum mass, and as a result, they were eliminated.

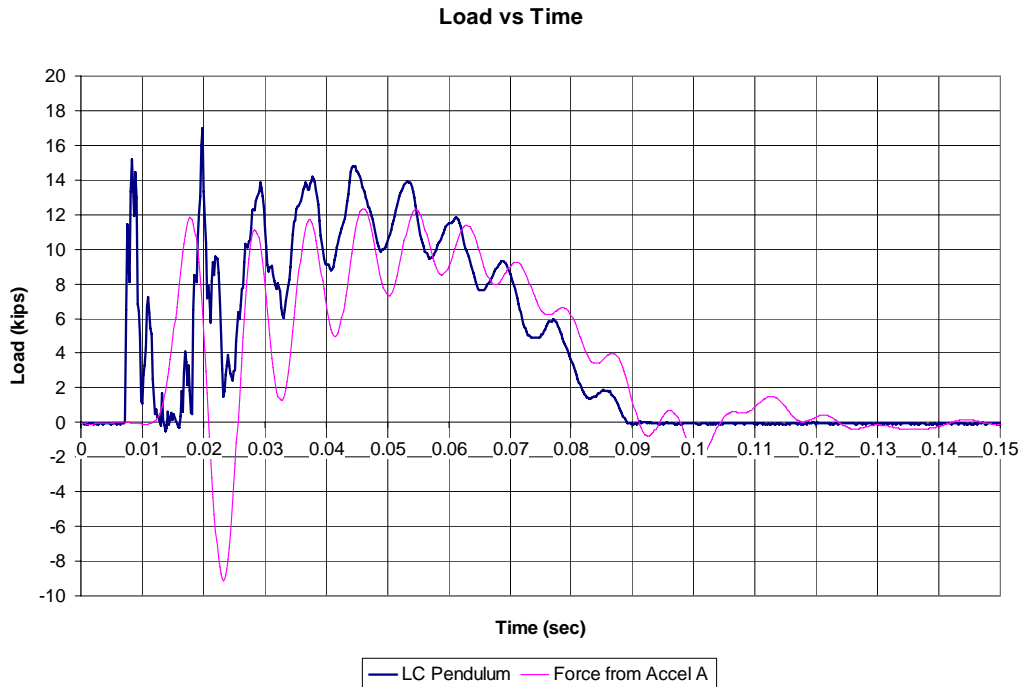


***Fig. 5-12: Load profile obtained from load cell (LC) in front of pendulum and from acceleration profile (6-in drop height).***

Useful information was also obtained from the string potentiometers. This information is presented in two charts. The first chart (Figure 5-13) shows the overall behavior of the beam during and after the impact. The second chart (Figure 5-14) shows only the initial impact. By analyzing the overall behavior of the laminated lumber beam, it can be seen that, after the initial impact, the midspan deflection vibrates back and forth along the zero axis until the movement damps out, ending up at zero deformation. Therefore, it was determined that the beam demonstrated elastic behavior.

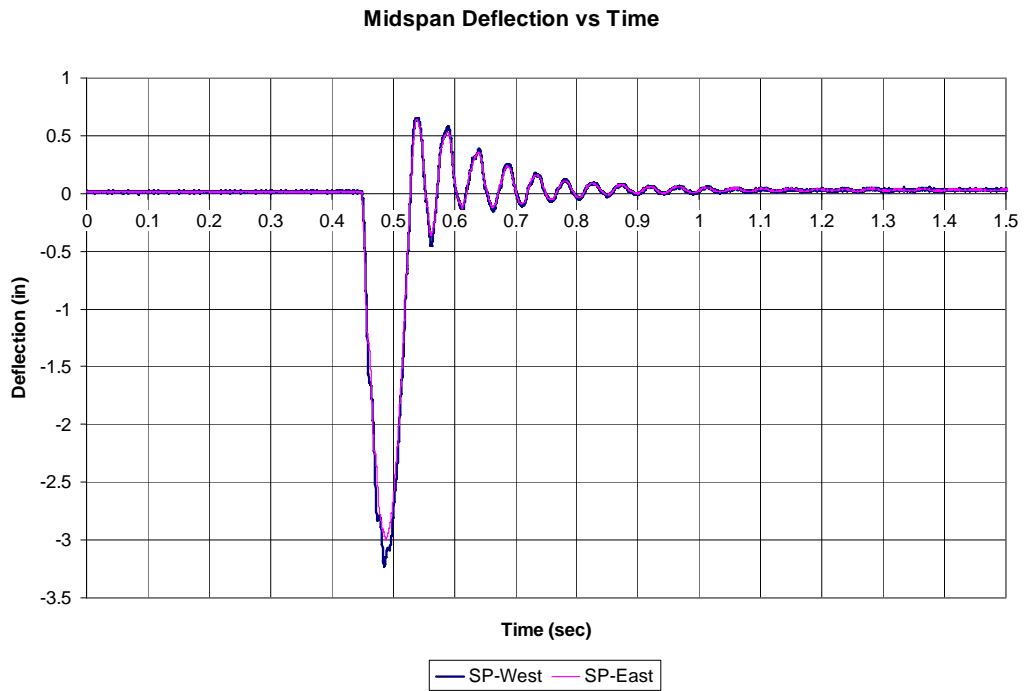


**Fig. 5-13: Midspan deflection measured using string potentiometers (SP).**

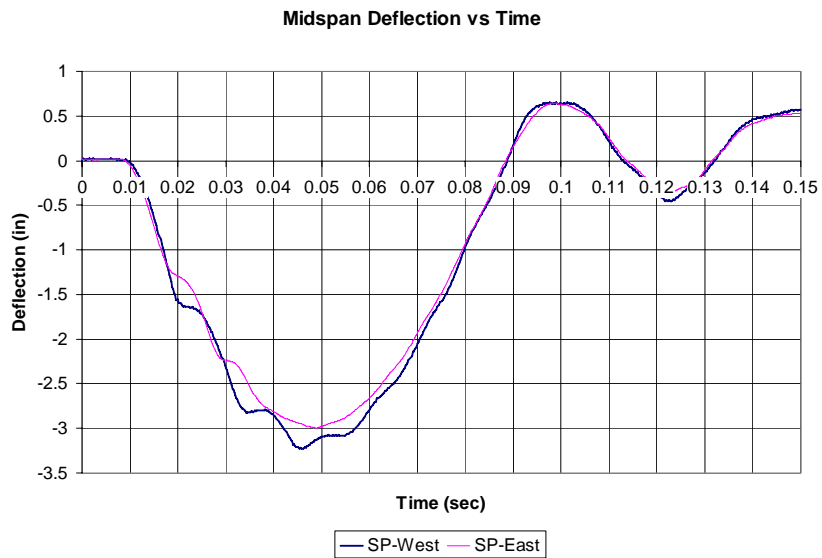


**Fig. 5-14: Midspan deflection during impact measured using string potentiometers (SP).**



#### 5.4.2 Laminated lumber beam – 6-in drop height

For the second test performed, a 6-in drop height with respect to the pendulum mass was used once again. The same drop height was used for this test in order to compare the results with the first test performed on the laminated lumber beam. The load profile from the load cells revealed the same behavior as that from the first test and shown in Figure 5-11. Figure 5-15 shows a comparison between the data obtained from the load cell in front of the pendulum in the first two tests. The difference obtained in maximum load between the two tests is 4.05% relative to the maximum value.

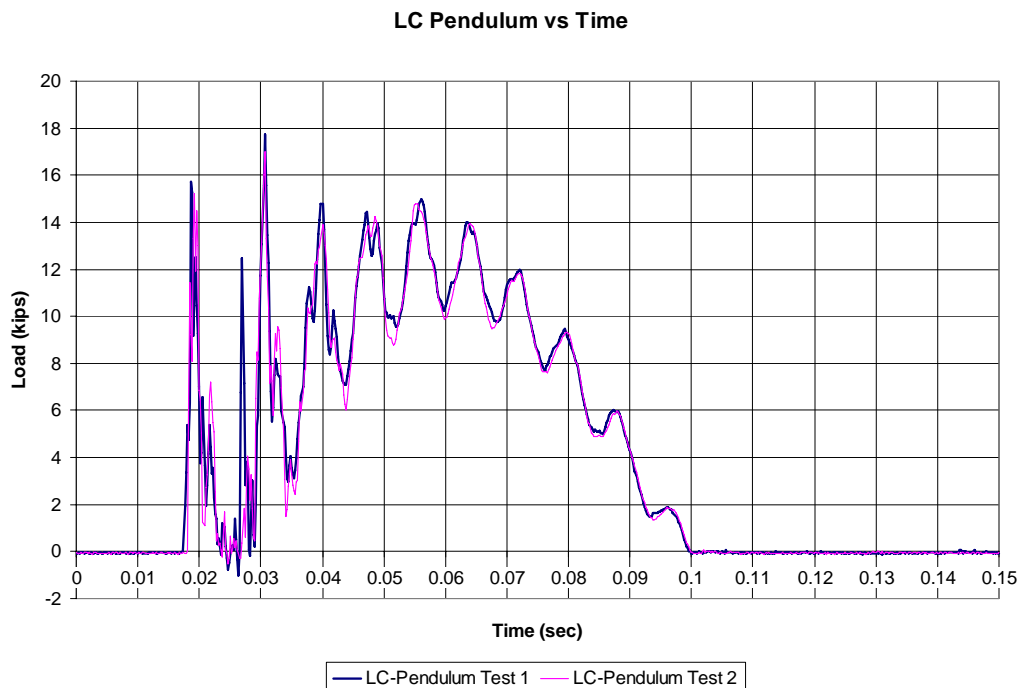


**Fig. 5-15: Load comparison between first two tests.**

The data registered by the 250-g accelerometer located on the pendulum mass was once again multiplied by the mass of the pendulum to obtain a force

profile of the impact. This force profile was then used to make a comparison with the data registered on the first test, which also used a drop height of 6 in. The similarity of the two tests is shown in Figure 5-16.

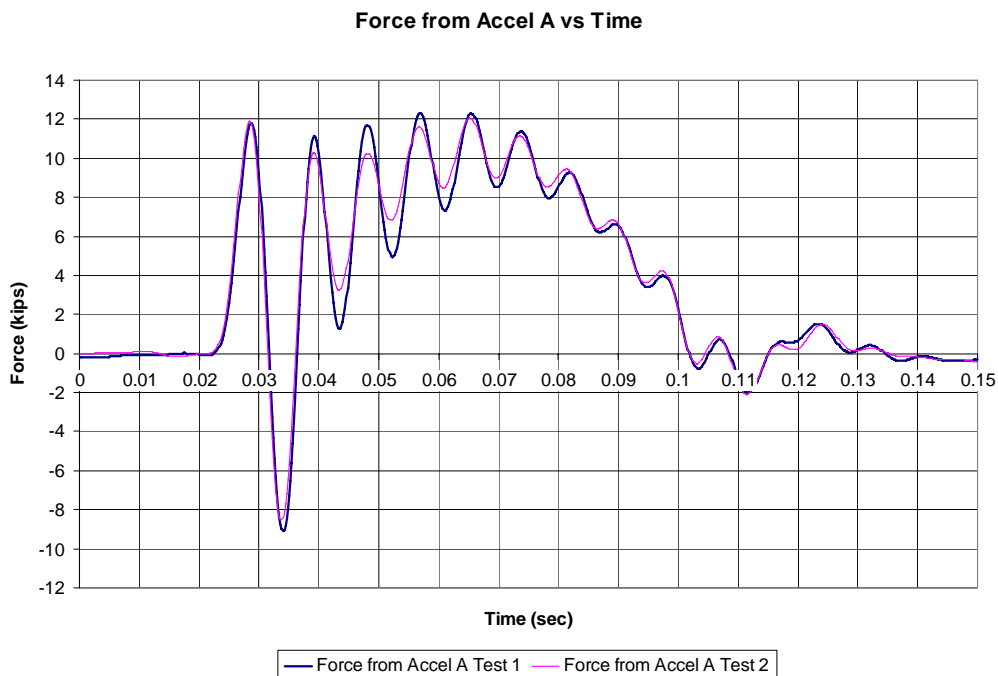


**Fig. 5-16: Force profile for first two tests obtained from acceleration data.**

The midspan deflections were the same for the second test as those obtained from the first test involving the laminated lumber beam. The specimen also behaved elastically for this test. Figure 5-17 shows two frames obtained from a video recorder during the testing of the specimen.



*Fig. 5-17: Frames from video recorded during impact (6-in drop height).*

#### **5.4.3 Laminated lumber beam – 12-in drop height**

For the third test performed on the laminated lumber beam, a 12-in drop height with respect to the pendulum mass was used. The maximum load registered by the load cell located in front of the pendulum mass was 31.15 kips. Figure 5-18 shows a comparison between load profiles obtained from the data registered by the load cell in front of the pendulum mass for the 6-in drop height test and the 12-in drop height. The maximum load recorded by the load cell in front of the pendulum mass for the second test (6-in drop height) was 17.72 kips. For the third test, the sum of the loads recorded by the load cells at the supports was 5.18 kips lower than the one obtained from the load cell on the pendulum mass. This difference is thought to be attributable to the contribution of inertial and damping effects in the dynamic equilibrium of the system. Hence, the load cell in front of the pendulum registers the load applied to the beam, and the load cells on the supports register the response of the beam. Therefore, the decision to only use the load data registered by the load cell on the pendulum mass was taken.

It was also observed that the maximum values registered by each of the three load cells occurred at different times. The load cell on the west support registered a maximum of 14.54 kips; then 0.0056 seconds later, the load cell in

front of the pendulum mass registered 31.15 kips. Finally, 0.0202 seconds afterward, the load cell on the east support registered a maximum of 11.43 kips. This difference might be attributed to the fact that the pendulum was not completely centered with respect to the beam. The pendulum mass was about 2.5 in off center.

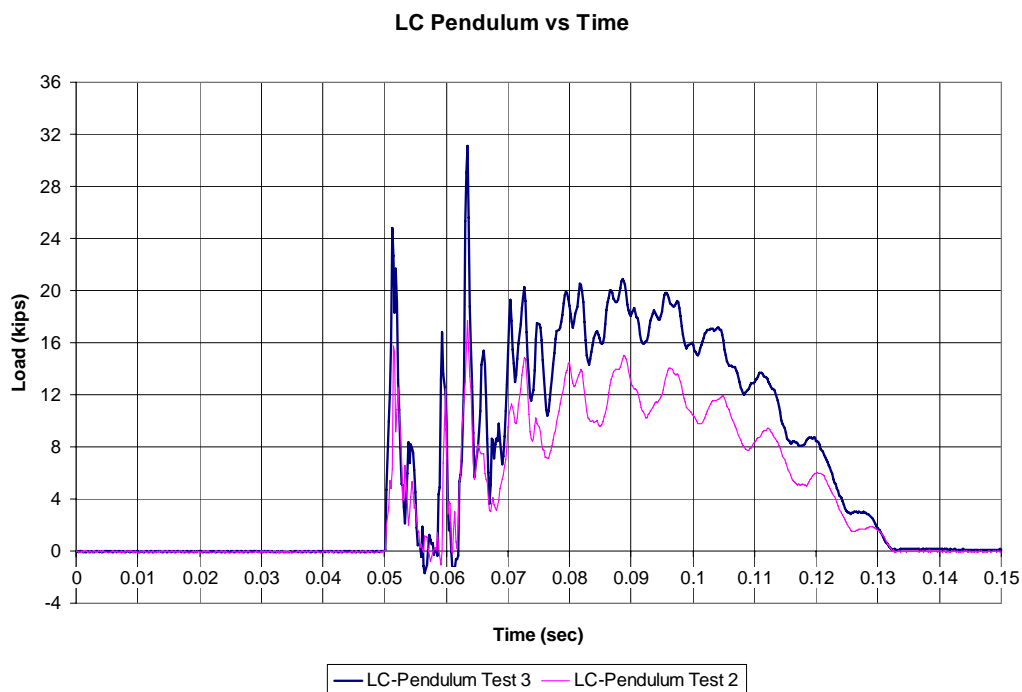


**Fig. 5-18: Load comparison between test 2 (6-in drop height) and test 3 (12-in drop height).**

The data from the accelerometers was once again used to obtain a force profile. Figure 5-19 shows the force obtained for test 2 with a 6-in drop height and for test 3 with a 12-in drop height. This graph has a similar form as the one presented in Figure 5-18, but the magnitudes of the loads are different. It would be desirable to calculate the area under the test 3 curve divided by the duration of

the impact to obtain a force of impact, but the duration of the impact is not known. As mentioned before, it can not be readily determined using the acceleration or load profiles.

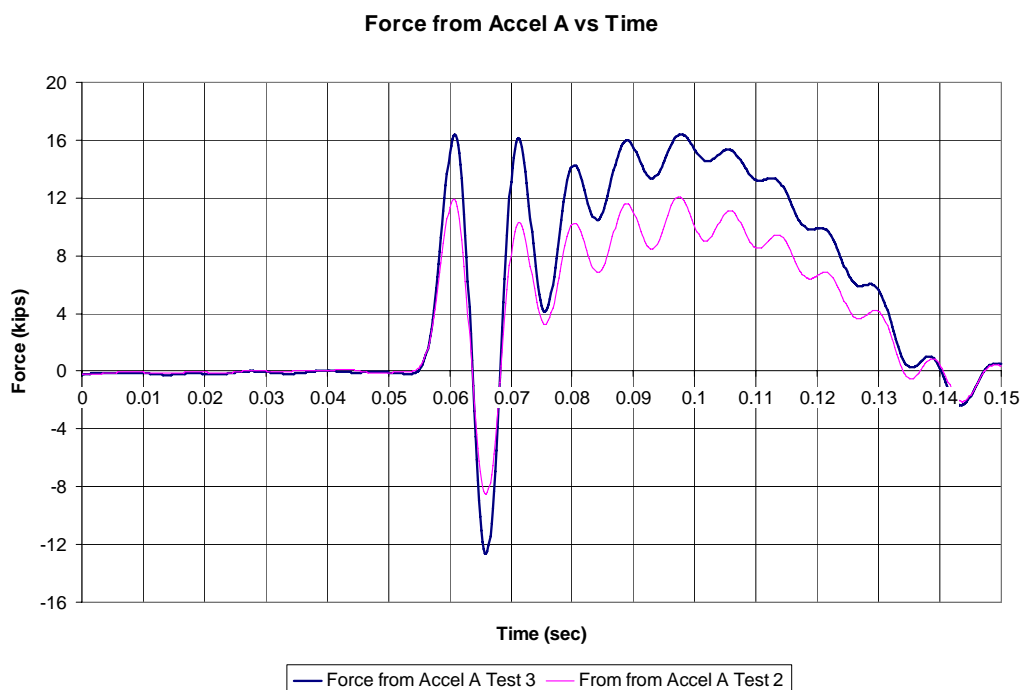


**Fig. 5-19: Force profile for test 2 (6-in drop height) and test 3 (12-in drop height).**

The behavior of the beam after the impact was very similar to that from the two previous tests. However, because the drop height was increased by 6 in, the displacements also increased. Nonetheless, the specimen remained in the elastic range. Figure 5-20 shows a graph with the midspan deflection recorded by the string potentiometers for a 6-in drop height and for a 12-in drop height. The two pictures presented in Figure 5-21 show the beam before the impact and during the impact for the 12-in drop height test.

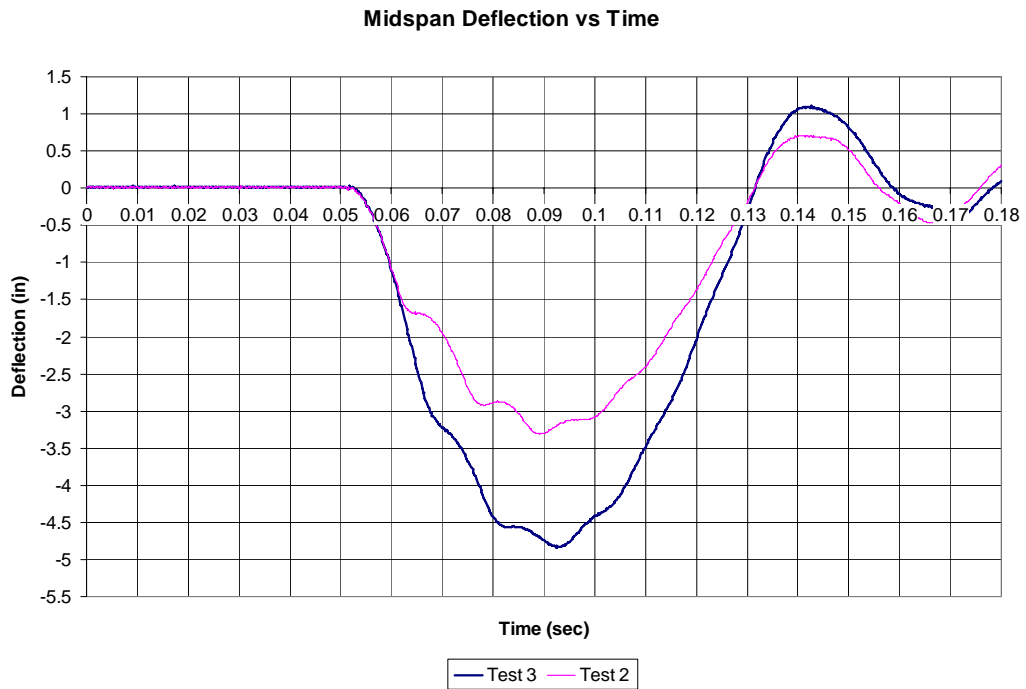


*Fig. 5-20: Midspan displacement for test 2 (6-in drop height) and test 3 (12-in drop height).*

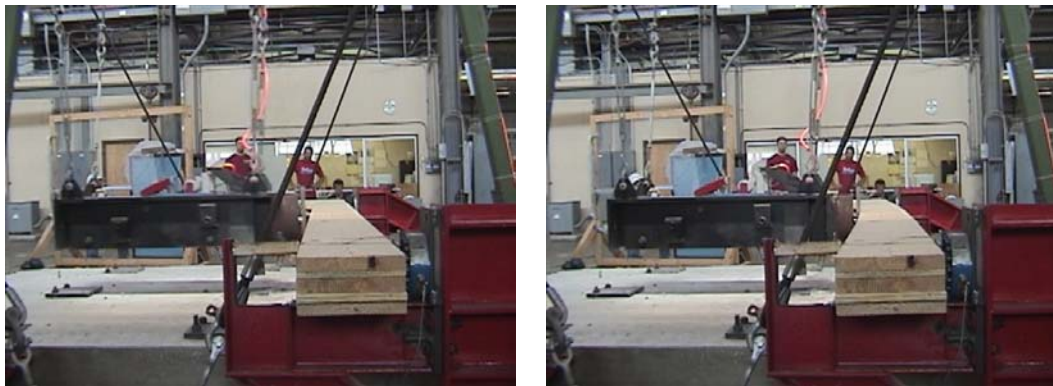


*Fig. 5-21: Frames from video recorded during impact (12-in drop height).*

#### 5.4.4 Laminated lumber beam – 18-in drop height

For the last test performed on the laminated lumber beam, the pendulum mass was raised to 18 in. This test was the last one performed because the impact caused partial failure of the beam, and, for safety reasons, it was decided not to perform another test with the same specimen. Figure 5-22 compares the loads recorded by the load cell on the pendulum mass for test 3 and test 4. The overall behavior is similar to the previous tests, but unlike before, the maximum load occurs at a different time. This result occurs because the beam fails after the initial impact. The same behavior as the previous test was obtained for the load cells on the supports; the sum of the two forces was 1.7 kips lower than that registered by the load cell on the pendulum mass. Reasons for this difference were previously addressed.

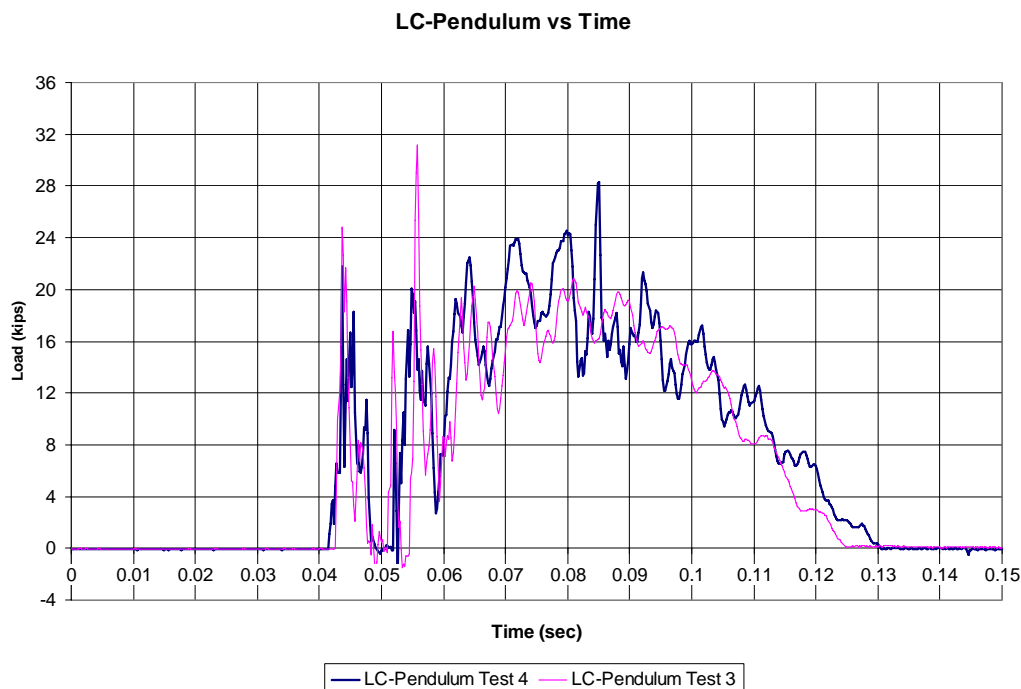


**Fig. 5-22: Load comparison between test 3 (12-in drop height) and test 4 (18-in drop height).**

Figure 5-23 shows the force profile obtained from the acceleration data for the three different drop heights used: 6 in, 12 in, and 18 in. Unlike the load profile presented in Figure 5-22, the maximum forces for the three tests are obtained at the same period of time, and, as expected, test 4 shows a higher force than test 3. The load profile obtained from the load cell data and the force profile obtained from the acceleration data do not show any signs of whether the specimen failed or not. Figure 5-24 shows the specimen after it partially failed.

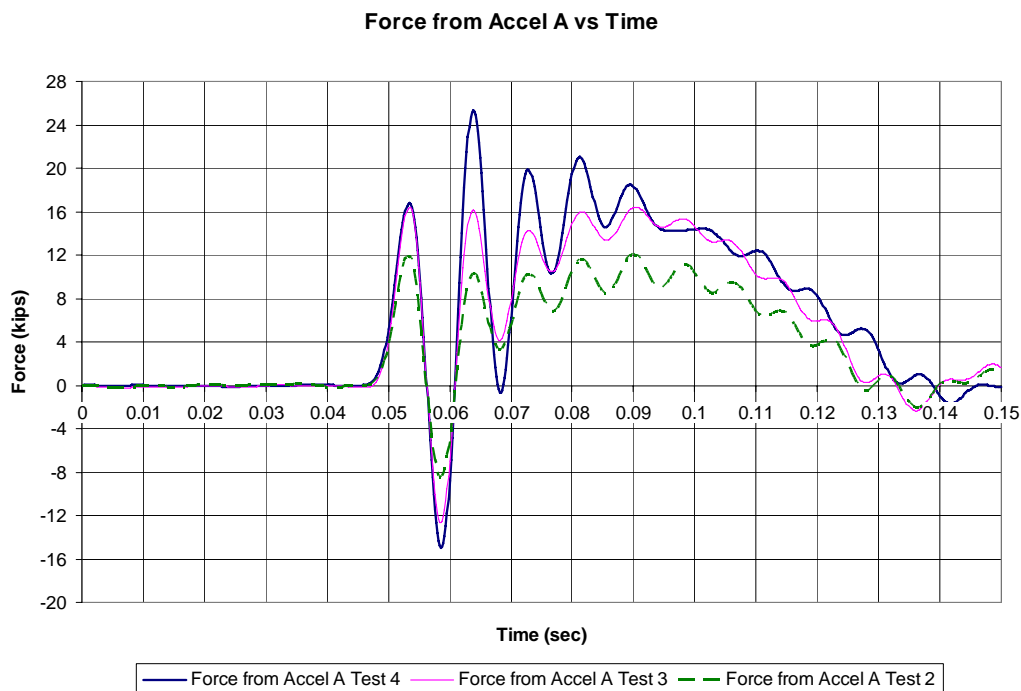


***Fig. 5-23: Force profile for test 2 (6-in drop height), test 3 (12-in drop height) and test 4 (18-in drop height).***





*Fig. 5-24: Pictures of laminated lumber beam after final test.*

The midspan deflections for the three different drop heights are presented in Figure 5-25. As it can be seen for all tests, after the initial impact, the beam vibrated back and forth about the zero axis until it comes to rest. However, for test four with a drop height of 18 in, the vibration does not only occur along the zero axis due to the fact that the beam partially failed. Nevertheless, it can be seen there was no permanent deformation associated with test four.

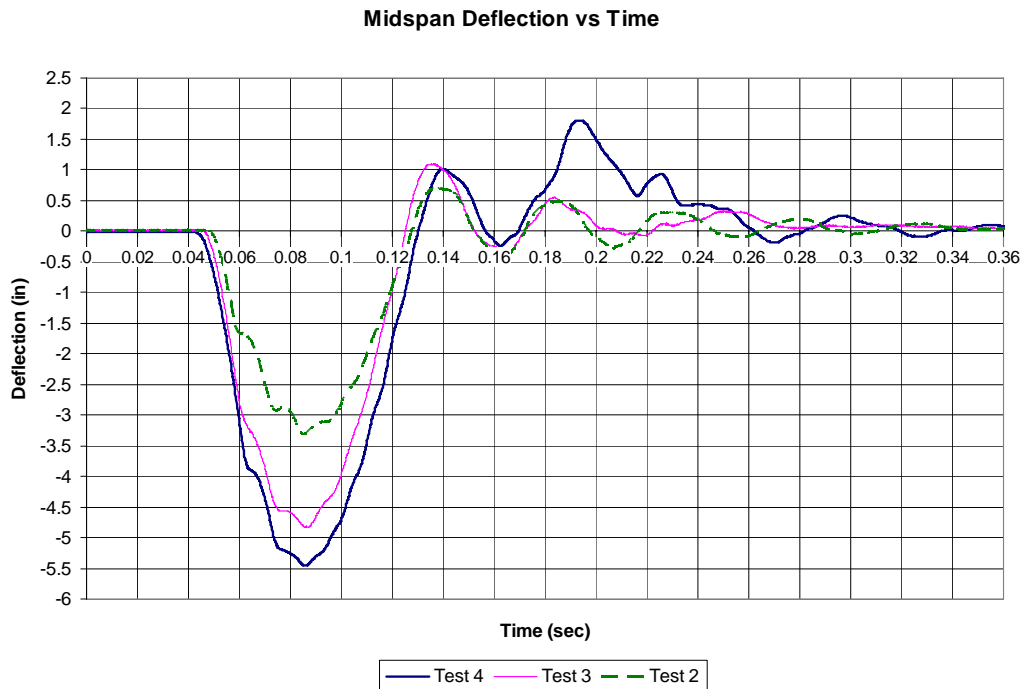


**Fig. 5-25: Midspan displacement for test 2 (6-in drop height), test 3 (12-in drop height) and test 4 (18-in drop height).**

For all tests, the profile between the measured force from the load cell and the computed force from the acceleration data are very different in terms of high frequency content or noise. This difference can clearly be seen in Figure 5-12, 5-26, and 5-27. As mentioned previously, the acceleration data is filtered, and the result is a smooth curve (Figure 5-23). The data from the load cell, however, was used without any filter, and it has many peaks (Figure 5-22). The data from the load cell is not filtered because, unlike the accelerometers, the load cell is not affected by “ringing” of the pendulum mass. For this reason, it is thought that the filter used for the acceleration data should be reviewed and possibly modified for tests that do not involve a crush package in front of the pendulum mass. The modification should consider allowing higher frequencies to pass during the initial

impact because the main difference between profiles occurs at the beginning of the impact. It is important to point out that there are no explicit guidelines for designing a filter for the raw accelerometer data, and it was originally designed by trial and error (Mitchell, 2005). Therefore, in order to be able to review the filter and possibly perform modifications to it, several tests would have to be performed, which falls outside the scope of this report.

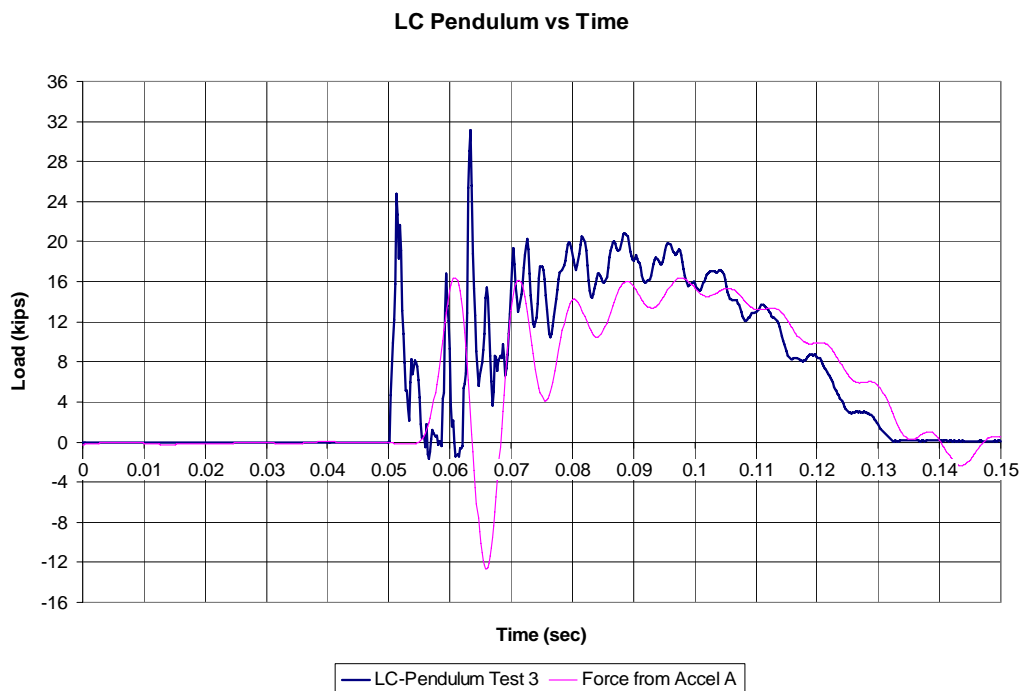


***Fig. 5-26: Load profile obtained from load cell (LC) in front of pendulum and from acceleration profile (12-in drop height).***

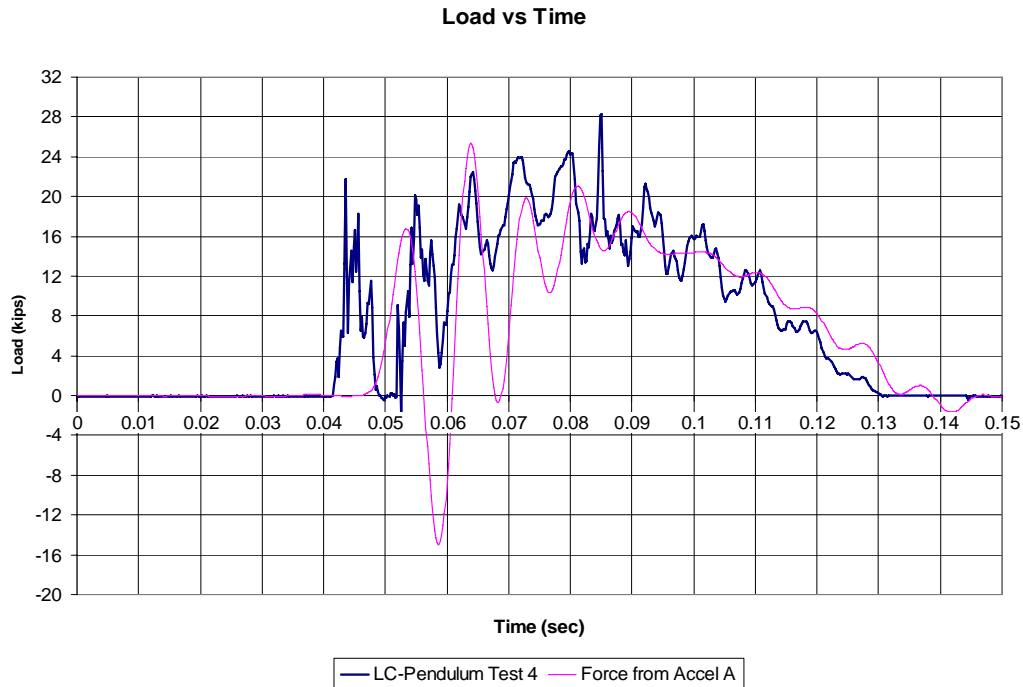


***Fig. 5-27: Load profile obtained from load cell (LC) in front of pendulum and from acceleration profile (18-in drop height).***

After analyzing the data obtained from the load cell located in front of the pendulum and comparing it with the one obtained from the accelerometer on the pendulum mass, it is difficult to conclude which one is better. However, by looking at Figure 5-12, 5-26, and 5-27 it can be seen that the load cell data has two very high peaks at the beginning of the profile, and if these two peaks are ignored, the load profiles are very similar. Therefore, any of the two can be used to compute the system response. However, as mentioned before, it is still recommended that the filter is reviewed in order to verify that response data is not being lost with this process.

## CHAPTER 6

### Conclusions and Recommendations

#### 6.1 SUMMARY

This report provides a description of five beams that were designed and fabricated for the purposes of impact testing. Two of the specimens are constructed using prestressed concrete, two are built using reinforced concrete, and one is fabricated with pine boards. The first type of specimen is representative of a prestressed AASHTO Type IV girder. These beams have not yet been tested. The reinforced concrete beams had the same dimensions and a similar flexural capacity as the prestressed beams. They were used to perform two tests where the main objective was to evaluate the behavior of the test setup and instrumentation. The third type of specimen was used to evaluate the behavior of the load cells installed on the supports and in front of the pendulum mass.

Two buttresses were also designed and fabricated. These buttresses serve as beam supports and are located 16 ft apart. They hold the specimen to be tested at a specific height. The original buttress design restricted the rotation at the ends of the beam, causing local failure of the concrete and to the nose of the support. After some minor modifications, the beams were able to undergo large end rotations without damaging the buttresses.

For the tests performed, different types of instrumentation were used to measure both force and displacement. To measure displacement, LVDTs and string potentiometers were employed. However, the accuracy of the data obtained for the midspan deflection was unknown due to the rapid movement of the beam after the initial impact. Accelerometers and load cells were used to measure the force applied to the specimen by the pendulum mass. The main difference between the data obtained from load cells and accelerometers occurs at the

beginning, where the load cell data shows two high peaks that are not shown by the force profiles obtained from the acceleration data. However, if these two peaks are ignored, the behavior profiles are very similar and any of the two can be used to compute the system response.

## **6.2 CONCLUSIONS**

- 1) The buttresses fabricated for this project are strong enough to hold the beam in place even with drop heights of up to 15 ft (measured with respect to the ground). The displacement of the buttresses after the impact can be assumed to be zero.
- 2) The string potentiometers located at midspan work accurately if the beam is not taken to complete failure, which was the case of the laminated lumber beam. If the beam is taken to complete failure, like in the case of the two reinforced concrete beams, the deflections are too big to be registered by the string potentiometers.
- 3) The accelerometer with a capacity of 100 g does not have enough capacity for this type of test because the actual acceleration plus the “ringing” of the pendulum mass exceed 100 g.
- 4) The 100-kip load cells located on the buttresses only register data from the response of the beam, which is not equal to the force registered by the 200-kip load cell in front of the pendulum mass. The difference can be attributable to the contribution of inertial and damping effects in the dynamic equilibrium of the system.
- 5) The data from the 200-kip load cell and from the accelerometer on the pendulum mass are close enough and either one can be used to compute system response.

### **6.3 RECOMMENDATIONS FOR FUTURE RESEARCH**

After performing several tests and analyzing the data obtained from them, the author recommends the following future research.

- The filter used to eliminate the “ringing” from the pendulum mass needs to be modified for this type of test. After comparing the acceleration data with the load cell data, it is thought that some useful response information from the actual impact is being eliminated by the filter.
- A high-speed camera should be employed to record the test and then visually obtain displacements due to the pendulum impact. The laser-type displacement sensor is another type of equipment that, with the proper research, might be effective in measuring displacements in dynamic impact tests.
- The maximum drop height of the pendulum mass used when the load cells were installed was 18 in. If the load cells are going to be used with a higher drop height, it should be done with the consent of faculty members and lab technicians because the author did not conduct any research on anything higher than 18 in.
- The prestressed specimens might need to be redesigned in order to place the strands at the bottom corners of the stirrups. In order to do so, two layers are required, and the current prestressing bed at Ferguson Laboratory allows for only one.

## APPENDIX A

### Calculations for Specimens

#### A.1 STRESS CALCULATION USING ALLOWABLE STRESS DESIGN

##### Concrete Properties

---

$f_{ci}$ =	5000	psi	Strength of concrete at release
$f_c$ =	12410	psi	Strength of concrete at 28 days
$\gamma$ =	0.15	k / ft <sup>3</sup>	Weight of concrete

##### Strand Properties

Type: Low Relaxation - 1/2"

Area = 0.153 in<sup>2</sup>/strand

$f_{pu}$  = 270 ksi

$$f_{py} = 0.9 f_{pu}$$

$f_{py}$  = 243 ksi

Allowed jacking stress is the lesser of: (ACI-05, prov. 18.5.1)

$0.94f_{py}$  = 228.42 ksi

$0.8f_{pu}$  = 216 ksi

$$P_{jack} = A_p \cdot (0.8 f_{pu})$$

$P_{jack}$  = 33.048 kips/strand

Jacking force

Initial P/S force

$T_{loss}$  = 7.5 %

Loss between jacking and transfer (Mitchell, 263)

$$P_i = P_{jack} \left( 1 - \frac{T_{loss}}{100} \right)$$

$P_i$  = 30.569 kips/strand

Initial prestressing force per strand

Total  $P_i$  = 61.139 kips

# of strands = 2 strands

##### Sectional Properties

---

L =	16.67	ft	Beam length
h =	11.5	in	Beam depth
b =	6.5	in	Beam width
A =	74.75	in <sup>2</sup>	Area of cross section
I =	823.807	in <sup>4</sup>	Moment of inertia
$Y_t$ =	5.75	in	Distance to outer top fiber
$Y_b$ =	5.75	in	Distance to outer bottom fiber
e =	2.75	in	Eccentricity of P/S force
Wsw =	0.078	kips/ft	Load due to Self Weight (SW)
V support =	0.649	kips	Reaction at support due to SW
Mmidspan =	32.444	kips-in	Moment at midspan due to SW
M50db =	14.175	kips-in	Moment at 50db from end of beam



### Stresses in Concrete Immediately After Prestress Transfer

---

#### Stresses at top fiber

$$f_{ct} = -\frac{P_i}{A} + \frac{P_i \cdot e \cdot Y_t}{I} - \frac{M_{sw} \cdot Y_t}{I}$$

$f_{ct}$ midspan =	0.129	ksi	$\leq 3 \cdot \sqrt{f'_{ci}} \rightarrow$	0.212	ksi	OK
$f_{ct}$ 50db =	0.257	ksi	$\leq 6 \cdot \sqrt{f'_{ci}} \rightarrow$	0.424	ksi	OK

#### Stresses at bottom fiber

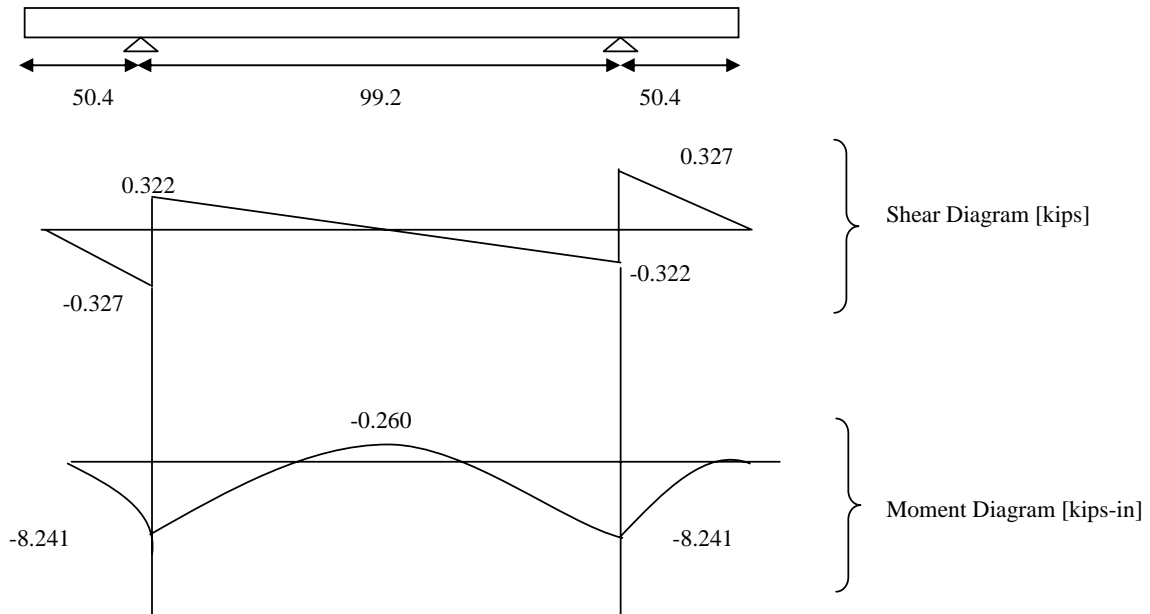
$$f_{cb} = -\frac{P_i}{A} - \frac{P_i \cdot e \cdot Y_b}{I} + \frac{M_{sw} \cdot Y_b}{I}$$

$f_{cb}$ midspan =	-1.765	ksi	$\leq 0.6 \cdot f'_c \rightarrow$	3	ksi	OK
$f_{cb}$ 50db =	-1.892	ksi				

### Stresses in Concrete During Lifting Operation

---

$f_{pf}$ =	165	ksi	Final prestressing stress (Mitchell, 264)
Total $P_f$ =	50.49	kips	Total final prestressing force
$W_{sw}$ =	0.0065	kips/in	Load due to Self Weight



$$M_{lift} = 8.241 \text{ kips-in}$$

Critical moment during lifting operation

Stresses at critical fiber

$$f_{ct} = -\frac{P_{pf}}{A} + \frac{P_{pf} \cdot e \cdot Y_t}{I} + \frac{M_{lift} \cdot Y_t}{I}$$

Stress at critical location during lifting operation

$$f_{ct} = 0.351 \text{ ksi} \quad \boxed{\leq 7.5 \cdot \sqrt{f'_c} \rightarrow} \quad 0.836 \text{ ksi} \quad \text{OK}$$

**Stresses in Concrete at Test Setup**

---

$$l = 16 \text{ ft}$$

Length between supports

$$M_{mst} = \frac{W_{sw} \cdot l^2}{8}$$

Moment due to self-weight at midspan in test setup

$$M_{mst} = 29.9 \text{ kip-in}$$

$$Y_{bw} = 3.25 \text{ in}$$

Distance to outer bottom fiber of weak axis

$$I_w = 263.18229 \text{ in}^4$$

Moment of inertia of weak axis

Stresses at critical fiber

$$f_{cb} = -\frac{P_f}{A} + \frac{P_f \cdot e \cdot Y_t}{I} + \frac{M_{mst} \cdot Y_{tw}}{I_w}$$

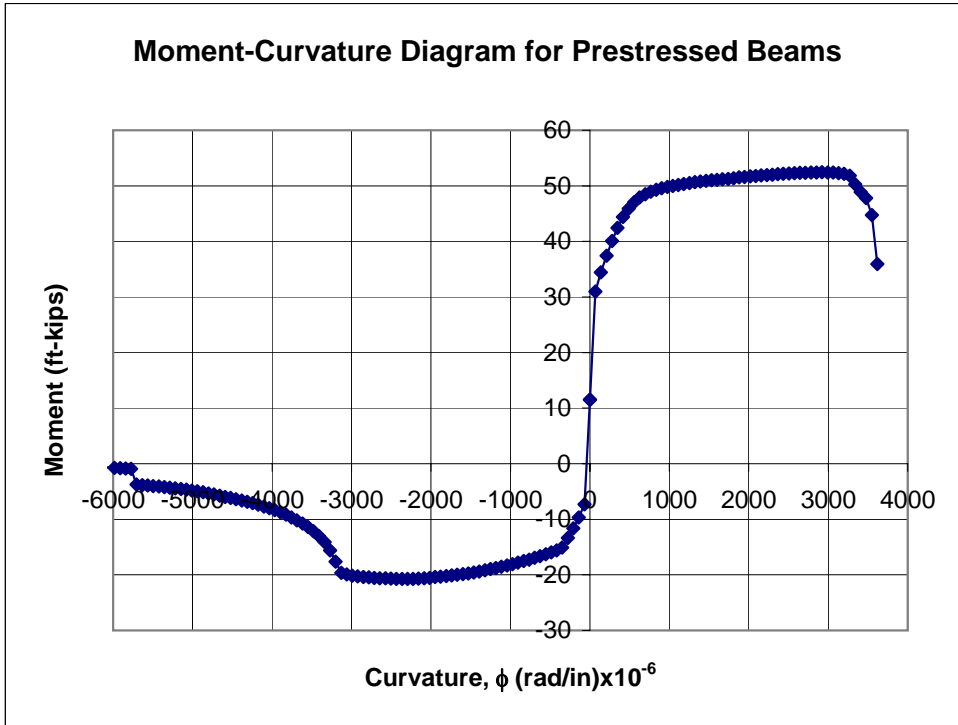
Stress at critical location at test setup

$$f_{cb} = 0.663 \text{ ksi} \quad \boxed{\leq 7.5 \cdot \sqrt{f'_c} \rightarrow} \quad 0.836 \text{ ksi} \quad \text{OK}$$

## A.2 FLEXURAL DESIGN OF TEST SPECIMENS

### A.2.1 Prestressed Concrete Specimen

The maximum flexural moment is obtained from the Moment-Curvature Diagram



$M_u = 52.43$  ft-kip  
 $L = 16$  ft  
 $W_{sw} = 0.078$  kips/ft  
 $M_{sw} = 2.492$  ft-kip

Max. Moment (from M- $\phi$  diagram)  
 Distance between supports  
 Distributed load due to self weight  
 Moment due to self weight

For a point load applied at midspan:

$$P_u = \frac{(M_u - M_{sw}) \cdot 4}{L}$$

$P_u = 12.485$  kips

Estimated Point Load at failure

### A.2.2 Reinforced Concrete Specimen

---

$M_n = 52.43$  k-ft Required Moment Capacity obtained  
 from capacity of Prestressed Beam  
 $M_{sw} = 2.492$  ft-kip Moment due to self weight

$d = 10.5$  in Effective depth of beam  
 $\phi = 0.9$   
 $f_y = 60$  ksi  
 $f'_c = 6.9$  ksi  
 $b = 6.5$  in  
 $M_n = 629.16$  k-in

$$C_c = 0.85 f'_c a b \quad \text{Compression force in concrete}$$

Where a is equal to:

$$a = \beta_1 c$$

$$T = A_s f_y \quad \text{Tension force in steel}$$

For equilibrium:

$$\begin{aligned}
 T &= C \\
 0.85 f'_c a b - A_s f_y &= 0 \\
 a &= \frac{A_s f_y}{0.85 f'_c b}
 \end{aligned}$$

The resisting moment is obtained by multiplying the tension force by the distance to the compression force provided by the concrete

$$\begin{aligned}
 \phi M_n &= A_s f_y \left( d - \frac{a}{2} \right) \\
 \phi M_n &= A_s f_y \left( d - \frac{A_s f_y}{1.7 f'_c b} \right) \\
 \left( \frac{\phi f_y^2}{1.7 f'_c b} \right) A_s^2 - (\phi f_y d) A_s + M_n &= 0
 \end{aligned}$$

Solving for  $A_s$

$$A_s = 1.221 \text{ in}^2 \quad \text{Required area of steel}$$

Req. #5 rebars:  $3.94 \text{ in}^2 \longrightarrow$  Use 4 #5 rebars

Because the amount of rebars cannot be placed on a single layer, it was decided to use three rebars #5

$$\begin{aligned}
 A_{\#5} &= 0.31 \text{ in}^2 \\
 \# \text{ rebars} &= 3 \\
 A_s \text{ to use} &= 0.93 \text{ in}^2 \\
 M_n &= 490.556 \text{ k-in} \\
 M_n &= 40.880 \text{ k-ft}
 \end{aligned}$$

Area of rebar #5

Total area of steel provided

Resisting moment for the steel provided

$$P_u = \frac{(M_n - M_{sw}) \cdot 4}{L}$$

$$P_u = 9.60 \text{ kips}$$

Estimated Point Load at failure

Estimated Point Load at failure

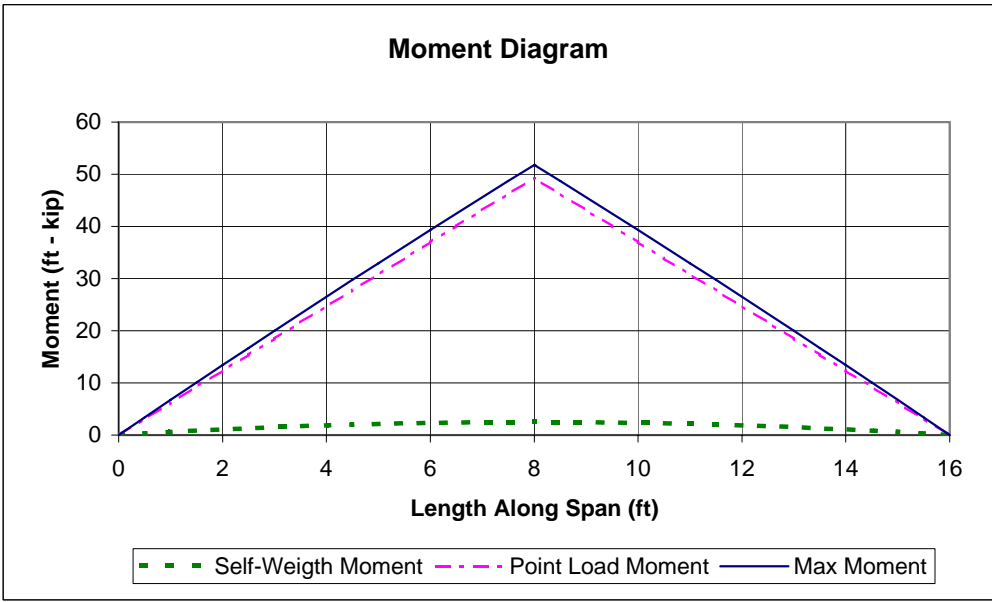
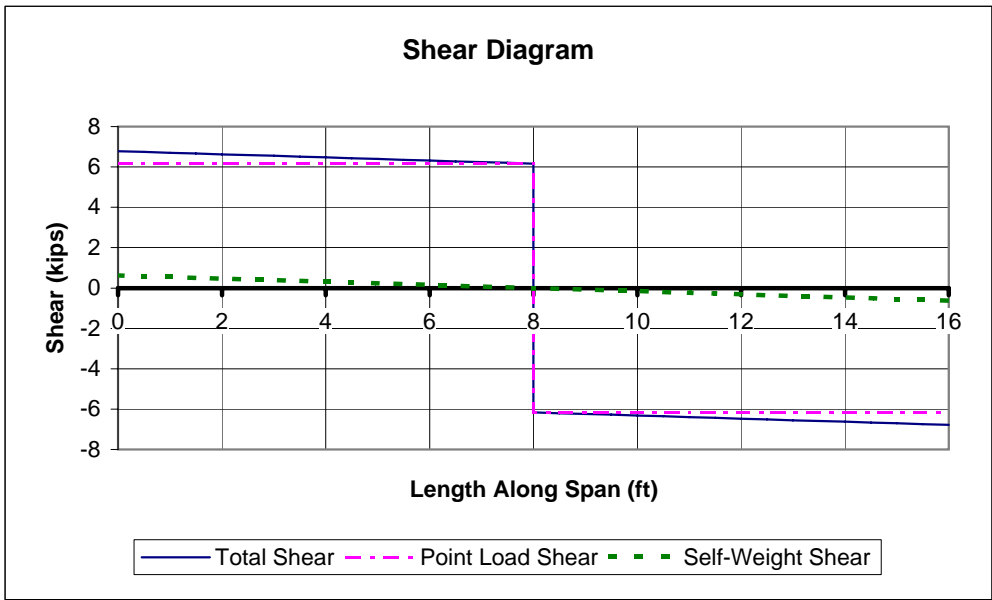
### A.3 SHEAR DESIGN OF TEST SPECIMENS

#### A.3.1 Prestressed Concrete Specimen

#### Shear and Moment Diagram

$f_{pf}$ =	165	kips	Final prestressing stress (Mitchell, 264)
$W_{sw}$ =	0.0778	k/ft	Beam self-weight
$P_u$ =	12.32	kips	Estimated Point Load at failure
$L$ =	16	ft	Span Length
R due to $W_{sw}$ =	0.6224	kips	Reaction due to Self-Weight
R due to $P_u$ =	6.1615227	kips	Reaction due to Point load
$M_{max}$ =	52.43	kips-ft	Max. Moment (from M- $\phi$ diagram)
$x_{tr} = L_{transfer} - L_{ex}$	21	in	Transfer length from edge of support

x (ft)	$V_d$ (kips)	$V_{pu}$ (kips)	$V_u$ (kips)	$M_{sw}$ (kips-ft)	$M_{pu}$ (kips-ft)	$M_{max}$ (kips-ft)
0	0.62	6.16	6.78	0.00	0.00	0.00
0.5	0.58	6.16	6.75	0.30	3.08	3.38
1	0.54	6.16	6.71	0.58	6.16	6.75
1.5	0.51	6.16	6.67	0.85	9.24	10.09
2	0.47	6.16	6.63	1.09	12.32	13.41
2.5	0.43	6.16	6.59	1.31	15.40	16.72
3	0.39	6.16	6.55	1.52	18.48	20.00
3.5	0.35	6.16	6.51	1.70	21.57	23.27
4	0.31	6.16	6.47	1.87	24.65	26.51
4.5	0.27	6.16	6.43	2.01	27.73	29.74
5	0.23	6.16	6.39	2.14	30.81	32.95
5.5	0.19	6.16	6.36	2.25	33.89	36.13
6	0.16	6.16	6.32	2.33	36.97	39.30
6.5	0.12	6.16	6.28	2.40	40.05	42.45
7	0.08	6.16	6.24	2.45	43.13	45.58
7.5	0.0389	6.16	6.20	2.48	46.21	48.69
8	0	6.16	6.16	2.49	49.29	51.78
8	0.00	-6.16	-6.16	2.49	49.29	51.78
8.5	-0.04	-6.16	-6.20	2.48	46.21	48.69
9	-0.08	-6.16	-6.24	2.45	43.13	45.58
9.5	-0.12	-6.16	-6.28	2.40	40.05	42.45
10	-0.16	-6.16	-6.32	2.33	36.97	39.30
10.5	-0.19	-6.16	-6.36	2.25	33.89	36.13
11	-0.23	-6.16	-6.39	2.14	30.81	32.95
11.5	-0.27	-6.16	-6.43	2.01	27.73	29.74
12	-0.31	-6.16	-6.47	1.87	24.65	26.51
12.5	-0.35	-6.16	-6.51	1.70	21.57	23.27
13	-0.39	-6.16	-6.55	1.52	18.48	20.00
13.5	-0.43	-6.16	-6.59	1.31	15.40	16.72
14	-0.47	-6.16	-6.63	1.09	12.32	13.41
14.5	-0.51	-6.16	-6.67	0.85	9.24	10.09
15	-0.54	-6.16	-6.71	0.5835	6.16	6.75
15.5	-0.58	-6.16	-6.75	0.301475	3.08	3.38
16	-0.62	-6.16	-6.78	0	0.00	0.00



## Shear Capacity Calculations

$f =$	0.75		Strength reduction factor
$f_y =$	60000	psi	Shear Steel Yield
$A_v =$	0.11	in <sup>2</sup>	Area of one legged stirrup (#3)
$f'_c =$	10000	psi	
$\sqrt{f'_c} =$	100.00	psi	Should be limited to 100 psi (ACI-05, prov. 11.1.2)
$b_w =$	6.5	in	Web Width
$A_p =$	0.306	in <sup>2</sup>	Area of prestressing strand
$f_{pu} =$	270	ksi	Ultimate strength of strands
$h =$	11.5	in	Depth of section
$d_p =$	8.41	in	Must be greater than $0.8h =$ 9.2 in

Shear Reinforcing (#3 double legged stirrups)

For section 1:

$s_1 =$	3.5	in	Proposed stirrup spacing
$A_{v1} =$	0.7542857	in <sup>2</sup> /ft	Proposed area of steel

For section 2:

$s_2 =$	7.5	in	Proposed stirrup spacing
$A_{v2} =$	0.352	in <sup>2</sup> /ft	Proposed area of steel

Minimum Shear Reinforcement and Spacing:

$s =$	12	in	Spacing to obtain area/ft of stirrup req.
-------	----	----	---

$$A_v > 0.75 \cdot \sqrt{f'_c} \cdot \frac{b_w \cdot s}{f_y}$$

(ACI-05 Eq 11-13)

$A_v >$	0.098	in <sup>2</sup> /ft	<b>Controls</b>
---------	-------	---------------------	-----------------

but not less than:

$$A_v \geq \frac{50 \cdot b_w \cdot s}{f_y}$$

$A_v >$	0.065	in <sup>2</sup> /ft
---------	-------	---------------------

$$A_v \geq \frac{A_p \cdot f_{pu} \cdot s}{80 \cdot f_y \cdot d_p} \cdot \sqrt{\frac{d_p}{b_w}}$$

(ACI-05, Eq 11-14)

$A_v >$	0.027	in <sup>2</sup> /ft
---------	-------	---------------------

$$s \leq 0.75 \cdot h$$

Max stirrup spacing (ACI-05, prov. 11.5.5.2)

$s <$	8.625	in
-------	-------	----



Web Shear Capacity ( $V_{cw}$ )

$L_s =$	4	in	Support Length
L transfer =	25	in	Transfer length ( $50d_b$ )
$P_f = f_{pf} A_p =$	50.49	kips	Total final prestressing force
A =	74.75	in <sup>2</sup>	Area of cross section
$V_p =$	0	lbs	Vertical component of effective prestress force

If  $x < 20"$  then Peffective:

$$P_{effective} = \frac{P_f \cdot (x + L_s)}{L_{transfer}}$$

$$f_{pc} = \frac{P_{effective}}{A}$$

Comp. stress in concrete at centroid of cross section

$$V_{cw} = (3.5 \cdot \sqrt{f'_c} + 0.3 \cdot f_{pc}) \cdot b_w \cdot d + V_p$$

(ACI-05, Eq 11.12)

x (ft)	x (in)	Peffective (kips)	$V_p$ (kips)	$f_{pc}$ (ksi)	$V_{cw}$ (kips)
0	0	0	0	0	20.93
0.5	6	20.20	0	0.27	25.78
1	12	32.31	0	0.43	28.69
1.5	18	44.43	0	0.59	31.59
2	24	50.49	0	0.68	33.05
2.5	30	50.49	0	0.68	33.05
3	36	50.49	0	0.68	33.05
3.5	42	50.49	0	0.68	33.05
4	48	50.49	0	0.68	33.05
4.5	54	50.49	0	0.68	33.05
5	60	50.49	0	0.68	33.05
5.5	66	50.49	0	0.68	33.05
6	72	50.49	0	0.68	33.05
6.5	78	50.49	0	0.68	33.05
7	84	50.49	0	0.68	33.05
7.5	90	50.49	0	0.68	33.05
8	96	50.49	0	0.68	33.05

Flexural Shear Capacity ( $V_{ci}$ )

$Y_b =$	5.75	in	Distance to outer bottom fiber
$e =$	2.75	in	Eccentricity
$I =$	823.81	in <sup>4</sup>	Moment of inertia of cross section
$V_i =$	6.16	kips	Min. shear value

$$f_{cr} = 6 \cdot \sqrt{f'_c}$$

$f_{cr} =$  0.6 ksi Cracking stress of concrete

$$f_{pe} = \frac{P_{effective}}{A} + \frac{P_{effective} \cdot e \cdot Y_b}{I}$$

Stress due to self-equilibrating loads

$$f_{sw} = \frac{M_{sw} \cdot Y_b}{I}$$

Stress due to self-weight

$$f_{cr} = -f_{pe} + f_{sw} + \frac{M_{cr} \cdot Y_b}{I}$$

$$M_{cr} = (f_{cr} + f_{pe} - f_{sw}) \cdot \frac{I}{Y_b}$$

Cracking Moment ( $M_{cr}$ )

$$V_{ci} = 0.6 \cdot \sqrt{f'_c} \cdot b_w \cdot d_p + V_d + \frac{V_i \cdot M_{cr}}{M_{max}}$$

ACI-05, Eq 11-10

$V_{ci}$  must be greater than:

$$V_{ci} > 1.7 \cdot \sqrt{f'_c} \cdot b_w \cdot d$$

x (ft)	$V_d$ (kips)	Peffective (kips)	$f_{pe}$ (ksi)	$f_{sw}$ (ksi)	$M_{cr}$ (kips-ft)	M max (kips-ft)	$V_i$ (kips)	$V_{ci}$ (kips)
0	0.62	0.00	0.00	0.00	7.16	0.00	6.16	$\infty$
0.5	0.58	20.20	0.66	0.00	14.99	3.38	6.16	31.48
1	0.54	32.31	1.05	0.00	19.68	6.75	6.16	22.11
1.5	0.51	44.43	1.45	0.01	24.37	10.09	6.16	18.98
2	0.47	50.49	1.64	0.01	26.71	13.41	6.16	16.32
2.5	0.43	50.49	1.64	0.01	26.69	16.72	6.16	13.85
3	0.39	50.49	1.64	0.01	26.67	20.00	6.16	12.19
3.5	0.35	50.49	1.64	0.01	26.66	23.27	6.16	11.00
4	0.31	50.49	1.64	0.01	26.64	26.51	6.16	10.17
4.5	0.27	50.49	1.64	0.01	26.63	29.74	6.16	10.17
5	0.23	50.49	1.64	0.01	26.62	32.95	6.16	10.17
5.5	0.19	50.49	1.64	0.02	26.61	36.13	6.16	10.17
6	0.16	50.49	1.64	0.02	26.60	39.30	6.16	10.17
6.5	0.12	50.49	1.64	0.02	26.60	42.45	6.16	10.17
7	0.08	50.49	1.64	0.02	26.59	45.58	6.16	10.17
7.5	0.04	50.49	1.64	0.02	26.59	48.69	6.16	10.17
8	0.00	50.49	1.64	0.02	26.59	51.78	6.16	10.17

Shear Strength Provided by Concrete ( $V_c$ )

$V_c$  is the smaller value of  $V_{cw}$  and  $V_{ci}$

x (ft)	$V_{cw}$ (kips)	$V_{ci}$ (kips)	$V_c$ (kips)	$\phi V_c$ (kips)
0	20.93	$\infty$	20.93	15.70
0.5	25.78	31.48	25.78	19.33
1	28.69	22.11	22.11	16.58
1.5	31.59	18.98	18.98	14.23
2	33.05	16.32	16.32	12.24
2.5	33.05	13.85	13.85	10.39
3	33.05	12.19	12.19	9.15
3.5	33.05	11.00	11.00	8.25
4	33.05	10.17	10.17	7.62
4.5	33.05	10.17	10.17	7.62
5	33.05	10.17	10.17	7.62
5.5	33.05	10.17	10.17	7.62
6	33.05	10.17	10.17	7.62
6.5	33.05	10.17	10.17	7.62
7	33.05	10.17	10.17	7.62
7.5	33.05	10.17	10.17	7.62
8	33.05	10.17	10.17	7.62

Shear Strength Provided by Steel ( $V_s$ )

$$V_s = \frac{A_v \cdot f_y \cdot d}{s}$$

If  $V_s > 4 \cdot \sqrt{f'_c} \cdot b_w \cdot d$

$S_{max}$  shall be reduced by 0.5

x (ft)	$V_s$ (kips)	$\phi V_s$ (kips)
0	34.70	26.02
0.5	34.70	26.02
1	34.70	26.02
1.5	34.70	26.02
2	34.70	26.02
2.5	16.19	12.14
3	16.19	12.14
3.5	16.19	12.14
4	16.19	12.14
4.5	16.19	12.14
5	16.19	12.14
5.5	16.19	12.14
6	16.19	12.14
6.5	16.19	12.14
7	16.19	12.14
7.5	16.19	12.14
8	16.19	12.14

Section 1

$4 \cdot \sqrt{f'_c} \cdot b_w \cdot d = \rightarrow 23.920$  kips

$S_{max} / 2 = 4.31$      **Controls**  
using 3.5"     **OK!**

Section 2

$4 \cdot \sqrt{f'_c} \cdot b_w \cdot d = \rightarrow 23.920$  kips

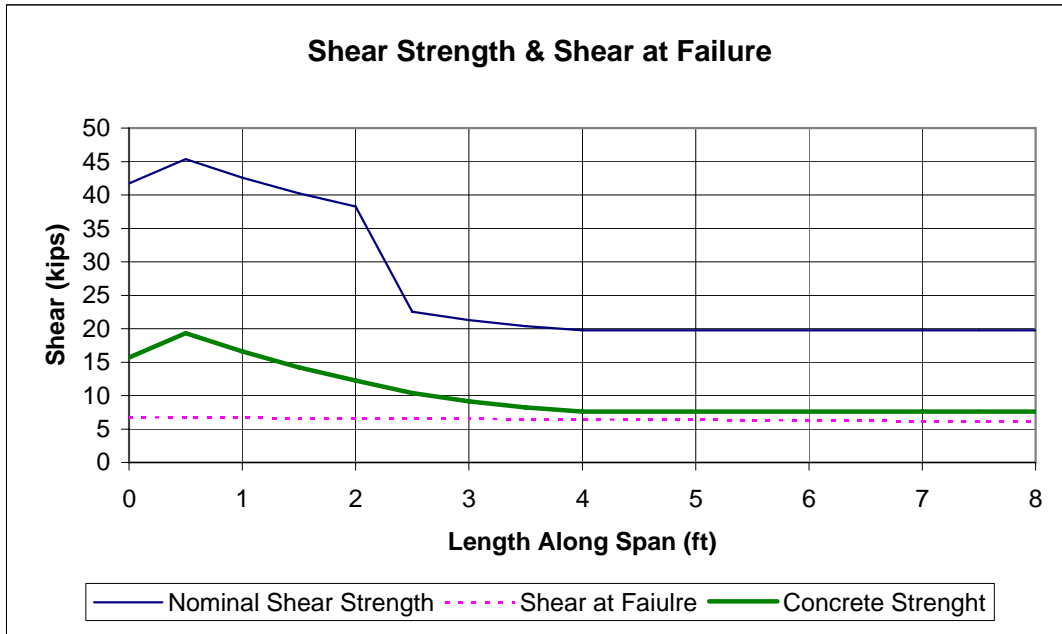
$S_{max} = 8.63$      **Controls**  
using 7.5"     **OK!**

Shear Strength Provided by Steel and Concrete

$$\phi V_n = \phi V_c + \phi V_s$$

x (ft)	$\phi V_n$ (kips)	$V_u$ (kips)
0	41.72	6.78
0.5	45.36	6.75
1	42.61	6.71
1.5	40.26	6.67
2	38.27	6.63
2.5	22.53	6.59
3	21.29	6.55
3.5	20.39	6.51
4	19.77	6.47
4.5	19.77	6.43
5	19.77	6.39
5.5	19.77	6.36
6	19.77	6.32
6.5	19.77	6.28
7	19.77	6.24
7.5	19.77	6.20
8	19.77	6.16

$\phi V_n > V_u$  OK

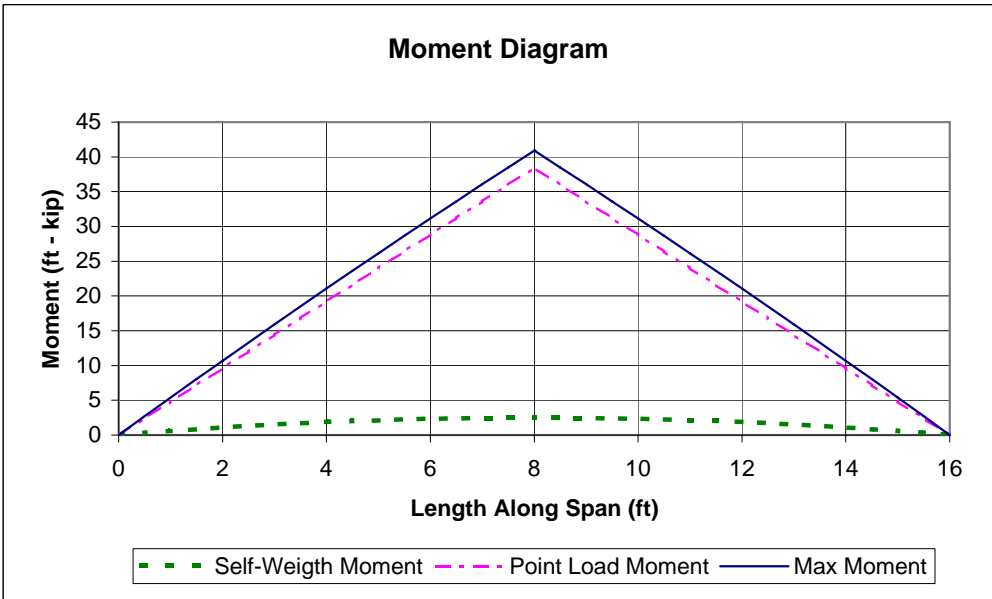
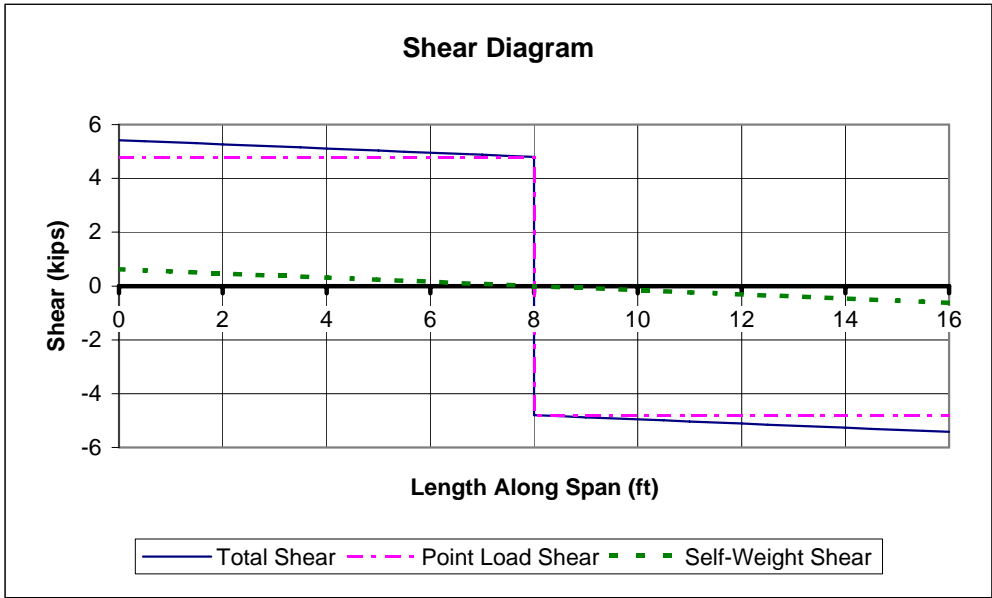


### A.3.2 Reinforced Concrete Specimen

#### Shear and Moment Diagram

W <sub>sw</sub> =	0.0778	k/ft	Beam self-weight
P <sub>u</sub> =	9.60	kips	Estimated Point Load at failure
L =	16	ft	Span Length
R due to W <sub>sw</sub> =	0.6224	kips	Reaction due to Self-Weight
R due to P <sub>u</sub> =	4.8	kips	Reaction due to Point load
M <sub>max</sub> =	40.88	kips-ft	Max. Moment (from M-φ diagram)

x (ft)	V <sub>d</sub> (kips)	V <sub>pu</sub> (kips)	V <sub>u</sub> (kips)	M <sub>sw</sub> (kips-ft)	M <sub>pu</sub> (kips-ft)	M max (kips-ft)
0	0.62	4.80	5.42	0.00	0.00	0.00
0.5	0.58	4.80	5.38	0.30	2.40	2.70
1	0.54	4.80	5.34	0.58	4.80	5.38
1.5	0.51	4.80	5.31	0.85	7.20	8.05
2	0.47	4.80	5.27	1.09	9.60	10.69
2.5	0.43	4.80	5.23	1.31	12.00	13.31
3	0.39	4.80	5.19	1.52	14.40	15.92
3.5	0.35	4.80	5.15	1.70	16.80	18.50
4	0.31	4.80	5.11	1.87	19.20	21.07
4.5	0.27	4.80	5.07	2.01	21.60	23.61
5	0.23	4.80	5.03	2.14	24.00	26.14
5.5	0.19	4.80	4.99	2.25	26.40	28.65
6	0.16	4.80	4.96	2.33	28.80	31.13
6.5	0.12	4.80	4.92	2.40	31.20	33.60
7	0.08	4.80	4.88	2.45	33.60	36.05
7.5	0.0389	4.80	4.84	2.48	36.00	38.48
8	0	4.80	4.80	2.49	38.40	40.89
8	0.00	-4.80	-4.80	2.49	38.40	40.89
8.5	-0.04	-4.80	-4.84	2.48	36.00	38.48
9	-0.08	-4.80	-4.88	2.45	33.60	36.05
9.5	-0.12	-4.80	-4.92	2.40	31.20	33.60
10	-0.16	-4.80	-4.96	2.33	28.80	31.13
10.5	-0.19	-4.80	-4.99	2.25	26.40	28.65
11	-0.23	-4.80	-5.03	2.14	24.00	26.14
11.5	-0.27	-4.80	-5.07	2.01	21.60	23.61
12	-0.31	-4.80	-5.11	1.87	19.20	21.07
12.5	-0.35	-4.80	-5.15	1.70	16.80	18.50
13	-0.39	-4.80	-5.19	1.52	14.40	15.92
13.5	-0.43	-4.80	-5.23	1.31	12.00	13.31
14	-0.47	-4.80	-5.27	1.09	9.60	10.69
14.5	-0.51	-4.80	-5.31	0.85	7.20	8.05
15	-0.54	-4.80	-5.34	0.5835	4.80	5.38
15.5	-0.58	-4.80	-5.38	0.301475	2.40	2.70
16	-0.62	-4.80	-5.42	0	0.00	0.00



### Shear Capacity Calculations

---

$f =$	0.75		Strength reduction factor
$f_y =$	60000	psi	Shear Steel Yield
$A_v =$	0.11	in <sup>2</sup>	Area of one legged stirrup (#3)
$f'_c =$	6900	psi	
$\sqrt{f'_c} =$	83.07	psi	Should be limited to 100 psi (ACI-05, prov. 11.1.2)
$b_w =$	6.5	in	Web Width
$h =$	11.5	in	Depth of section
$d =$	11	in	Effective depth of section

Shear Reinforcing (#3 double legged stirrups)

For section 1:

$s_1 =$	5.5	in	Proposed stirrup spacing
$A_{v1} =$	0.48	in <sup>2</sup> /ft	Proposed area of steel

### Shear Strength Provided by Concrete

---

$$\phi V_c = \phi 2 \sqrt{f'_c} b_w d$$

Shear strength provided by concrete (ACI-05, Eq. 11-3)

$$\phi V_c = 8.91 \text{ kips}$$

Since  $V_c > V_u$  use minimum shear reinforcement

### Minimum Shear Reinforcement and Spacing:

---

$A_v$  min:

Min. area of steel for non-prestressed members

$$A_v > 0.75 \cdot \sqrt{f'_c} \cdot \frac{b_w \cdot s}{f_y}$$

(ACI-05, Eq 11-13)

If two legged #3 stirrups are used

$$A_v = 0.22 \text{ in}^2 \quad \text{Area of two legged stirrups \#3}$$

Minimum spacing if two legged #3 stirrups are used:

$$s = \frac{A_v f_y}{0.75 \sqrt{f'_c} b_w}$$

$$s = 32.60 \text{ in}$$

But shall not exceed  $d/2$

(ACI-05, prov. 11.5.5.1)

$$d/2 = 5.5 \text{ in}$$

**Controls**

## APPENDIX B

### Drawings

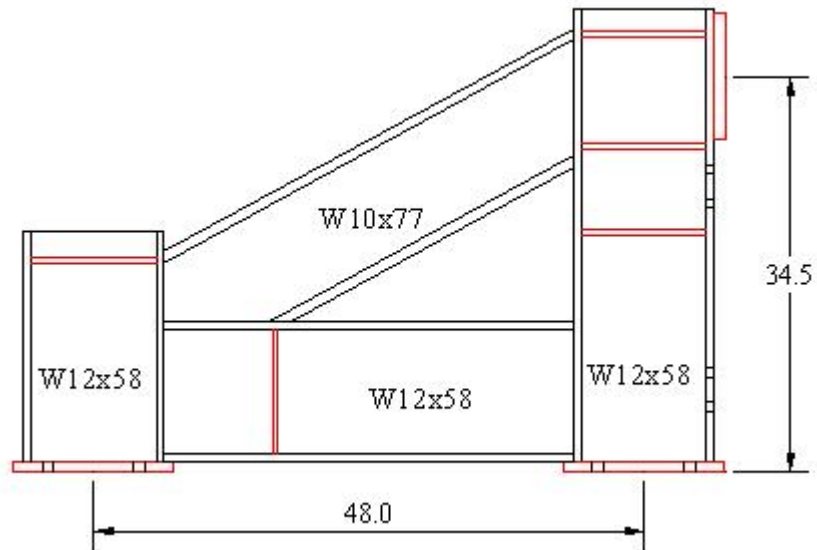


*Fig. B-1: Elevation view of buttress (units in inches).*

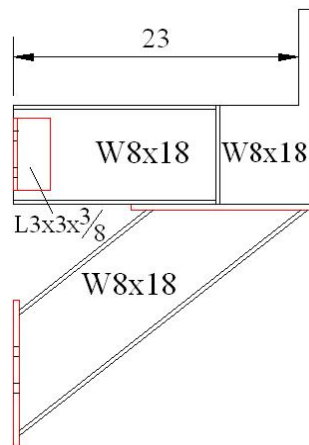


*Fig. B-2: Elevation view of nose of support buttress (units in inches).*



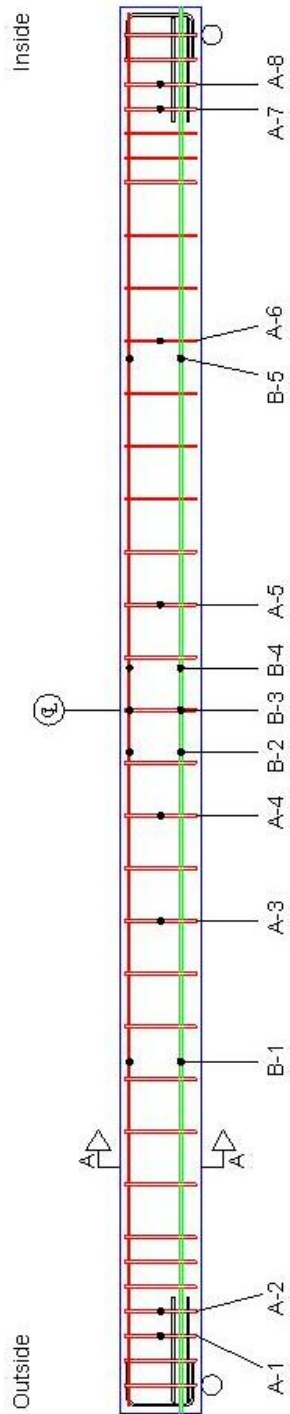
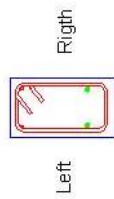


**Fig. B-3a: Location of stain gauges in prestressed beam (see Fig. B-3b).**



Section - A-A

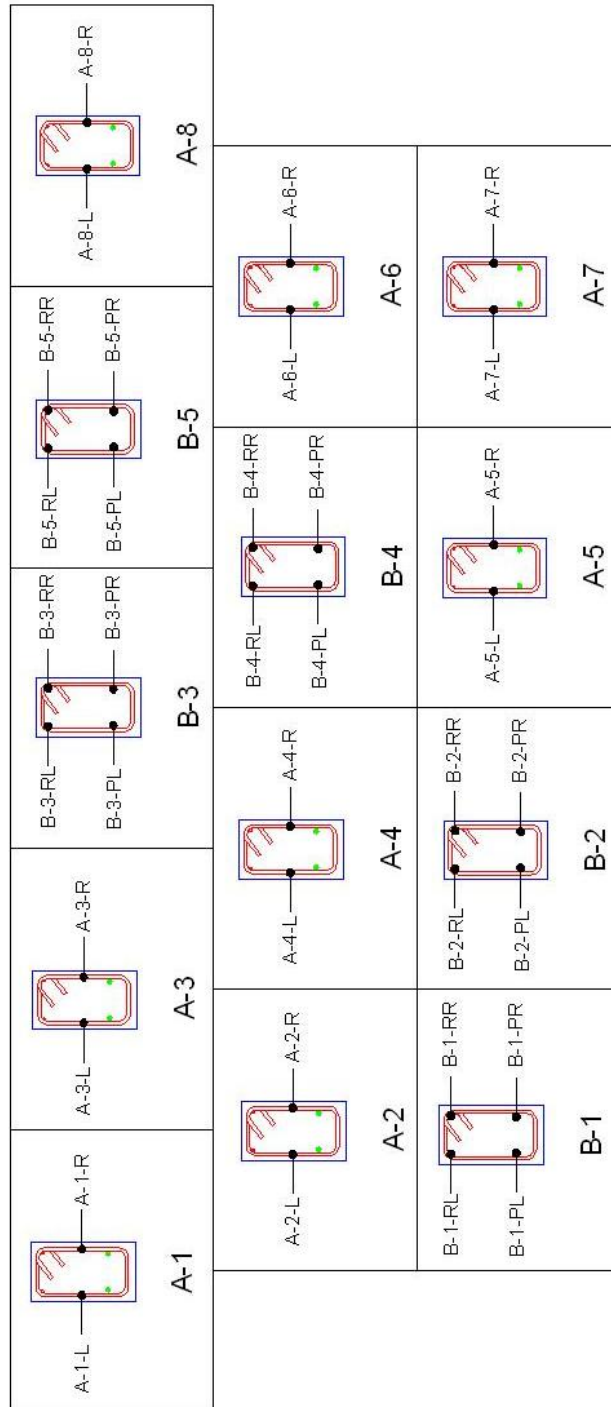
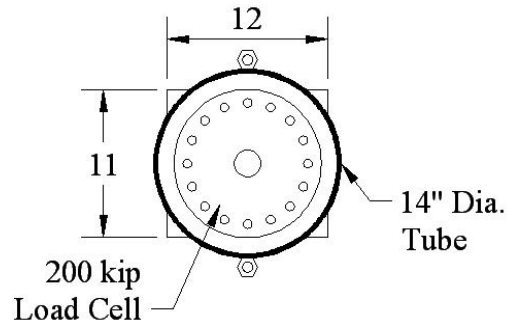
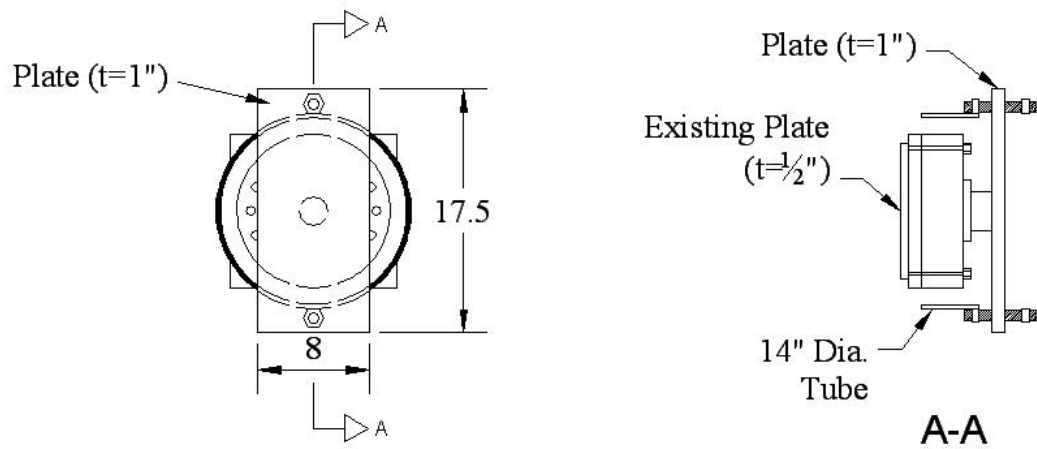


Fig. B-3b: Location of stain gauges in prestressed beam (see Fig. B-3a).



**Fig. B-4: 200 kip load cell located in front of pendulum mass.**



**Fig. B-5: 200 kip load cell located in front of pendulum mass.**

## APPENDIX C

### Pictures

#### C.1 CONSTRUCTION OF BUTTRESSES



(a)



(b)

*Fig. C-1: Cutting of a (a) W12×58, (b) W10×77.*



*Fig. C-2: Cutting of W10×77.*



(a)



(b)

**Fig. C-3: Welding of (a) A-frame, (b) Nose of support.**

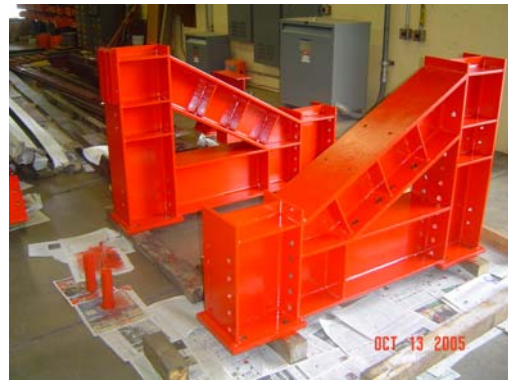


**Fig. C-4: Painting of buttresses.**



**Fig. C-5: Base plate for load cell on A-frame.**

## C.2 FORMWORK FOR PRESTRESSED BEAMS



*Fig. C-6: Formwork for prestressed beams.*

**C.3 REBAR CAGE FOR PRESTRESSED BEAMS**



*Fig. C-7: Reinforcement at beam ends.*



*Fig. C-8: Rebar cage for prestressed beam.*

#### C.4 STRAIN GAUGES IN PRESTRESSED BEAM



(a)



(b)

*Fig. C-9: (a) Grained surface for installation of strain gauge, (b) strain gauge on prestressing strand*



*Fig. C-10: Installed strain gauges on longitudinal and transverse reinforcement.*



## C.5 PLACING CONCRETE FOR PRESTRESSED BEAMS



*Fig. C-11: Pouring of concrete.*

## C.6 STRIPPING FORMWORK FOR PRESTRESSED BEAMS



*Fig. C-12: Stripping formwork.*

## C.7 FORMWORK FOR REINFORCED CONCRETE BEAMS



*Fig. C-13: Formwork for reinforced concrete beam.*

## C.8 REBAR CAGE FOR REINFORCED CONCRETE BEAMS

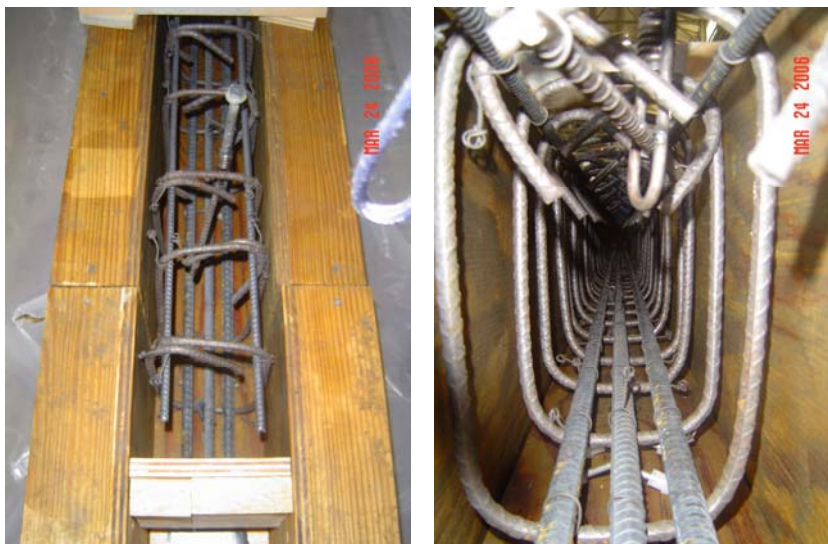


*Fig. C-14: Rebar cage for reinforced concrete beam.*

## C.9 PLACING CONCRETE FOR REINFORCED CONCRETE BEAMS



*Fig. C-15: Placing of concrete for reinforced concrete beam.*

## C.10 PLACING FRP ON CONCRETE SPECIMENS



*Fig. C-16: Placing FRP at ends of beam.*

## C.11 LAMINTATED LUMBER BEAM



*Fig. C-17: Fabrication of laminated lumber beam.*

## C.12 TEST 1 – REINFORCED CONCRETE BEAM

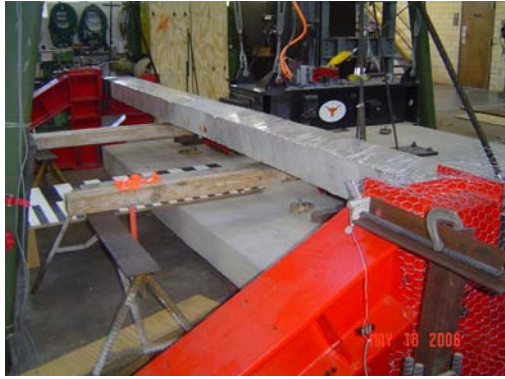


*Fig. C-18: Test setup for first specimen.*



*Fig. C-19: Midspan failure.*

### C.13 TEST 2 – REINFORCED CONCRETE BEAM



(a)



(b)

*Fig. C-20: (a) LVDT at support (b) Conditions of test setup after impact.*



*Fig. C-21: Midspan failure.*

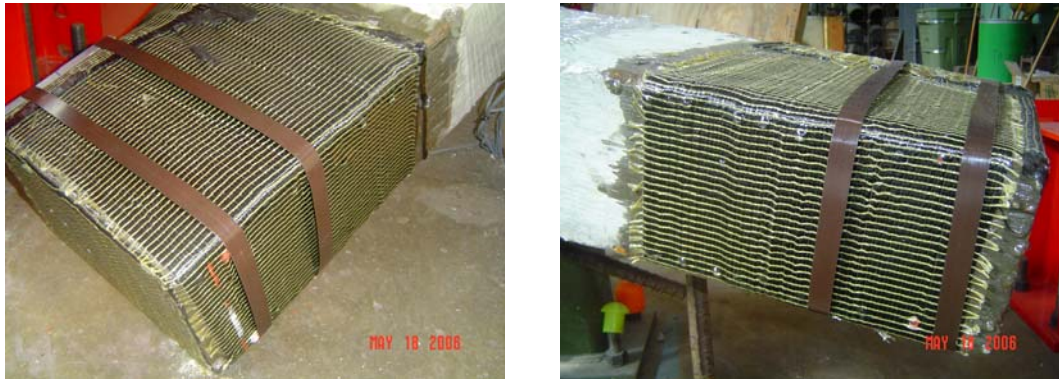


*Fig. C-22: Ends of beam after test.*

#### **C.14 TEST 3 – LAMINATED LUMBER BEAM**



*Fig. C-23: Scale used to measure the drop height of the pendulum mass.*



**Fig. C-24: Test setup for laminated lumber beam.**



(a)



(b)

**Fig. C-25: (a) Leveling of the pendulum mass. (b) Stopper for left support.**





*Fig. C-26: Failure of laminated lumber beam.*

### C.15 LOAD CELLS



*Fig. C-27: Protection ring for load cell in front of pendulum mass.*

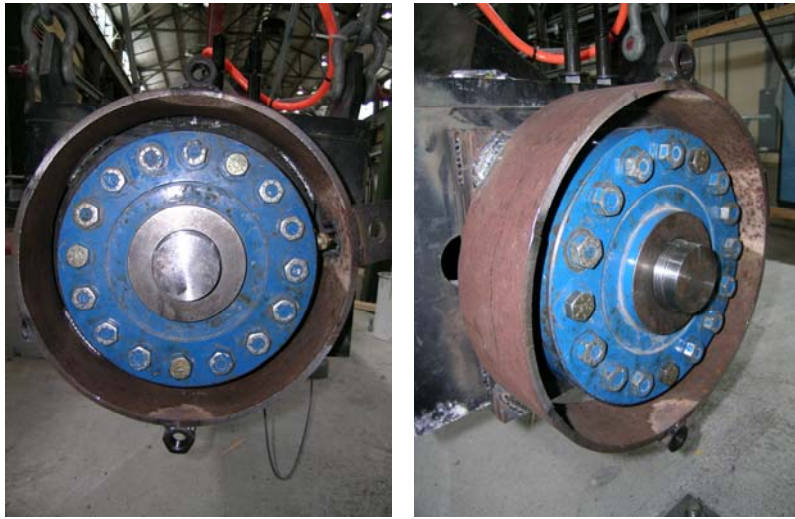


*Fig. C-28: 200 kip load cell in front of pendulum mass.*



*Fig. C-29: 200 kip load cell in front of pendulum mass.*

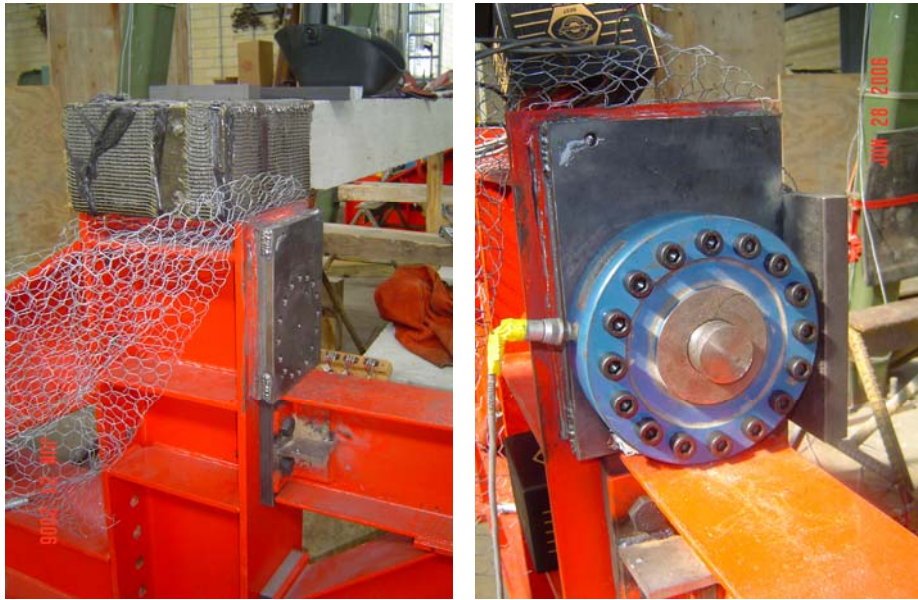


*Fig. C-30: 100 kip load cell on A-frames.*

## REFERENCES

- ACI 318-05: ACI Committee 318, *Building Code Requirements for Structural Concrete (ACI 318-05)*, American Concrete Institute, Farmington Hills, MI.
- BBC News (2005). [http://newsimg.bbc.co.uk/media/images/40886000/jpg/40886412\\_ghazali\\_ya\\_ap203b.jpg](http://newsimg.bbc.co.uk/media/images/40886000/jpg/40886412_ghazali_ya_ap203b.jpg) (accessed July 31, 2006).
- Collins, M., and Mitchell, D. (1997). “*Prestressed Concrete Structures*,” Response Publications, Canada, pp. 256-296.
- elmundo.es (2005). <http://www.elmundo.es/elmundo/2005/01/11/madrid/1105430419.html> (accessed July 31, 2006).
- Felber, Andreas J. (1990). “*RESPONSE: A Program to Determine the Load-Deformation Response of Reinforced Concrete Sections*” Department of Civil Engineering, University of Toronto.
- Jones, Norman. (2000). “*Structures Under Shock and Impact VI*,” WIT Press, pp. 247-256.
- Mitchell, Geoffrey T. (2005). “*Pendulum Simulation of Vehicular Impact on Retrofit Bridge Barriers*”, Department of Civil, Architectural and Environmental Engineering, The University of Texas at Austin.
- Sea Ice Studies. (2005). *Thumbnails: Confederation Bridge*, [http://www.mar.dfo-mpo.gc.ca/science/ocean/seaice/bridge\\_gallery\\_e.html](http://www.mar.dfo-mpo.gc.ca/science/ocean/seaice/bridge_gallery_e.html) (accessed July 31, 2006).
- Tuchscherer, Robin G. (2006). “*Investigation of the Cracking Problem of Short Type IV Girders*,” Department of Civil, Architectural and Environmental Engineering, The University of Texas at Austin.
- Prestressed Concrete I-Beams*, Texas Department of Transportation, <http://www.dot.state.tx.us/insdtdot/orgchart/cmd/cserve/standard/bridge-e.htm> (accessed June 15, 2006).
- Washington State University. (2005). *Prestressed Girder Blast Test*, [http://www.ce.wsu.edu/trac/Research\\_WSU.htm](http://www.ce.wsu.edu/trac/Research_WSU.htm) (accessed July 31, 2006).

## VITA

Luis Alberto Orozco was born in Monterrey, Mexico on January 24, 1981, son of Felipe de Jesus Orozco and Miriam Lorena Villaseñor. Brother to Luis Felipe and Alejandro Orozco. He attended high school at Preparatoria Eugenio Garza Lagüera in Monterrey, Mexico and graduated in 1999. After high school he was admitted to the Instituto Tecnológico y de Estudios Superiores de Monterrey at Monterrey, Mexico and, in December of 2003, was awarded the degree of Bachelor of Science in Civil Engineering. After graduating he worked for a year as a project and structural designer in Gutierrez Ingenieros. In January of 2005, he entered The Graduate School at The University of Texas to pursue a Master of Science degree in Engineering. While pursuing his graduate degree, he worked at the Ferguson Structural Engineering Laboratory as a Graduate Research Assistant under Prof. Eric B. Williamson and Prof. Oguzhan Bayrak.

Permanent Address: Montes Claros #3413, Col. Villasol

Monterrey, N.L., C.P. 64949

Mexico

This report was typed by the author.